

# RESOLVED MASSIVE STAR CLUSTERS IN THE MILKY WAY AND ITS SATELLITES: BRIGHTNESS PROFILES AND A CATALOGUE OF FUNDAMENTAL PARAMETERS

DEAN E. MCLAUGHLIN

University of Leicester, Dept. of Physics and Astronomy, University Road,  
 Leicester, UK LE1 7RH

AND

ROELAND P. VAN DER MAREL

Space Telescope Science Institute, 3700 San Martin Drive, Baltimore, MD 21218

*Published in the Astrophysical Journal Supplement Series, 2005 Dec: ApJS, 161, 304-360*

## ABSTRACT

We present a database of structural and dynamical properties for 153 spatially resolved star clusters in the Milky Way, the Large and Small Magellanic Clouds, and the Fornax dwarf spheroidal. This database complements and extends others in the literature, such as those of Harris (1996) and Mackey & Gilmore (2003a,b,c). Our cluster sample comprises 50 “young massive clusters” in the LMC and SMC, and 103 old globular clusters between the four galaxies. The parameters we list include central and half-light averaged surface brightnesses and mass densities; core and effective radii; central potentials, concentration parameters, and tidal radii; predicted central velocity dispersions and escape velocities; total luminosities, masses, and binding energies; central phase-space densities; half-mass relaxation times; and “ $\kappa$ -space” parameters. We use publicly available population-synthesis models to compute stellar-population properties (intrinsic  $B - V$  colors, reddenings, and  $V$ -band mass-to-light ratios) for the same 153 clusters plus another 63 globulars in the Milky Way. We also take velocity-dispersion measurements from the literature for a subset of 57 (mostly old) clusters to derive dynamical mass-to-light ratios for them, showing that these compare very well to the population-synthesis predictions. The combined dataset is intended to serve as the basis for future investigations of structural correlations and the fundamental plane of massive star clusters, including especially comparisons between the systemic properties of young and old clusters.

The structural and dynamical parameters are derived from fitting three different models—the modified isothermal sphere of King (1966); an alternate modified isothermal sphere based on the ad hoc stellar distribution function of Wilson (1975); and asymptotic power-law models with constant-density cores—to the surface-brightness profile of each cluster. Surface-brightness data for the LMC, SMC, and Fornax clusters are based in large part on the work of Mackey & Gilmore (2003a,b,c), but include significant supplementary data culled from the literature and important corrections to Mackey & Gilmore’s  $V$ -band magnitude scale. The profiles of Galactic globular clusters are taken from Trager, King, & Djorgovski (1995). We address the question of which model fits each cluster best, finding in the majority of cases that the Wilson models—which are spatially more extended than King models but still include a finite, “tidal” cut-off in density—fit clusters of any age, in any galaxy, as well as or better than King models. Untruncated, asymptotic power laws often fit about as well as Wilson models but can be significantly worse. We argue that the extended halos known to characterize many Magellanic Cloud clusters may be examples of the *generic* envelope structure of self-gravitating star clusters, not just transient features associated strictly with young age.

*Subject headings:* globular clusters: general — galaxies: star clusters — Magellanic Clouds

## 1. INTRODUCTION

Next to elliptical galaxies, globular clusters are the most thoroughly modeled and best understood class of “hot” stellar system. The simple models of single-mass, isotropic, lowered isothermal spheres developed by King (1966) have been fit to a large majority of the  $\sim 150$  Galactic globulars currently known, yielding comprehensive catalogues of cluster structural parameters and derived physical properties (Djorgovski 1993; Pryor & Meylan 1993; Trager, King, & Djorgovski 1995; Harris 1996). These have been used to explore a multitude of scaling relations and interdependences between the various properties (Djorgovski & Meylan 1994), leading to the definition of a fundamental plane for globular clusters which is analogous to but physically distinct from that for early-type

galaxies and bulges (e.g., Djorgovski 1995; Burstein et al. 1997; Bellazzini 1998; McLaughlin 2000). Spectroscopic and HST imaging data have also been collected, and fit with King (1966) models, for a large number of globulars in M31 (e.g., Djorgovski et al. 1997; Dubath & Grillmair 1997; Barmby, Holland, & Huchra 2002), M33 (Larsen et al. 2002), and NGC 5128 = Centaurus A (Holland, Côté, & Hesser 1999; Harris et al. 2002; Martini & Ho 2004). These clusters appear to follow essentially the same scaling relations and lie on the same fundamental plane as Galactic globulars.

That these data contain important information on the formation and evolution of globular clusters (GCs) is clear. But cleanly separating formative from evolutionary influences on the present-day form of GC structural correlations and the fundamental plane is difficult in the absence of any rigorous, first-principles predictions for the systemic properties of newly born star clusters. This issue only gains in importance with the emergent consensus that the “super” star clusters now

forming in nearby starbursts and galaxy mergers, and even massive young clusters in more quiescent disks, may well be close analogues to what globular clusters were a Hubble time ago. What, then, can the properties of GCs tell us about how star clusters form in general? Conversely, what can a comparison between the properties of young clusters and GCs add to our understanding of the globulars?

Important steps towards addressing these questions have been made by studies of the mass-radius relations for young massive clusters in merging galaxies (e.g., Zepf et al. 1999) and relatively nearby spiral disks (Larsen 2004), and, on a somewhat different scale, for the (young) nuclear clusters in very late-type spirals (Böker et al. 2004; Walcher et al. 2005). However, the data on these clusters—all of which are at distances of many Mpc—are necessarily much less complete, and in some respects more uncertain, than those for globular clusters in the Milky Way and even out to NGC 5128. A comprehensive study of young cluster properties vs. GC properties requires a catalogue for the former which includes the full suite of physical parameters routinely calculated for Galactic GCs, preferably obtained within the same modeling framework and to comparable precision and accuracy.

Our main goal in this paper is to contribute to such a database, focusing specifically on the nearby populations of massive clusters in the Large and Small Magellanic Clouds. In particular, we fit a variety of models to obtain derived parameters for 53 LMC clusters and 10 SMC clusters with high-quality, HST-based surface-density profiles of their inner parts measured by Mackey & Gilmore (2003a,b). Thirteen of these objects are globular clusters older than 10 Gyr; the other 50 range in age from several Myr to a few Gyr. At the same time, Mackey & Gilmore (2003c) have published new surface-brightness profiles for the 5 old GCs in the Fornax dwarf spheroidal, so we include these in our catalogue as well. As we describe below, some aspects of our analyses of these LMC, SMC, and Fornax clusters go beyond what is normally done for GCs. Thus, we also take surface-brightness profiles for globulars in the Milky Way from the collection of Trager, King, & Djorgovski (1995), and some supplementary data from the catalogue of Harris (1996), in order to model as many Galactic GCs as is practical in precisely the same way that we treat the Mackey & Gilmore datasets. The exact number of Galactic GCs that we include depends on the context of our various calculations.

Much in the existing catalogues of Galactic GC properties is based on the same surface-brightness data from Trager, King, & Djorgovski (1995) that we employ here; and, as we said above, the catalogues already contain the results of reasonably uniform modeling of the clusters. However, all of this is within the context of the theoretical King (1966) isotropic, modified isothermal spheres. Mackey & Gilmore (2003a,b,c), for their part, tabulate estimates of cluster central surface brightnesses, core radii, total luminosities, and total masses derived from fits of power-law models for their surface-density profiles:  $I(R) \propto [1 + (R/r_0)^2]^{-(\gamma-1)/2}$ . (Mackey & Gilmore’s cluster masses further depend on their application of population-synthesis models.) One of our aims here is to homogenize the analysis of the basic data on young and globular clusters alike, and thus we completely re-fit all of the LMC, SMC, Fornax, and Milky Way cluster profiles with *both* King (1966) *and* power-law models. It is then important to recognize Mackey & Gilmore’s motivation for fitting asymptotic power laws to their cluster sample in the first place.

In their pioneering study of the structure of young clusters in the LMC, Elson, Fall, & Freeman (1987) found that King (1966) models are not always capable of describing the outer-envelope structures of these objects, which are very extended spatially and may be better fit by power laws that do not include the sharp tidal cut-offs built into King models. Some subsequent studies of other young massive clusters have come to the same conclusion (e.g., Larsen 2004; Schweizer 2004). It has been argued that this reflects the presence of rather massive halos of unbound stars around the clusters, which (it is presumed) will eventually be stripped away by tides to leave behind a more familiar, King-like body. However, so far as we are aware, there have not been any systematic attempts made to fit large samples of young clusters with structural models that are more extended than King (1966) but still spatially truncated rather than formally infinite like power laws. Nor, for that matter, has any such test been performed on old GCs. Thus, in this paper we also fit our combined LMC/SMC/Fornax/Milky Way cluster sample with a third type of model which is intermediate to King and power-law models. For this we have chosen a spherical and isotropic version of the model originally developed by Wilson (1975) for application to elliptical galaxies. Wilson’s model is essentially a single-mass, modified isothermal sphere like a King (1966) model in its core but with an ad hoc change in the “lowering” term in the stellar distribution function to give more extended (though still finite) halos for otherwise similar clusters.

In §2 below, we discuss in detail the surface-brightness data that we use to fit models to the clusters in our sample. In the LMC and SMC, we supplement many of the HST-derived profiles in Mackey & Gilmore (2003a,b) with older (ground-based) starcount densities for the same clusters. In many cases this allows the density profiles to be defined out to substantially larger projected radii. For the Fornax clusters, we rely exclusively on the Mackey & Gilmore (2003c) data. We work in the V band, and in all cases we check Mackey & Gilmore’s magnitude scales against ground-based aperture magnitudes from the literature. We find it necessary to recalibrate Mackey & Gilmore’s surface brightnesses, since as published they lead to integrated magnitudes that are always too faint—often by several tenths of a mag—relative to the ground-based numbers. The zeropoint correction for every cluster is tabulated. Our discussion of the Milky Way GC surface-brightness data is very brief, as we simply take them (also in the V band) from Trager, King, & Djorgovski (1995) with minor modifications.

Following that, in §3 we explore the use of population-synthesis models to infer an extinction  $A_V$  and mass-to-light ratio  $\Upsilon_V$  for each of the 68 LMC, SMC, and Fornax clusters from Mackey & Gilmore (2003a,b,c)—who have also provided an age and metallicity for every cluster, either compiled from CMD studies in the literature or estimated themselves—and for 148 Galactic GCs with metallicities listed in the catalogue of Harris (1996). We resort to the use of extinctions based on population-synthesis model colors to derive intrinsic luminosities, etc., from the observations of LMC and SMC clusters, because direct measurements of reddening are not available for the majority of that sample. (Measured extinctions are available for the Fornax and Milky Way GCs, and we use those as a check on our population-synthesis model values.) We need theoretical mass-to-light ratios for most of the clusters in all four galaxies in order to convert from luminosity to mass when determining

a number of dynamical cluster parameters (velocity dispersions have been observed for only a fraction of the clusters under consideration here). We tabulate  $A_V$  and  $\Upsilon_V$  for every cluster as determined using each of two publicly available population-synthesis codes (Fioc & Rocca-Volmerange 1997; Bruzual & Charlot 2003) under a number of different assumptions on the form of the stellar IMF. For our subsequent modeling, however, we only use the values predicted by the code of Bruzual & Charlot (2003) with the disk-star IMF of Chabrier (2003). Mackey & Gilmore (2003a,b,c) also used population-synthesis modeling to estimate mass-to-light ratios for their LMC/SMC/Fornax clusters; but they assumed a much steeper IMF than we do and obtained systematically different numbers for  $\Upsilon_V$ .

Section 4 first describes (§4.1) some salient aspects of King, power-law, and Wilson models. Then §4.2 shows in detail how each compares to the observed surface-brightness and internal velocity-dispersion profiles of the well studied GC  $\omega$  Centauri (see also McLaughlin & Meylan 2003), before presenting the bulk of our results, the basic parameters of each model fit to each of the 68 LMC, SMC, and Fornax clusters and 85 Galactic globulars. These are accompanied by a number of derived cluster properties, all evaluated within each of the three fitted models: central and half-light averaged surface brightnesses and mass densities; core and effective radii; concentrations and tidal radii (or infinite power-law slope); predicted central velocity dispersions and escape velocities; total luminosities, masses, and binding energies; central phase-space densities; and half-mass relaxation times. In §4.3 we compare our fits to those in existing catalogues (when the latter overlap with our work), and we check that our derived cluster properties are generally well defined regardless of which model is fit to the data.

We also investigate in §4.3 the question of which model tends to fit these clusters best. We find that, for  $\approx 90\%$  of our full sample of young massive clusters *and* old globular clusters, the more extended Wilson (1975) models provide equally good or significantly better fits than King (1966) models. Untruncated power laws generally describe the young clusters about as well as the spatially limited Wilson models; only occasionally are they slightly better. Thus, we conclude that (1) unlimited power laws are not the only description possible for the halos of young LMC/SMC clusters in particular, and (2) structure extending beyond what is predicted by King (1966) models is a fairly generic feature of any star cluster, rather than something present only at young ages. *It is not obvious that all such extended halos must necessarily be unbound*, but it is a subtle problem to measure accurately the tidal radius of a cluster and to compare it properly to the theoretical Roche lobe defined by a galaxy's tidal field. We do not tackle the issue in any detail in this paper.

In §5 we collect velocity-dispersion data from the literature for a subset of 19 Magellanic Cloud and Fornax clusters and 38 Galactic GCs, and use these in conjunction with our surface-brightness fits to derive dynamical mass-to-light ratios for them. We compare these directly to the population-synthesis model values which we used to derive all mass-dependent cluster properties. The agreement is very good on average.

Finally, §6 presents the “ $\kappa$ -space” parameters of Bender, Burstein, & Faber (1992) and Burstein et al. (1997) (or, more precisely, mass-equivalent versions of these) for the 153 young and globular clusters to which we fit all three of our structural models. We also tabulate in this Section

the galactocentric radii of all the objects. These quantities complete what is needed to construct the fundamental plane of star clusters in any of the equivalent formulations that can be found in the current literature. However, we leave the actual delineation and interpretation of all cluster correlations, including discussion of young vs. old populations, for future work.

## 2. STARCOUNT DATA, APERTURE PHOTOMETRY, AND SURFACE-BRIGHTNESS PROFILES

In this Section we collect and combine, in a uniform fashion, available data defining the run of surface brightness as a function of radius in a significant number of nearby and well-resolved globular and young, massive star clusters.

In the case of the Milky Way globular cluster (GC) system, this task has in fact already been completed by Trager, King, & Djorgovski (1995), who gathered inhomogeneous surface-brightness (SB) and starcount data from the literature for 124 GCs and combined them objectively into a single, zeropointed  $V$ -band SB profile for each cluster.<sup>1</sup> This database has served as the raw material for the standard catalogues (Djorgovski 1993; Harris 1996, updated 2003 February<sup>2</sup>) of King (1966) model parameters for Galactic GCs. Here we similarly work from the Trager, King, & Djorgovski (1995) GC profile data for our modeling of Milky Way globulars. Although some of these profiles have been superseded by more recent work on a few individual clusters, we have not attempted to incorporate any such updates into the Trager et al. catalogue, preferring instead to draw on data that have been processed in a homogeneous way by a single set of authors. A few further details on our handling of the Trager et al. data are given in §2.2 below.

The situation for well-resolved massive clusters in the Magellanic Clouds and the Fornax dwarf spheroidal is not quite as simple, although in these cases the recent studies of Mackey & Gilmore (2003a,b,c) have gone a long way towards providing a close analogue to the Trager, King, & Djorgovski (1995) dataset for Milky Way globulars. Mackey & Gilmore performed starcounts on the inner  $\approx 100''$  of 68 massive clusters (including 18 old globulars) from archival HST (WFPC2) images, providing the most accurate definitions of the *core* structures of these objects. (In the LMC, at a distance of  $D = 50.1$  kpc,  $100''$  corresponds to 24.2 pc; in the SMC, with  $D = 60.0$  kpc,  $100'' = 29.1$  pc; for the Fornax dwarf,  $D = 137$  kpc and  $100'' = 66.4$  pc.) Mackey & Gilmore further converted their starcount densities to  $V$ -band fluxes and published their results as standard surface-brightness profiles.

Our modeling of the LMC/SMC/Fornax clusters is therefore based in largest part on the work of Mackey & Gilmore (2003a,b,c). Again in the interest of confining our attention to as uniform a raw dataset as possible, we have not brought into the sample any other Magellanic Cloud clusters studied by other authors. (Note however, that Mackey & Gilmore's clusters do include many previously observed from the ground and modeled by other authors; see their papers for details of the overlap and comparisons with earlier work.)

We did, however, find it useful to go back through the literature to supplement Mackey & Gilmore's HST data with

<sup>1</sup> We note in passing that Trager et al. give the number of clusters in their catalogue as 125. However, according to Harris (1996), the GCs Terzan 5 and Terzan 11, which appear separately in Trager, King, & Djorgovski (1995), are in fact the same object.

<sup>2</sup> Available online at <http://physwww.mcmaster.ca/%7Eharris/mwgc.dat>.

(1) any available ground-based starcount data at projected radii  $R \gtrsim 100''$ , and (2) all available concentric-aperture photometry for these 68 clusters. The detailed comparison of the HST data against ground-based aperture photometry and large-radius starcounts, and our combination of these into a single, properly zeropointed  $V$ -band SB profile for each cluster, are what we describe now.

### 2.1. LMC, SMC, and Fornax Clusters

Table 1 lists all sources of star counts that we have taken from the literature for the 53 massive clusters (including 12 old globulars) studied by Mackey & Gilmore (2003a) in the Large Magellanic Cloud; the 10 (including one GC) studied by Mackey & Gilmore (2003b) in the SMC; and the 5 globular clusters of the Fornax dwarf spheroidal (Mackey & Gilmore 2003c). We note again that, although Mackey & Gilmore have published their data as SB profiles, they are in fact number densities converted to net mag arcsec<sup>-2</sup>; the other papers listed in Table 1 publish their results directly as number densities  $N$  per unit area on the sky, either already corrected for or accompanied by an estimate of background contamination. The older data can be combined with those of Mackey & Gilmore by transforming the ground-based  $N$  as  $\mu = C - 2.5 \log N$ , with the constant  $C$  chosen to provide the best average agreement with the HST surface brightnesses at clustercentric radii where the observations overlap.

For each of their 68 clusters in these three Galactic satellites, Mackey & Gilmore (2003a,b,c, hereafter referred to collectively as MG03) have produced a “primary” surface brightness profile in the  $V$  band and a “secondary” profile in one of  $B$  or  $I$ . We have chosen to work on the  $V$  magnitude scale, but to make maximal use of the new HST data, we have combined the data in the secondary bands with the main  $V$ -band data by applying a constant color term to the former. These instrumental colors are determined simply from integrating to find the total magnitude of every MG03 cluster in both  $V$  and  $B$  or  $I$ , and then adding the difference ( $V - B$ ) or ( $V - I$ ) to every point in the secondary SB profile. This produces a single profile with two independent estimates of  $\mu_V$ —both used in our model fitting below—at every clustercentric radius. The instrumental colors we applied are listed for reference in Table 2 and are in agreement with the total cluster magnitudes already calculated by MG03.

After combining the primary  $V$  and secondary  $B/I$  SB data for each cluster, we parsed them to be left only with strictly independent surface brightnesses. MG03 performed starcounts in four different series of concentric apertures covering each cluster, each series using a different width for the annuli. Within a given series, the annuli are all of the same width and not overlapping, but there is annulus overlap between the series. Thus, the SB profile tabulations from MG03 include interdependent data points. To avoid such correlations during our model fitting, we simply adopted only the ( $V + B/I$ ) surface brightnesses derived by MG03 in their narrowest annuli ( $\Delta R = 1.''5$ ) for the inner regions of every cluster, and switched over to take only the widest-annulus results ( $\Delta R = 4.''$ ) in the outer parts. We discarded altogether the SB points estimated from the intermediate annulus widths. Additionally, to each annulus that we kept we assigned an average (median) radius determined by the local slope of the surface-brightness distribution, as described in King (1988) (rather than associating each SB point with the straight mean of the inner and outer radii of its annulus, as MG03 do).

At this point we were able to match the ground-based starcounts to the combined HST SB profiles, on the  $V$ -band magnitude scale defined by MG03. Background-corrected stellar number densities  $N$  and uncertainties are tabulated for 32 LMC clusters in the Mackey & Gilmore sample, and for all 10 of the SMC clusters, in the papers listed in Table 1. We first converted all of these to uncalibrated “surface brightnesses,”  $-2.5 \log N$ . In many cases, multiple plates with different exposure times and limiting magnitudes were used by the original authors to derive independent estimates of the density throughout overlapping ranges of radius  $R$  within a single cluster. We shifted such partial  $N(R)$  profiles by constants chosen to make the median difference of the various  $\log N(R)$ , taken over all radii where any count sets overlap, vanish. The single, ground-based profile in  $-2.5 \log N(R)$  that resulted always extended inward to at least  $R = 100''$  in each cluster, thus overlapping with the MG03 HST  $\mu_V$  data. The difference  $[\mu_V(R_i) + 2.5 \log N(R_i)]$  averaged over the radii where ground- and space-based data overlap then defined a constant  $C$  which, when added to  $-2.5 \log N(R)$ , brings the older starcount data onto the  $V$ -band surface brightness scale of Mackey & Gilmore. In determining these “calibrations,” we never included the ground-based density at the innermost or outermost radius of any count set, as these are the radii potentially most susceptible, respectively, to crowding and background errors.

With these combined, parsed, and extended  $\mu_V(R)$  profiles in hand, and in effect calibrated by Mackey & Gilmore (2003a,b,c), we found it necessary to re-examine this calibration—the zeropoint of their conversion from HST starcounts to  $V$ -band fluxes—itsself. To check it, we used the  $\mu_V$  profiles as published in MG03 to calculate the integrated (enclosed) magnitude,  $V(\leq R)$ , as a function of projected radius on scales  $R \lesssim 100''$  in each cluster in the total LMC+SMC+Fornax sample. We then compared these integrated profiles against appropriate ground-based aperture magnitudes. Photometry within apertures  $R_{\text{ap}} \lesssim 100''$  exists in the literature for all but two of the clusters under consideration, and the sources that we have used are listed in Table 3. In principle, we might have simply used true SB profiles from the literature to compare directly against Mackey & Gilmore’s surface brightness calibration without any integration; but such profiles exist for a much smaller fraction of the clusters in this sample, so for reasons of homogeneity we took the aperture-photometry approach in all cases.

Table 4 presents the results of this comparison for all 68 clusters from MG03. Each cluster has six columns in this table: first is the cluster name; next, the aperture size,  $R_{\text{ap}}$ , associated with a ground-based magnitude measurement; then the  $V$  magnitude from the literature and the specific source of this  $V(\leq R_{\text{ap}})$  combination; next, the integrated  $V$  magnitude within  $R_{\text{ap}}$  implied by Mackey & Gilmore’s SB profile as published; and finally, the difference  $\Delta\mu_V$  of the ground-based aperture magnitude minus the MG03  $V$  magnitude.

For the majority of clusters, the  $V$ -band magnitudes implied by the MG03 surface-brightness calibration are significantly fainter—sometimes by a full magnitude or more—than any independent aperture photometry. This appears to be related to the fact that, in performing their number counts, MG03 necessarily had to mask out some bright stars, whether because of issues with saturation or scattered light, or because they disturbed the smoother overall distribution of the underlying, more numerous fainter stars in the cluster. The flux from these stars was *not* added back in when the stellar counts

TABLE 1  
PUBLISHED STARCOUNT DATA FOR MAGELLANIC CLOUD AND FORNAX CLUSTERS

Source	Clusters
LMC:	
Kontizas, Chrysovergis, & Kontizas (1987)	NGC 1711, 1786, 1835, 1847, 1850, 1856, 2019, 2100
Kontizas, Hadjidimitriou, & Kontizas (1987)	NGC 1777, 1868; Hodge 14; SL 842
Chrysovergis, Kontizas, & Kontizas (1989)	NGC 1754, 1805, 1898, 2031, 2121, 2136, 2173, 2210, 2213, 2231
Elson, Fall, & Freeman (1987)	NGC 1818, 1831, 1866, 2004, 2156, 2157, 2159, 2164, 2172, 2214
Mackey & Gilmore (2003a)	all of the above, plus: NGC 1466, 1651, 1718, 1841, 1860, 1916, 1984, 2005, 2011, 2153, 2155, 2162, 2193, 2209, 2249, 2257; Hodge 4, 11; R136 (30 Dor); SL 663, 855
SMC:	
Kontizas, Danezis, & Kontezis (1982)	Kron 3; NGC 152, 176, 361, 458
Kontizas & Kontizas (1983)	NGC 121, 330, 339, 411, 416
Mackey & Gilmore (2003b)	all of the above
Fornax Dwarf Spheroidal:	
Mackey & Gilmore (2003c)	FORNAX 1, 2, 3, 4, 5

TABLE 2  
INSTRUMENTAL COLORS OF MAGELLANIC CLOUD AND FORNAX CLUSTERS

Cluster (1)	Color (2)	Value (3)	Cluster (1)	Color (2)	Value (3)
LMC-HODGE11	( <i>B</i> − <i>V</i> )	0.35 ± 0.09	LMC-NGC2156	( <i>V</i> − <i>I</i> )	0.04 ± 0.14
LMC-HODGE14	( <i>B</i> − <i>V</i> )	0.41 ± 0.26	LMC-NGC2157	( <i>B</i> − <i>V</i> )	−0.12 ± 0.08
LMC-HODGE4	( <i>B</i> − <i>V</i> )	0.42 ± 0.11	LMC-NGC2159	( <i>V</i> − <i>I</i> )	0.10 ± 0.11
LMC-NGC1466	( <i>V</i> − <i>I</i> )	0.77 ± 0.06	LMC-NGC2162	( <i>B</i> − <i>V</i> )	0.46 ± 0.11
LMC-NGC1651	( <i>B</i> − <i>V</i> )	0.49 ± 0.11	LMC-NGC2164	( <i>V</i> − <i>I</i> )	0.13 ± 0.06
LMC-NGC1711	( <i>V</i> − <i>I</i> )	0.21 ± 0.06	LMC-NGC2172	( <i>V</i> − <i>I</i> )	0.12 ± 0.12
LMC-NGC1718	( <i>B</i> − <i>V</i> )	0.50 ± 0.10	LMC-NGC2173	( <i>B</i> − <i>V</i> )	0.49 ± 0.10
LMC-NGC1754	( <i>V</i> − <i>I</i> )	1.02 ± 0.07	LMC-NGC2193	( <i>B</i> − <i>V</i> )	0.50 ± 0.14
LMC-NGC1777	( <i>B</i> − <i>V</i> )	0.39 ± 0.10	LMC-NGC2209	( <i>B</i> − <i>V</i> )	0.09 ± 0.20
LMC-NGC1786	( <i>V</i> − <i>I</i> )	0.87 ± 0.05	LMC-NGC2210	( <i>V</i> − <i>I</i> )	0.82 ± 0.06
LMC-NGC1805	( <i>V</i> − <i>I</i> )	0.08 ± 0.10	LMC-NGC2213	( <i>B</i> − <i>V</i> )	0.47 ± 0.12
LMC-NGC1818	( <i>V</i> − <i>I</i> )	0.05 ± 0.06	LMC-NGC2214	( <i>B</i> − <i>V</i> )	0.00 ± 0.09
LMC-NGC1831	( <i>B</i> − <i>V</i> )	0.19 ± 0.05	LMC-NGC2231	( <i>B</i> − <i>V</i> )	0.42 ± 0.13
LMC-NGC1835	( <i>V</i> − <i>I</i> )	1.02 ± 0.06	LMC-NGC2249	( <i>B</i> − <i>V</i> )	0.27 ± 0.08
LMC-NGC1841	( <i>V</i> − <i>I</i> )	0.88 ± 0.11	LMC-NGC2257	( <i>B</i> − <i>V</i> )	0.37 ± 0.10
LMC-NGC1847	( <i>B</i> − <i>V</i> )	−0.05 ± 0.11	LMC-R136	( <i>V</i> − <i>I</i> )	0.36 ± 0.08
LMC-NGC1850	( <i>B</i> − <i>V</i> )	0.18 ± 0.06	LMC-SL663	( <i>B</i> − <i>V</i> )	0.29 ± 0.21
LMC-NGC1856	( <i>B</i> − <i>V</i> )	0.26 ± 0.04	LMC-SL842	( <i>B</i> − <i>V</i> )	0.40 ± 0.19
LMC-NGC1860	( <i>B</i> − <i>V</i> )	−0.07 ± 0.14	LMC-SL855	( <i>B</i> − <i>V</i> )	0.17 ± 0.27
LMC-NGC1866	( <i>V</i> − <i>I</i> )	0.18 ± 0.05	SMC-KRON3	( <i>B</i> − <i>V</i> )	0.42 ± 0.09
LMC-NGC1868	( <i>B</i> − <i>V</i> )	0.29 ± 0.07	SMC-NGC121	( <i>B</i> − <i>V</i> )	0.49 ± 0.06
LMC-NGC1898	( <i>V</i> − <i>I</i> )	0.86 ± 0.07	SMC-NGC152	( <i>B</i> − <i>V</i> )	0.39 ± 0.11
LMC-NGC1916	( <i>V</i> − <i>I</i> )	1.12 ± 0.04	SMC-NGC176	( <i>B</i> − <i>V</i> )	−0.01 ± 0.18
LMC-NGC1984	( <i>V</i> − <i>I</i> )	0.56 ± 0.12	SMC-NGC330	( <i>B</i> − <i>V</i> )	−0.06 ± 0.07
LMC-NGC2004	( <i>B</i> − <i>V</i> )	−0.13 ± 0.11	SMC-NGC339	( <i>B</i> − <i>V</i> )	0.44 ± 0.11
LMC-NGC2005	( <i>V</i> − <i>I</i> )	0.92 ± 0.08	SMC-NGC361	( <i>B</i> − <i>V</i> )	0.37 ± 0.11
LMC-NGC2011	( <i>V</i> − <i>I</i> )	0.29 ± 0.16	SMC-NGC411	( <i>B</i> − <i>V</i> )	0.44 ± 0.11
LMC-NGC2019	( <i>V</i> − <i>I</i> )	0.94 ± 0.06	SMC-NGC416	( <i>B</i> − <i>V</i> )	0.36 ± 0.08
LMC-NGC2031	( <i>V</i> − <i>I</i> )	0.28 ± 0.06	SMC-NGC458	( <i>B</i> − <i>V</i> )	0.07 ± 0.11
LMC-NGC2100	( <i>B</i> − <i>V</i> )	0.02 ± 0.11	FORNAX1	( <i>V</i> − <i>I</i> )	0.64 ± 0.12
LMC-NGC2121	( <i>B</i> − <i>V</i> )	0.39 ± 0.10	FORNAX2	( <i>V</i> − <i>I</i> )	0.78 ± 0.09
LMC-NGC2136	( <i>B</i> − <i>V</i> )	0.17 ± 0.11	FORNAX3	( <i>V</i> − <i>I</i> )	0.89 ± 0.08
LMC-NGC2153	( <i>B</i> − <i>V</i> )	0.30 ± 0.15	FORNAX4	( <i>V</i> − <i>I</i> )	1.06 ± 0.13
LMC-NGC2155	( <i>B</i> − <i>V</i> )	0.51 ± 0.13	FORNAX5	( <i>V</i> − <i>I</i> )	0.90 ± 0.09

NOTE. — Cluster colors are those implied by the integrated magnitudes derived from surface-brightness profiles out to  $R \approx 100''$  as published by Mackey & Gilmore (2003a,b,c). Colors are strictly instrumental, in that the published surface brightnesses have not been corrected for any zeropoint changes in any bandpass. For clusters with instrumental (*B* − *V*) colors given here, compare with the *true* colors listed in Column (4) of Table 8.

TABLE 3  
PUBLISHED APERTURE PHOTOMETRY FOR MAGELLANIC CLOUD AND FORNAX CLUSTERS

Source	Clusters
LMC:	
Bernard & Bigay (1974)	NGC 1835, 2019
Bernard (1975)	NGC 2173
van den Bergh (1981)	Mackey & Gilmore (2003a) sample excluding SL 663, 855
Gordon & Kron (1983)	NGC 1835, 1841, 1856, 1916, 2121
Elson, Fall, & Freeman (1987)	NGC 1818, 1831, 1866, 2004, 2156, 2157, 2159, 2164, 2172, 2214
Bica et al. (1996)	Mackey & Gilmore (2003a) sample excluding SL 663, 855
SMC:	
van den Bergh (1981)	full Mackey & Gilmore (2003b) sample
Gordon & Kron (1983)	full Mackey & Gilmore (2003b) sample
Fornax Dwarf Spheroidal:	
Hodge (1965, 1969); Webbink (1985)	FORNAX 1
de Vaucouleurs & Ables (1970)	FORNAX 2, 3, 4, 5
Gordon & Kron (1983)	FORNAX 3, 4

TABLE 4  
ZEROPOINT OFFSETS APPLIED TO MACKEY & GILMORE *V*-BAND SURFACE BRIGHTNESS

Cluster	$R_{\text{ap}}$ [sec]	$V_{\text{ap}}$ [lit.]	Ref.	$V_{\text{ap}}$ [MG03]	$\Delta\mu_V$	Cluster	$R_{\text{ap}}$ [sec]	$V_{\text{ap}}$ [lit.]	Ref.	$V_{\text{ap}}$ [MG03]	$\Delta\mu_V$
(1)	(2)	(3)	(4)	(5)	(6)	(1)	(2)	(3)	(4)	(5)	(6)
LMC-HODGE11	30.5	11.93	1	12.158	$-0.228 \pm 0.046$	LMC-NGC2156	27.6	11.38	3	12.670	$-1.290 \pm 0.104$
LMC-HODGE14	31.0	13.42	2	13.571	$-0.151 \pm 0.084$	LMC-NGC2157	30.0	10.16	2	10.920	$-0.760 \pm 0.074$
LMC-HODGE4	19.0	13.33	1	13.489	$-0.159 \pm 0.080$	LMC-NGC2159	36.0	11.38	2	12.569	$-1.189 \pm 0.065$
LMC-NGC1466	30.0	11.59	2	11.963	$-0.373 \pm 0.040$	LMC-NGC2162	31.0	12.70	2	12.814	$-0.114 \pm 0.079$
LMC-NGC1651	50.0	12.28	1	12.254	$0.026 \pm 0.063$	LMC-NGC2164	30.0	10.34	2	11.603	$-1.263 \pm 0.040$
LMC-NGC1711	30.0	10.11	2	11.431	$-1.321 \pm 0.041$	LMC-NGC2172	36.0	11.75	2	12.976	$-1.226 \pm 0.069$
LMC-NGC1718	31.0	12.25	2	12.219	$0.031 \pm 0.059$	LMC-NGC2173	75.0	11.88	1	11.901	$-0.021 \pm 0.059$
LMC-NGC1754	50.0	11.57	1	11.907	$-0.337 \pm 0.052$	LMC-NGC2193	19.0	13.42	1	13.582	$-0.162 \pm 0.089$
LMC-NGC1777	19.0	12.80	1	12.997	$-0.197 \pm 0.048$	LMC-NGC2209	34.0	13.15	2	13.940	$-0.790 \pm 0.147$
LMC-NGC1786	30.0	10.88	2	11.453	$-0.573 \pm 0.029$	LMC-NGC2210	34.0	10.94	2	11.492	$-0.552 \pm 0.033$
LMC-NGC1805	30.0	10.63	2	11.945	$-1.315 \pm 0.073$	LMC-NGC2213	31.0	12.38	2	12.466	$-0.086 \pm 0.076$
LMC-NGC1818	36.0	9.70	2	11.181	$-1.481 \pm 0.047$	LMC-NGC2214	30.0	10.93	2	11.408	$-0.478 \pm 0.088$
LMC-NGC1831	30.0	11.18	2	11.219	$-0.039 \pm 0.040$	LMC-NGC2231	22.0	13.20	2	13.516	$-0.316 \pm 0.105$
LMC-NGC1835	31.0	10.17	2	10.652	$-0.482 \pm 0.037$	LMC-NGC2249	75.0	11.94	1	12.035	$-0.095 \pm 0.060$
LMC-NGC1841	93.5	11.43	1	12.164	$-0.734 \pm 0.087$	LMC-NGC2257	30.5	12.62	1	12.747	$-0.127 \pm 0.066$
LMC-NGC1847	36.0	11.06	2	11.512	$-0.452 \pm 0.076$	LMC-R136	30.0	8.27	2	8.985	$-0.715 \pm 0.078$
LMC-NGC1850	25.0	9.57	1	9.721	$-0.151 \pm 0.060$	LMC-SL663	...	...	-	...	0
LMC-NGC1856	31.0	10.06	2	10.042	$0.018 \pm 0.032$	LMC-SL842	19.0	14.15	1	14.196	$-0.046 \pm 0.160$
LMC-NGC1860	36.0	11.04	2	12.852	$-1.812 \pm 0.134$	LMC-SL855	...	...	-	...	0
LMC-NGC1866	36.0	9.73	2	10.838	$-1.108 \pm 0.034$	SMC-KRON3	31.0	12.05	2	12.198	$-0.148 \pm 0.046$
LMC-NGC1868	31.0	11.57	2	11.633	$-0.063 \pm 0.044$	SMC-NGC121	31.0	11.24	2	11.548	$-0.308 \pm 0.034$
LMC-NGC1898	20.0	11.86	1	12.463	$-0.603 \pm 0.049$	SMC-NGC152	31.0	12.92	2	12.946	$-0.026 \pm 0.077$
LMC-NGC1916	22.0	10.38	2	10.868	$-0.488 \pm 0.028$	SMC-NGC176	31.0	12.70	2	13.441	$-0.741 \pm 0.123$
LMC-NGC1984	25.0	9.99	1	12.922	$-2.932 \pm 0.086$	SMC-NGC330	31.0	9.60	2	10.621	$-1.021 \pm 0.065$
LMC-NGC2004	36.0	9.60	2	10.380	$-0.780 \pm 0.090$	SMC-NGC339	31.0	12.84	2	12.873	$-0.033 \pm 0.079$
LMC-NGC2005	12.5	11.57	2	12.052	$-0.482 \pm 0.058$	SMC-NGC361	31.0	12.12	4	12.690	$-0.570 \pm 0.085$
LMC-NGC2011	20.0	10.58	1	13.353	$-2.773 \pm 0.175$	SMC-NGC411	31.0	12.21	2	12.234	$-0.024 \pm 0.088$
LMC-NGC2019	36.0	10.86	2	11.314	$-0.454 \pm 0.043$	SMC-NGC416	31.0	11.42	2	11.609	$-0.189 \pm 0.038$
LMC-NGC2031	36.0	10.83	2	11.560	$-0.730 \pm 0.039$	SMC-NGC458	31.0	11.73	2	11.832	$-0.102 \pm 0.092$
LMC-NGC2100	30.0	9.60	2	10.184	$-0.584 \pm 0.101$	FORNAX1	70.0	15.57	5	15.395	0
LMC-NGC2121	31.0	12.37	2	12.581	$-0.211 \pm 0.058$	FORNAX2	32.5	13.73	6	14.017	$-0.287 \pm 0.050$
LMC-NGC2136	30.0	10.54	2	10.733	$-0.193 \pm 0.089$	FORNAX3	32.5	12.74	6	13.177	$-0.437 \pm 0.047$
LMC-NGC2153	50.0	13.05	1	13.472	$-0.422 \pm 0.103$	FORNAX4	32.5	13.49	6	14.069	$-0.579 \pm 0.090$
LMC-NGC2155	31.0	12.60	2	12.542	$0.058 \pm 0.091$	FORNAX5	32.5	13.55	6	14.009	$-0.459 \pm 0.055$

REFERENCES. — (1)—Bica et al. (1996); (2)—van den Bergh (1981); (3)—Elson, Fall, & Freeman (1987); (4)—Gordon & Kron (1983); (5)—Webbink (1985); (6)—de Vaucouleurs & Ables (1970).

NOTE. — Six columns for each of 68 star clusters in the LMC, SMC, and Fornax studied by Mackey & Gilmore (2003a,b,c, collectively MG03):

**Column (1)**—Cluster name.

**Column (2)**—Aperture radius, in arcsec, of a ground-based magnitude measurement from previous literature.

**Column (3)**—Ground-based *V* magnitude of the cluster within the radius in Column (2).

**Column (4)**—Source of the cited ground-based aperture magnitude.

**Column (5)**—*V*-band magnitude within  $R_{\text{ap}}$  obtained by integrating the published surface-brightness profile of MG03.

**Column (6)**—Zeropoint correction to be *added* to MG03 *V*-band surface brightnesses to bring their cluster magnitudes into agreement with the earlier, ground-based data.

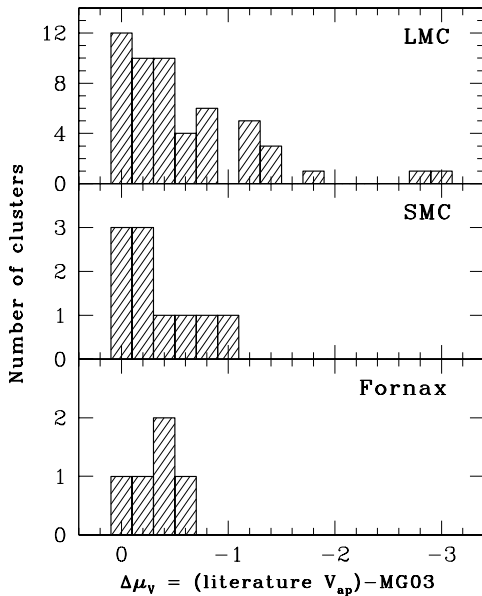


FIG. 1.— Histogram of zeropoint corrections  $\Delta\mu_V$  to the  $V$ -band surface brightness scale defined for LMC, SMC, and Fornax clusters in Mackey & Gilmore (2003a,b,c). Values of  $\Delta\mu_V$  are given for individual clusters in Table 4.

were converted to  $\text{mag arcsec}^{-2}$ , so that the  $V$ -band surface brightnesses published in MG03 are systematically too faint (see the discussion in Mackey & Gilmore 2003a, especially; also, Mackey 2003, private communication).

Figure 1 is a histogram of the zeropoint corrections required to bring the MG03 surface brightnesses into agreement with the independent aperture photometry we have taken from the literature. Some of these offsets are rather surprisingly large, particularly in a few of the LMC clusters, and the possibility exists in principle that the older aperture magnitudes could be the ones in error—if, say, a bright foreground star were unwittingly included in the ground-based aperture but properly excluded from the HST analysis. However, a detailed examination of several specific cases has shown that the ground-based numbers are *not* the ones at fault (Mackey 2003, private communication). More general support for the same conclusion comes from the fact that, as we describe just below, there is typically good agreement between the integrated  $V(\leq R)$  profile *shapes* from the MG03 and ground-based data in many clusters where multiple aperture magnitudes can be found in the literature—suggesting that if the ground-based data were erroneously brightened by foreground stars, these would have had to be projected essentially onto the very centers of the clusters in an inordinate number of cases. And the instrumental colors (Table 2) of those clusters for which MG03 publish both  $B$  and  $V$  surface-brightness profiles do not agree with the aperture-photometry colors from the literature [Column (4) of Table 8 below], even when the  $V$ -band zeropoint correction that we infer is negligible (implying that the missing  $V$  flux in MG03 is not generally consistent with a regular population of foreground stars). Thus, when fitting models and deriving physical parameters for the Magellanic Cloud and Fornax clusters (§4.2), we always add the (generally negative) offsets  $\Delta\mu_V$  listed in Table 4 to the  $V$ -band profile numbers published in MG03.

Note that for two of the LMC clusters (SL-663 and SL-855) we could find no independent  $V$  photometry against which to compare the MG03 calibration; while for Globular Cluster 1 in Fornax, various estimates of the total  $V$  magnitude from Webbink (1985) and Hodge (1965, 1969) differ from each other by at least as much as they do from the implied MG03 magnitude. In these three cases, we do not apply any zeropoint correction to the MG03 surface brightnesses, but we recognize that the adopted numbers could be in error by tenths of a magnitude in each case.

For 32 of the clusters, ground-based  $V$  magnitudes are available in the literature for more than one aperture—allowing for further checks in these cases, both of the consistency between the various old magnitude estimates and of the overall *shape* of the new Mackey & Gilmore profiles. These checks are presented in Figure 2. Each panel here corresponds to a different cluster, and all points plotted are aperture magnitudes from the sources listed in Table 3. Measurements of  $V_{\text{ap}}$  from van den Bergh (1981) and Bica et al. (1996)—the most comprehensive listings—are set apart as a large open square in every panel, while the smaller filled circles refer to reliable data from any other source. The large open circles, which are particularly evident in the Fornax globular clusters, denote published magnitudes which the original authors have indicated are especially uncertain. In all panels of Fig. 2, the solid line is the integrated magnitude profile derived from the  $V$ -band surface brightness data of MG03, *after* a shift brightward by the offset  $\Delta\mu_V$  from Table 4, which is listed in each panel. As was mentioned above, these comparisons show generally rather good agreement between the shapes of the cluster profiles as measured by MG03, and what can be inferred from the ground. In the few cases where the two do appear to differ at some significant level (e.g., NGC 1916 in the LMC), we simply view the newer HST data as providing an improved estimate of the true relative density distribution inside these distant clusters.

Table 5 contains the final surface-brightness profiles of the 68 LMC, SMC, and Fornax clusters to which we fit models in §4 below. This table is published in its entirety in the electronic version of ApJS; only a short excerpt is presented here. Each cluster is given several tens of lines in the table. The first column of each line is the cluster name, followed by: a radius in arcsec (the median of an annulus, determined, as mentioned above, according to King 1988); the logarithmic radius; the  $V$ -band surface brightness measured at that radius *after adjusting the magnitude scale of Mackey & Gilmore by the zeropoint offset from Table 4*; the faint and bright limits on  $\mu_V$  (reflecting the possibility of asymmetric errorbars, especially at faint intensity levels); the bandpass from which the datapoint originally came (with  $G$  denoting ground-based number densities scaled as described above); an estimate of the  $V$ -band extinction towards the cluster (assumed spatially constant in each cluster), and its uncertainty; and a flag indicating whether or not the point was included explicitly when fitting the models of §4.

To determine whether or not any given point should contribute to the weighting of the model fits—i.e., in setting the “fit flag” of Table 5 to 1 or 0—we first used all the tabulated  $V-B/I$ -ground-based SB values for a cluster to produce a smoothed (nonparametric) density profile. Any individual points that fell more than  $2\sigma$  away from this smoothed approximation were assigned a fit flag of 0.

The  $V$ -band extinctions in Table 5 require further explanation, since direct estimates of the reddening of individual

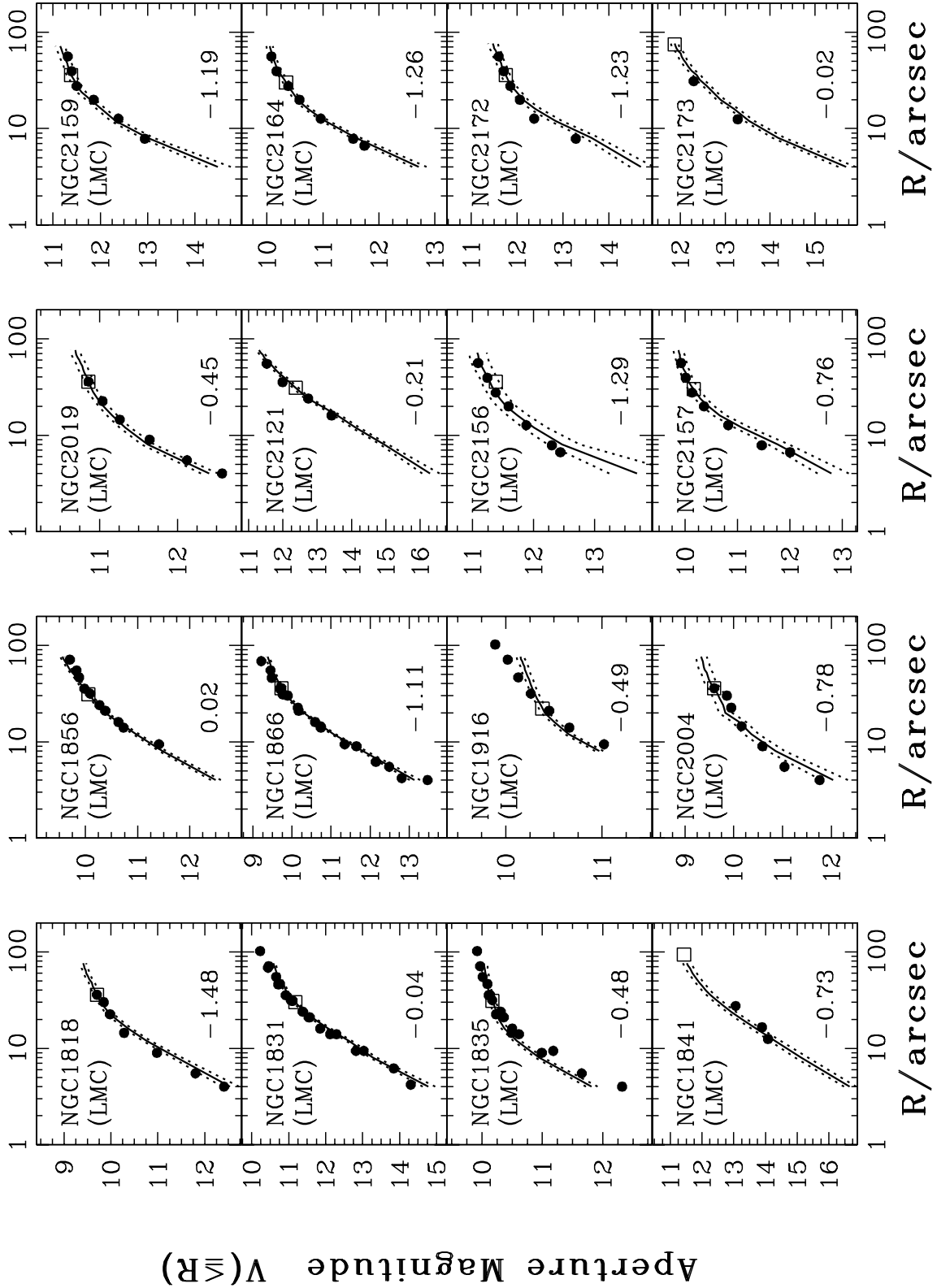


FIG. 2.— Aperture magnitude vs. radius for LMC, SMC, and Fornax clusters from the sample of Mackey & Gilmore (2003a,b,c). Only clusters with more than one ground-based  $V_{\text{ap}}$  found in the literature are shown. Solid line in each panel is the integrated magnitude  $V(\leq R)$  as a function of radius from the SB profile published by MG03, *after* applying the zeropoint correction given in Table 4. Dotted lines demark the uncertainties derived from the MG03 profiles. Open squares in all panels denote aperture magnitudes taken from either Bica et al. (1996) or van den Bergh (1981), filled circles are aperture magnitudes from any other source (see Table 3), and open circles are measurements cited as uncertain by the original authors.



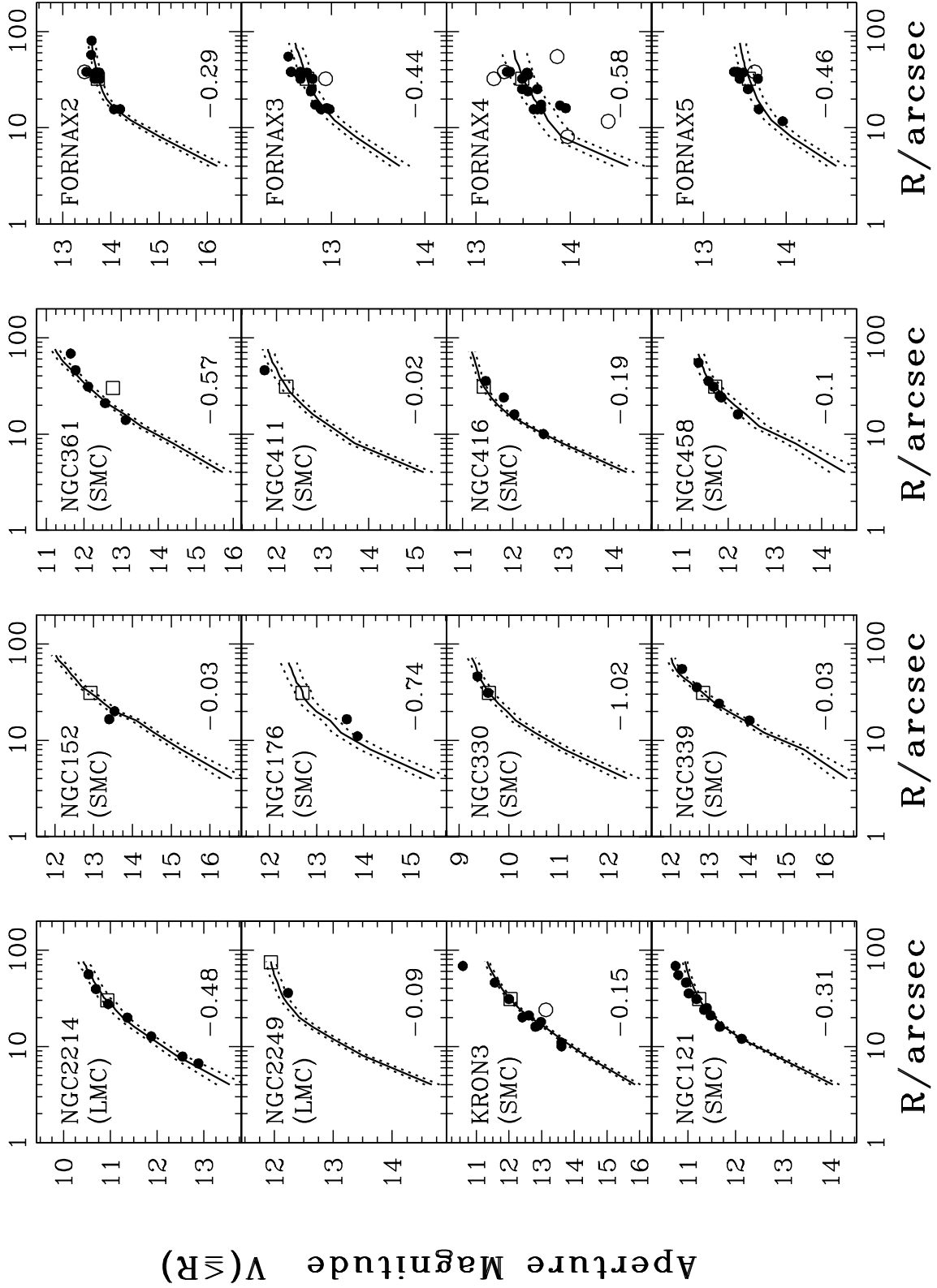


FIG. 2 [CONTINUED].—

TABLE 5  
CALIBRATED *V*-BAND SURFACE-BRIGHTNESS PROFILES OF LMC, SMC, AND FORNAX CLUSTERS

Cluster	$R$ [sec]	$\log R$	$\mu_V^a$	(max)	(min)	band <sup>b</sup>	$A_V^c$	uncertainty	fit flag <sup>d</sup>
(1)	(2)	(3)	(4)	(5)	(6)	(7)	(8)	(9)	(10)
LMC-HODGE11	1.06	0.025	18.82	19.21	18.43	<i>V</i>	0.143	0.077	1
LMC-HODGE11	1.06	0.025	19.00	19.35	18.65	<i>B</i>	0.143	0.077	1
LMC-HODGE11	2.37	0.374	19.53	19.78	19.28	<i>B</i>	0.143	0.077	1
SMC-KRON3	1.06	0.027	19.76	20.10	19.42	<i>V</i>	0.050	0.081	1
SMC-KRON3	1.06	0.027	19.75	20.07	19.43	<i>B</i>	0.050	0.081	1
SMC-KRON3	2.37	0.375	20.08	20.26	19.90	<i>B</i>	0.050	0.081	1
FORNAX1	1.41	0.150	22.84	23.29	22.39	<i>V</i>	0.220	0.077	1
FORNAX1	1.41	0.150	22.61	23.08	22.14	<i>I</i>	0.220	0.077	1
FORNAX1	3.16	0.500	23.41	23.60	23.22	<i>I</i>	0.220	0.077	1

NOTE. — A machine-readable version of the complete Table 5 is published in the electronic edition of the *Astrophysical Journal Supplement Series*; only a portion is shown here, for guidance regarding its form and content.

<sup>a</sup>Surface brightnesses  $\mu_V$  in Column (4) are on our *calibrated V*-band scale, with the zeropoint corrections to the Mackey & Gilmore (2003a,b,c) numbers already applied (see Table 4). Maximum and minimum surface brightnesses in Columns (5) and (6) define the errorbars on  $\mu_V$ , which are asymmetric in general. The uncertainty in the zeropoint correction  $\Delta\mu_V$  from Table 4 is a source of systematic error; it is *not* accounted for in Columns (5) and (6) but is added in quadrature to the formal,  $\chi^2$ -based uncertainties in all fitted and derived cluster parameters relating to surface brightness.

<sup>b</sup>*V*, *B*, or *I* denotes the original bandpass of a Mackey & Gilmore (2003a,b,c) surface-brightness datapoint, with *B* or *I* data shifted in zeropoint as in Table 2, and then again by an amount  $\Delta\mu_V$  from Table 4, to match onto our calibrated  $\mu_V$  scale. *G* denotes a surface density taken from ground-based starcounts in the literature (Table 1), transformed to a surface-brightness and zeropointed to the  $\mu_V$  scale of column (4).

<sup>c</sup>*V*-band extinction  $A_V = 3.1 E(B - V)$ , with  $E(B - V)$  taken from literature values compiled by Mackey & Gilmore (2003c) for the Fornax globular clusters but inferred from our population-synthesis modeling in §3 (Table 8) for LMC and SMC clusters.  $A_V$  must be *subtracted* from columns (4), (5), and (6); it is spatially constant in each cluster but is listed at every radius as a convenience.

<sup>d</sup>1 = point used in fitting of structural models in §4; 0 = point *not* used in model fitting.

Magellanic Cloud clusters do not exist for the majority in this sample. However, in order to accurately determine cluster physical parameters—true central surface brightnesses, total luminosities and masses, etc.—some knowledge of the extinction is clearly required. MG03 assign a single, average extinction to all LMC clusters, and another average to all SMC clusters; but the reddening is known to vary across these systems. We have instead used population-synthesis modeling, given an age and a metallicity for each cluster as compiled from the literature by MG03, to *predict* an intrinsic  $(B - V)_0$  color for every object here. Observed  $(B - V)$  colors from the aperture-photometry literature listed in Table 3 then imply reddenings  $E(B - V)$ , and extinctions  $A_V = 3.1 E(B - V)$  follow. More details of this procedure are given in §3, where we also use population-synthesis models to produce estimates of cluster mass-to-light ratios. In the next subsection, we first briefly describe some points related to our handling of the Trager, King, & Djorgovski (1995) catalogue data for Milky Way globular clusters.

## 2.2. Milky Way Globular Clusters

As was mentioned above, Trager, King, & Djorgovski (1995) have already taken steps, similar to those we have outlined above and applied to LMC, SMC, and Fornax clusters, to combine heterogeneous data into unique, calibrated *V*-band SB profiles for 124 Galactic globular clusters. However, their results as published do not include any estimates of uncertainty in the individual surface-brightness points. The profiles defined above for the MG03 cluster sample *do* include errorbars, and we use these during our model fitting in §4 to estimate the uncertainties in all basic and derived physical parameters of the clusters, via a standard analysis of  $\chi^2$  variations over grids of model fits. We would like to proceed in the same way with the Milky Way GC sample, and thus we

have attempted to estimate errorbars for the  $\mu_V$  values given by Trager, King, & Djorgovski (1995).

In lieu of absolute errorbars, Trager, King, & Djorgovski give each point in their brightness profiles a relative weight  $w_i \in [0, 1]$ . As they discuss, these weights were assigned “by eye” to reflect the authors’ judgement of the overall quality of the source dataset. They are therefore not connected rigorously to relative errors, and their precise meaning is left somewhat open to interpretation. Initially, we proceeded under the natural assumption that the weights were proportional to the inverse square of the surface-brightness uncertainties, or  $\sigma_i \propto 1/\sqrt{w_i}$ . When fitting models by minimizing an error-weighted  $\chi^2$  statistic, this led to some cases where the best-fit model parameters were unduly influenced by just a few discrepant points with low weights from Trager, King, & Djorgovski. Thus, we decided instead to de-weight such points even further by adopting the heuristic prescription that the relative surface-brightness errorbars grow as  $\sigma_i \propto 1/w_i$ .

Given this choice, we estimated the uncertainties as follows. Trager, King, & Djorgovski (1995) also tabulate the value at each radius in each cluster, of interpolating (Chebyshev) polynomials that provide reasonably accurate, model-independent approximations to the overall SB profile. We assume that the reduced  $\chi^2$  per degree of freedom for these polynomial fits is exactly 1 for every cluster. Typically, the polynomials fit by Trager, King, & Djorgovski are of third order, so for a surface-brightness profile with  $N$  datapoints there are  $N - 4$  degrees of freedom. Then, with our prescription  $\sigma_i \equiv \sigma_\mu/w_i$ , where  $\sigma_\mu$  is a different constant for each GC, and writing  $C(R_i)$  for the value of the polynomial fit at each radius  $R_i$  in any one cluster, we have that  $\frac{1}{N-4} \sum_{i=1}^N (w_i^2/\sigma_\mu^2) [C(R_i) - \mu_V(R_i)]^2 = 1$ . We have solved this

TABLE 6  
BASE ERRORBARS ASSIGNED TO MILKY WAY GLOBULAR-CLUSTER SURFACE  
BRIGHTNESSES IN CATALOGUE OF TRAGER ET AL. (1995)

Cluster	$\sigma_\mu$	Cluster	$\sigma_\mu$	Cluster	$\sigma_\mu$	Cluster	$\sigma_\mu$
AM1	0.300	NGC5986	0.081	NGC6397	0.199	NGC6752	0.173
ARP2	0.200	NGC6093	0.171	NGC6401	0.119	NGC6760	0.207
HP	0.248	NGC6101	0.182	NGC6402	0.137	NGC6779	0.207
IC1276	0.259	NGC6121	0.180	NGC6426	0.238	NGC6809	0.197
IC4499	0.218	NGC6139	0.136	NGC6440	0.110	NGC6864	0.138
NGC104	0.082	NGC6144	0.155	NGC6441	0.076	NGC6934	0.173
NGC1261	0.187	NGC6171	0.143	NGC6453	0.150	NGC6981	0.223
NGC1851	0.249	NGC6205	0.128	NGC6496	0.307	NGC7006	0.165
NGC1904	0.094	NGC6218	0.182	NGC6517	0.098	NGC7078	0.178
NGC2298	0.147	NGC6229	0.151	NGC6522	0.140	NGC7089	0.107
NGC2419	0.120	NGC6235	0.188	NGC6528	0.283	NGC7099	0.115
NGC2808	0.124	NGC6254	0.137	NGC6535	0.348	NGC7492	0.253
NGC288	0.158	NGC6256	0.197	NGC6539	0.235	PAL1	0.202
NGC3201	0.206	NGC6266	0.126	NGC6541	0.201	PAL10	0.075
NGC362	0.097	NGC6273	0.124	NGC6544	0.205	PAL11	0.220
NGC4147	0.242	NGC6284	0.122	NGC6553	0.162	PAL12	0.395
NGC4372	0.428	NGC6287	0.158	NGC6558	0.117	PAL13	0.454
NGC4590	0.176	NGC6293	0.146	NGC6569	0.240	PAL14	0.140
NGC5024	0.153	NGC6304	0.148	NGC6584	0.148	PAL2	0.359
NGC5053	0.244	NGC6316	0.139	NGC6624	0.130	PAL3	0.120
NGC5139	0.142	NGC6325	0.162	NGC6626	0.137	PAL4	0.129
NGC5272	0.191	NGC6333	0.169	NGC6637	0.093	PAL5	0.190
NGC5286	0.128	NGC6341	0.119	NGC6638	0.111	PAL6	0.098
NGC5466	0.120	NGC6342	0.165	NGC6642	0.140	PAL8	0.220
NGC5634	0.220	NGC6352	0.269	NGC6652	0.190	TERZAN1	0.142
NGC5694	0.120	NGC6355	0.152	NGC6656	0.173	TERZAN2	0.157
NGC5824	0.106	NGC6356	0.074	NGC6681	0.186	TERZAN5	0.129
NGC5897	0.118	NGC6362	0.136	NGC6712	0.218	TERZAN6	0.099
NGC5904	0.104	NGC6366	0.217	NGC6715	0.117	TERZAN7	0.236
NGC5927	0.089	NGC6380	0.173	NGC6717	0.215	TERZAN9	0.128
NGC5946	0.136	NGC6388	0.101	NGC6723	0.212	TON2	0.162

NOTE. —  $\sigma_\mu$  is a constant for each Galactic globular cluster in the catalogue of Trager, King, & Djorgovski (1995), used to estimate errorbars on individual surface-brightness datapoints. Given a relative weight  $w_i$  ( $0 \leq w_i \leq 1$ ) from Trager et al. for each datapoint in a cluster, we define the uncertainty in  $\mu_V$  to be  $\sigma_i \equiv \sigma_\mu / w_i$ .

identity for the “base” errorbar  $\sigma_\mu$  of each of the 124 clusters in the collection of Trager, King, & Djorgovski (1995), and reported the results in Table 6. Again, the uncertainty in  $\mu_V$  at any single radius  $R_i$  in any one cluster is taken as  $\sigma_\mu / w_i$ , assumed to be symmetric about the measured surface brightness.

For two globular clusters—Palomar 10 and Terzan 7—Trager et al. only present uncalibrated surface brightnesses,  $\mu_V$  profiles relative to an unknown central value. Subsequently, the central brightnesses of these objects have been determined, and they are tabulated in the catalogue of Harris (1996):  $\mu_{V,0} = 22.12$  for Palomar 10, and  $\mu_{V,0} = 20.69$  for Terzan 7. We have used these values as zeropoint “corrections” to the Trager et al. data, and treated them subsequently in the same fashion as our zeropoint shifts to all of the Mackey & Gilmore LMC/SMC/Fornax cluster surface brightnesses.

Aside from these two small points, we have proceeded with modeling the Trager et al. data as published, with no further embellishments nor any attempted updates. There are another 26 globular clusters included in the more recent catalogue of Harris (1996), but we have not made any attempt to model their density structures: the raw profiles of these additional clusters have not been gathered into a uniform collection on par with the Trager et al. database, and indeed many of them are rather obscure and not studied well enough for our purposes in the first place. For completeness, we list them in Table 7 as objects that we have not fit with structural models in

§4. We do, however, include most of them in the population-synthesis modeling of §3, since only estimates of their metallicities are required there.

We originally attempted to fit all 124 globulars from Trager, King, & Djorgovski (1995) with the variety of models that we also fit to the massive clusters in the Magellanic Clouds and Fornax. In doing so we found that for several clusters the effective (projected half-light) radius  $R_h$  returned by the fits was of order or larger than the projected radius  $R_{\text{last}}$  of the outermost SB datapoint tabulated by Trager et al. In particular, there are 34 GCs for which  $R_h / R_{\text{last}} > 0.9$ , signifying either that the observations are too sparse to significantly constrain important aspects of the models, or that the models we fit are simply poor descriptions of the data. In fact, these 34 objects include a majority of those designated as core-collapse or “possible” core-collapse candidates by Trager, King, & Djorgovski (1995), and subsequently in the catalogues of Djorgovski (1993) and Harris (1996). As Trager et al. make very clear, their own estimation of King (1966) model parameters for such globulars are essentially rough guesses and not quantitatively trustworthy. Our fits to the 34 GCs with  $R_h / R_{\text{last}} > 0.9$  are likewise rather uncertain, and we do not present any detailed results for them in §4 and later sections. Again, however, we name the clusters in Table 7 for completeness, and we include them in the population-synthesis analysis that we describe next.<sup>3</sup> After making this

<sup>3</sup> In §4.3.2 it will be seen that there are also 4 LMC clusters in the MG03

TABLE 7  
MILKY WAY GLOBULAR CLUSTERS NOT FIT BY STRUCTURAL MODELS

Reason	Clusters
Clusters in Harris (1996) but not in Trager, King, & Djorgovski (1995)	1636–283; 2MS–GC01, GC02; AM4; BH176; DJORG 1, 2; E 3; ERIDANUS; ESO–SC06; IC 1257; LILLER 1; LYNKA 7; NGC 4833, 6540, 6749, 6838; PAL 15; PYXIS; RUP 106; TERZAN 3, 4, 8, 10, 12; UKS 1
Clusters in Trager, King, & Djorgovski (1995) with large fitted $R_h$ (see text)	NGC 4372, 5927, 5946, 6144, 6256, 6284, 6293, 6304, 6325, 6342, 6352, 6355, 6380, 6401, 6426, 6453, 6517, 6522, 6544, 6558, 6624, 6626, 6642, 6717; HP; PAL 6, 8, 13; TERZAN 1, 2, 5, 6, 9; TON 2
Core-collapsed clusters	NGC 6397, 6681, 6752, 7078, 7099

cut, five other core-collapsed globulars remain in the Trager et al. sample. These are known a priori not to be properly described by King models (or others with constant-density cores) and so we remove them as well from consideration for structural modeling, but list them in Table 7 and include them in our population-synthesis modeling.

### 3. POPULATION-SYNTHESIS MODELS: REDDENINGS AND MASS-TO-LIGHT RATIOS

Before proceeding with the structural and dynamical modeling of the clusters in our Magellanic Cloud, Fornax, and Milky Way sample, we discuss some aspects of population-synthesis modeling. We have folded this into our derivation of physical cluster parameters from model fits to the cluster SB distributions. There are two main issues at hand that necessitate these considerations:

First, in order to move from a description of the observed surface brightness profile of a cluster to one of the true luminosity density profile, we need information on the extinction towards the cluster. For each of the Milky Way globular clusters that we model, an estimate of the foreground reddening  $E(B-V)$  is available in the catalogue of Harris (1996); the extinction follows directly, and the required corrections are straightforward. The same is true of the globulars in Fornax; Mackey & Gilmore (2003c), for example, have tabulated measurements from the literature of the reddenings  $E(B-V)$  of each cluster. But, as was mentioned above, there is no such information in the literature for many of the 63 LMC and SMC clusters being analyzed here. Aperture measurements (ground-based) of the clusters’  $(B-V)_{\text{ap}}$  colors do exist, however (see the references in Table 3), as do individual estimates of their ages and metallicities (compiled from the literature, again, by Mackey & Gilmore 2003a,b). We therefore use the cluster ages and  $[\text{Fe}/\text{H}]$  values to derive an expected intrinsic  $(B-V)_0$  from population-synthesis models, and then  $E(B-V) = (B-V)_{\text{ap}} - (B-V)_0$  and  $A_V = 3.1 E(B-V)$ . The fact that direct reddening measurements do exist for the Milky Way and Fornax globular clusters allows us to perform the same analysis on them, and then compare our “theoretical”  $E(B-V)$  values to the known ones—a valuable check on the method, albeit only in the extreme of old ages.

Second, to go from a description of the de-reddened luminosity density profile of a cluster to its *mass* density dis-

tribution, knowledge of an average mass-to-light ratio is required. Given a sample of clusters of a roughly common age (and a common stellar IMF), the mass-to-light ratio typically can also be treated as roughly constant, at least to within a factor of order unity which depends on  $[\text{Fe}/\text{H}]$  differences. Luminosity differences are then essentially proportional to mass differences, and detailed knowledge of the exact mass-to-light ratio is not critical to the accurate discernment of relative trends in physical cluster properties (such as mass-radius, mass-velocity dispersion, or other fundamental-plane correlations). In our case, however, we aim ultimately to compare these sorts of correlations for the old globular clusters in the Milky Way and other galaxies (ages  $\tau \sim 13$  Gyr for the most part), against those for the much younger massive clusters in the Magellanic Clouds ( $\tau < 10^9$  yr and as young as  $\tau \simeq 3 \times 10^6$  yr for R136=30 Doradus). Trends or correlations in luminosity then reflect a complex mix of age and mass effects which must be separated to make sense of the physical situation. Ideally, we would have liked to use measurements of the stellar velocity dispersions in the clusters to compute their mass-to-light ratios directly; but, as for the reddenings, such measurements exist for only a handful of the young LMC/SMC clusters, and they tend to be highly uncertain. Even in the Milky Way globular cluster system, reliable velocity-dispersion measurements and dynamical  $M/L$  ratios exist for fewer than half of the 85 clusters that we model here. Therefore, we also use population-synthesis models to define a  $V$ -band mass-to-light ratio for every cluster in our total sample. In §5 we compare these predicted values with the dynamical mass-to-light ratios that can be computed for the minority of (mostly old) clusters with measured velocity dispersions.

The population-synthesis model that we have chosen to use to derive cluster reddenings and mass-to-light ratios is that of Bruzual & Charlot (2003), using the Padova 1994 stellar-evolution tracks and assuming a stellar IMF following that of Chabrier (2003) for the Galactic disk population. The results are presented in §3.2. However, since they are so central to the establishment of all final, physical (mass-based) cluster properties and to the definition of systematic interdependencies between these properties, we have also carried through the full suite of calculations with the alternate population-synthesis code PÉGASE (Fioc & Rocca-Volmerange 1997, version 2.0) and under different assumptions on the form of the stellar IMF. In §3.1, then, we first present point-by-point comparisons between the  $E(B-V)$  and  $\Upsilon_V \equiv M/L_V$  values predicted by various combinations of codes and IMFs. Note, however, that we *always* assume that every clus-

sample which have  $R_h/R_{\text{last}} > 1$  and particularly uncertain fit extrapolations. In these cases, however, this is because the clusters have rather large cores rather than any hint of a post-collapse morphology. Given this, and the fact that they have not been fully modeled before, we do report all of our results for these objects.

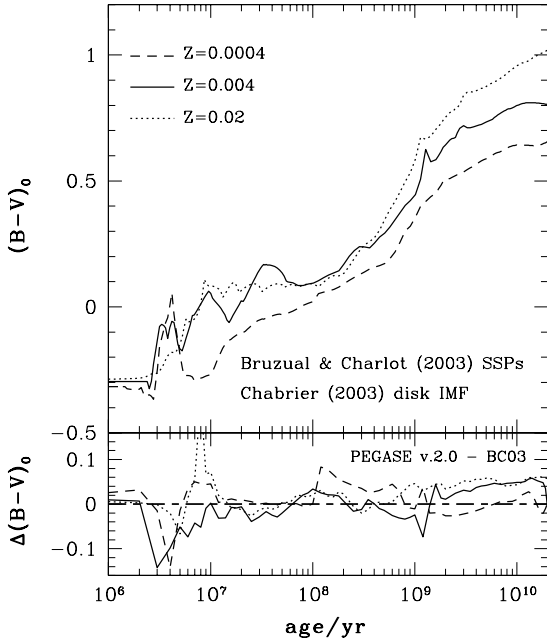


FIG. 3.— *Top panel:* Intrinsic color as a function of age for single-burst stellar populations of three different metallicities, as predicted by the population-synthesis code of Bruzual & Charlot (2003) assuming the disk-star IMF of Chabrier (2003). *Bottom panel:* Difference in  $(B-V)_0$  for the same model clusters as predicted by the PÉGASE (v.2.0) population-synthesis code of Fioc & Rocca-Volmerange (1997).

ter is a single-age population formed instantaneously in one coherent burst of star formation, and that all clusters, of any age or metallicity in any galaxy, share a common stellar IMF. Also, both Bruzual & Charlot (2003) and Fioc & Rocca-Volmerange (1997) have coded prescriptions for mass loss over time due to stellar-evolution debris (from winds and supernovae, essentially) that is assumed to be swept out of a cluster. When using either code, we always employ these prescriptions.

### 3.1. Comparison of Codes and Stellar IMFs

The Chabrier (2003) disk-star IMF that we adopt for our primary calculations is a Salpeter (1955) power law ( $dN/dm \propto m^{-2.35}$ ) for stellar masses  $m \geq 1 M_\odot$ , and a much flatter, lognormal distribution below  $m \leq 1 M_\odot$ . Figures 3 and 4 show, in their larger (upper) panels, the intrinsic colors  $(B-V)_0$  and V-band mass-to-light ratios  $\Upsilon_V$  predicted by the Bruzual & Charlot (2003) code for a single-burst (or “simple”) stellar population with this IMF, as functions of cluster age for three set heavy-element abundances roughly spanning the range appropriate for our combined sample of globular and young massive clusters. The smaller (bottom) panels in these figures show the *differences* in  $(B-V)_0$  and  $\log \Upsilon_V$  as predicted by the PÉGASE code of Fioc & Rocca-Volmerange (1997) given the same IMF and the same metallicities. Aside from the problematic region around ages  $10^6 \lesssim \tau \lesssim 10^7$  yr, there is generally good agreement between the two codes.

Figure 5 expands somewhat on these plots, showing  $(B-V)_0$  and  $\Upsilon_V$  predicted as functions of cluster  $[\text{Fe}/\text{H}]$  at various ages, all for a Chabrier (2003) disk IMF. The logarithm of cluster age is labeled in the upper panel of each pair

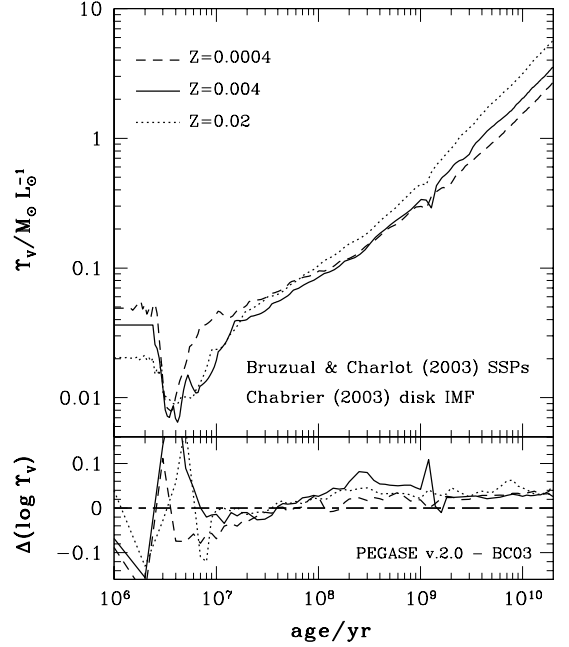


FIG. 4.— *Top panel:* V-band mass-to-light ratio as a function of age for single-burst stellar populations of three different metallicities, as predicted by the population-synthesis code of Bruzual & Charlot (2003) assuming the disk-star IMF of Chabrier (2003). *Bottom panel:* Difference in  $\log \Upsilon_V$  for the same model clusters as predicted by the PÉGASE (v.2.0) population-synthesis code of Fioc & Rocca-Volmerange (1997). Both codes allow for mass loss from the clusters due to the evacuation of stellar-wind and supernova debris over time. This amounts to a  $\sim 30\%$  reduction in total cluster mass after a Hubble time.

in this figure. Filled circles are the quantities predicted by Bruzual & Charlot (2003) at the six metallicities for which their code has stellar-evolution tracks. The solid curve joining these points is a spline interpolation, which we use to infer  $(B-V)_0$  and  $\Upsilon_V$  for clusters with metallicities between the few that are explicitly calculable (at any age) with the Bruzual-Charlot code. The open squares in every panel are the synthetic colors and mass-to-light ratios predicted by PÉGASE v.2.0, again at the six metallicities for which that code has explicit stellar-evolution tracks (these metallicities, and indeed the tracks themselves, are the same as those used by Bruzual & Charlot). The dashed lines joining the squares are linear interpolations for determining quantities at intermediate  $[\text{Fe}/\text{H}]$ . (The PÉGASE code does this interpolation internally, given any arbitrary  $[\text{Fe}/\text{H}]$  specified by the user.)

More detailed discussion of the comparison between the PÉGASE and Bruzual-Charlot codes—including the difficulties at young ages  $\tau < 10^7$  years, which fortunately are not relevant to us in general—may be found in Bruzual & Charlot (2003). The plots we have presented have vertical-axis scales chosen deliberately to emphasize the differences between the codes for one IMF. Evidently, although there are some exceptions, these differences are generally slight: at the level of  $\lesssim 0.05$  mag in  $(B-V)_0$  and  $\lesssim 10\%$  in  $\Upsilon_V$ . Again, we have adopted the Bruzual & Charlot code to define the intrinsic colors and mass-to-light ratios for our clusters, and we can proceed with some confidence that this choice is not introducing sizeable systematic errors in our subsequent analyses.

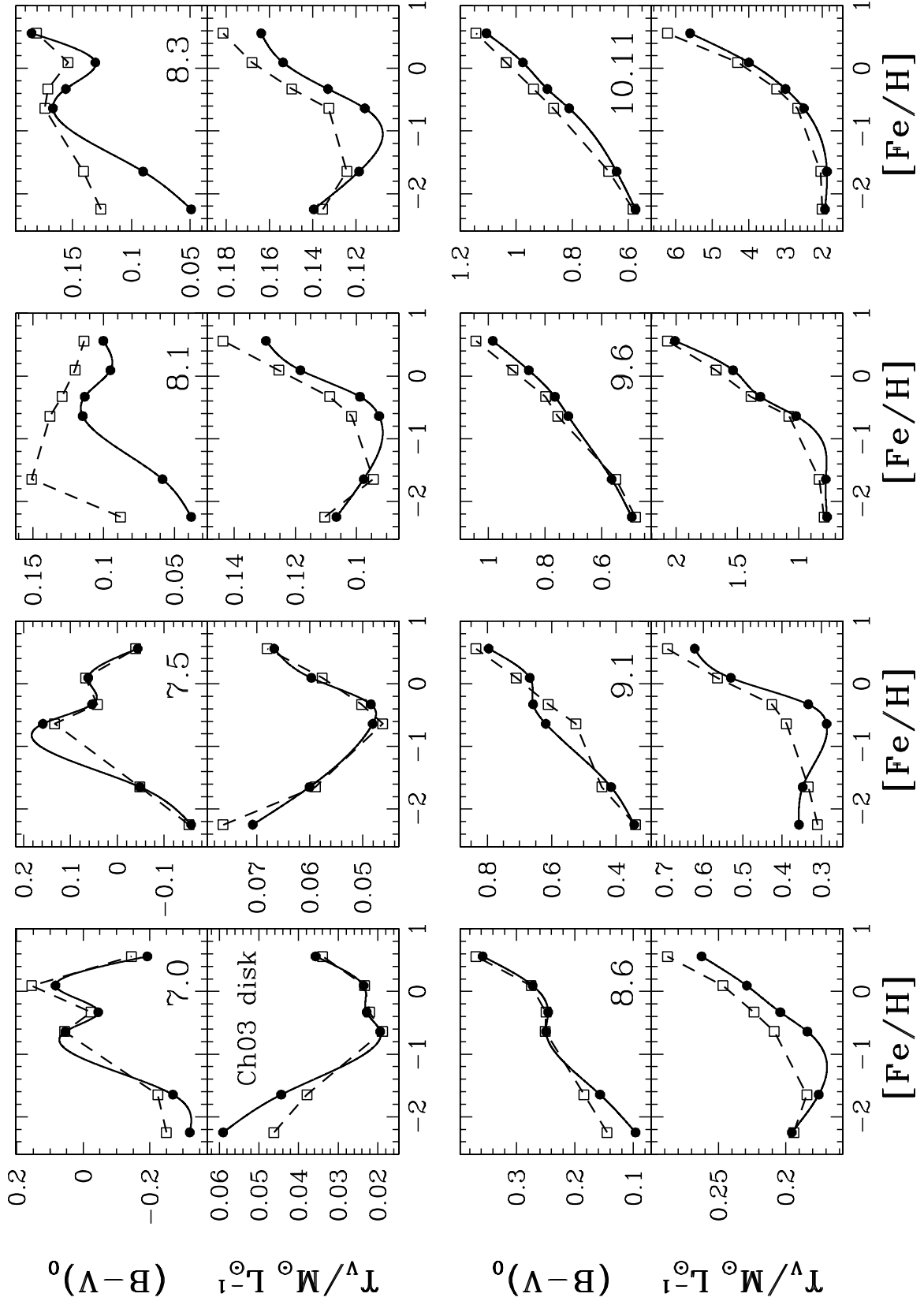


FIG. 5.— Intrinsic  $(B-V)$  colors and V-band mass-to-light ratios as functions of metallicity for single-burst stellar populations at a range of fixed ages. Filled circles and solid lines in every panel refer to predictions from the population-synthesis code of Bruzual & Charlot (2003); open squares and dashed lines refer to predictions from the code of Fioc & Rocca-Volmerange (1997, PÉGASE v.2.0). The logarithm of the cluster age is given in the upper  $(B-V)_0$  panel of each pair. All calculations employ the disk-star IMF of Chabrier (2003).

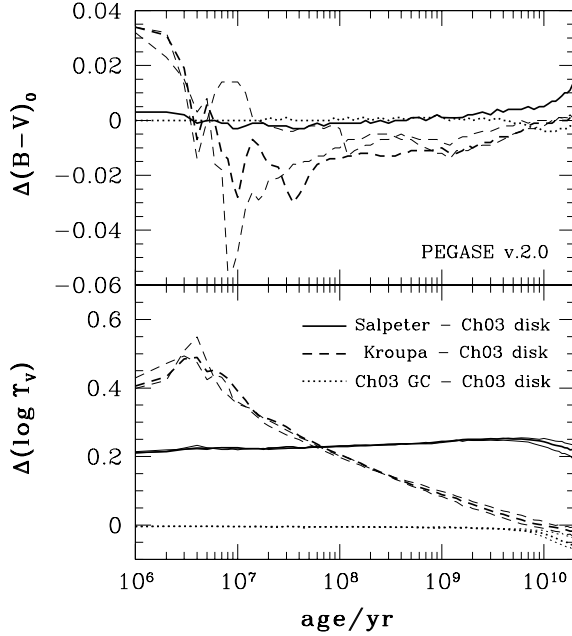


FIG. 6.— *Top panel:* IMF dependence of intrinsic color  $(B-V)_0$  of a single-burst stellar population in the population-synthesis code PÉGASE (v.2.0) (Fioc & Rocca-Volmerange 1997). *Bottom panel:* IMF dependence of the logarithm of V-band mass-to-light ratio  $\log \Upsilon_V$  in the PÉGASE code. Results are shown as differences of the computed quantities using the various IMFs indicated, minus the “reference” values obtained with a Chabrier (2003) disk-star IMF. Bold lines show the differences as functions of cluster age for a metal abundance  $Z = 0.004 = 0.2Z_\odot$ ; lighter lines, when shown, correspond to  $Z = 0.0004$  and  $Z = 0.02$ .

The next question concerns the implications of our choice of the Chabrier (2003) disk-star IMF for the population-synthesis calculations. The Bruzual-Charlot code offers only the choice between this option or a pure Salpeter (1955) power law at all stellar masses (which is well known by now to be an incorrect description of the true IMF below  $\sim 1 M_\odot$ , but is still commonly used for reference calculations). By contrast, the PÉGASE code of Fioc & Rocca-Volmerange can produce models for any user-defined IMF. We have therefore used PÉGASE to calculate  $(B-V)_0$  and  $\Upsilon_V$  as functions of age for clusters of three different metal abundances ( $Z = 0.0004$ ,  $Z = 0.004$ , and  $Z = 0.02$ , as in Figs. 3 and 4), given three stellar IMFs besides our preferred Chabrier (2003) disk-star distribution.

The alternate IMFs that we have examined are those of Salpeter (1955) (a single power law,  $dN/dm \propto m^{-2.35}$  at all masses); Kroupa, Tout, & Gilmore (1993) (a three-part piecewise power law which, with  $dN/dm \propto m^{-2.7}$  above  $m > 1 M_\odot$ , is significantly steeper than either Salpeter or Chabrier at high masses, but significantly shallower than Salpeter—and not substantially different from Chabrier’s disk IMF—at lower masses); and the “globular cluster” IMF of Chabrier (2003) (which is nearly the same as his disk-star IMF but for a somewhat narrower and displaced lognormal peak below  $1 M_\odot$ ). Figure 6 shows the differences in the predicted  $(B-V)_0$  and logarithmic  $\Upsilon_V$  predicted by PÉGASE for these IMFs vs. the Chabrier (2003) disk-star function.

The bold solid lines in both panels of Figure 6 compare

the Chabrier disk and Salpeter (1955) IMFs; the bold dashed lines, the Chabrier disk and Kroupa, Tout, & Gilmore (1993) IMFs; and the bold dotted lines, the Chabrier disk and “globular cluster” IMFs. All of these bold lines correspond to a cluster metal abundance  $Z = 0.004 = 0.2Z_\odot$ ; the thinner lines around them refer to  $Z = 0.0004 = 0.02Z_\odot$  and  $Z = 0.02 = Z_\odot$  (for clarity, in the upper panel the lines for different metallicities are only shown for the Chabrier disk vs. Kroupa et al. IMF comparison). Clearly, the choice of IMF has little bearing on the intrinsic  $(B-V)_0$  color of a cluster at a given age, with changes of less than a few hundredths of a magnitude—within the differences between the PÉGASE and Bruzual-Charlot codes—typically being implied. Given that the color is the ratio of the total cluster luminosity in two bandpasses, and the two codes employ essentially identical treatments of stellar evolution, its robustness against even major changes in the IMF is expected.

The V-band mass-to-light ratio is, however, naturally more sensitive to details of the IMF. The Salpeter IMF gives  $\Upsilon_V$  consistently higher than the Chabrier disk IMF (by factors of  $\sim 60\% - 75\%$ ), because of the much higher proportion of the total cluster mass that the former distribution places in very faint, low-mass stars. As we mentioned just above, however, it is known that the Salpeter IMF is not a good description of the real distribution at low stellar masses (see, e.g., Chabrier 2003). The difference in  $\Upsilon_V$  between Chabrier’s disk and “globular cluster” IMFs is essentially negligible until very old ages, where the GC IMF would predict slightly lower mass-to-light ratios. This is because the two IMFs are identical at stellar masses  $m \gtrsim 1 M_\odot$ , where both take on the Salpeter power-law shape. It is only after these relatively massive stars have all evolved significantly that the slight difference between the two IMFs at lower stellar masses has a measurable effect. Even then the effect is small, however, and in any case Chabrier’s disk IMF is better constrained empirically than his GC IMF—both arguments for our use of the disk-star IMF to make predictions for all of our clusters, GCs as well as the massive young objects in the LMC and SMC.

By contrast, the difference between  $\Upsilon_V$  as computed for the Chabrier (2003) disk IMF vs. the Kroupa, Tout, & Gilmore (1993) IMF is rather dramatic and, more worrisome, varies systematically with cluster age. This is a direct result of the much steeper slope specified by the Kroupa et al. IMF for stellar masses above  $1 M_\odot$ . For a given total cluster mass, the Kroupa et al. model initially puts a much smaller fraction into massive (and bright) stars, yielding significantly higher mass-to-light ratios at young ages. Over time,  $\Upsilon_V$  for the Kroupa et al. IMF approaches  $\Upsilon_V$  for the Chabrier IMF, because the two IMFs are effectively the same at stellar masses  $m \lesssim 1 M_\odot$ —which, of course, contribute all the cluster light at ages of 10 Gyr and more.

Clearly, the choice between these two IMFs has a direct impact on the mass-to-light ratios and all dependent physical parameters of clusters younger than  $\tau \lesssim 10^{10}$  yr—which is to say, all of the young LMC and SMC clusters that we model. In principle, given the strong systematics in the bottom panel of Fig. 6, choosing between these two particular IMFs might even influence the ultimate inference of correlations between (mass-based) cluster properties. We much prefer the Chabrier (2003) disk-star IMF, which has stronger and more recent empirical support than the older Kroupa et al. function. But it is important to note that Mackey & Gilmore (2003a,b,c) adopted the Kroupa et

al. IMF for their own population-synthesis modeling. *Our estimates below of the young LMC/SMC cluster mass-to-light ratios therefore differ significantly from those presented by Mackey & Gilmore.* However, the lower  $\Upsilon_V$  implied by our choice of IMF combines with our generally brighter  $V$ -band surface-brightness scale (§2.1) to produce cluster masses and mass densities that often differ less strongly from those in MG03.

### 3.2. Results for our Cluster Sample

Table 8 (a sample of which can be found at the end of this preprint, and which can be downloaded in full from the electronic edition of the *Astrophysical Journal Supplement Series*) presents in full the results of our population-synthesis modeling of the 53 LMC clusters, 10 SMC clusters, and 5 Fornax globular clusters in the combined MG03 database, as well as for 148 Galactic globular clusters with  $[\text{Fe}/\text{H}]$  values given in the catalogue of Harris (1996) (that is, 58 GCs in addition to the 90 that we fit with structural models in §4). In every case, to predict an intrinsic  $(B-V)_0$  color and average (global)  $\Upsilon_V$  ratio, we require only an estimate of the cluster age and metallicity. In the LMC, SMC, and Fornax cases, these quantities have been either derived or recovered from the literature by MG03, and we have generally taken their tabulated values, with the single exception that we assign an age of  $\tau = 13 \pm 2$  Gyr ( $\log \tau = 10.11 \pm 0.07$ ) to every cluster that they list as older than 13 Gyr. In the Milky Way, we have taken  $[\text{Fe}/\text{H}]$  from the Harris (1996) catalogue, and assigned a single age of  $13 \pm 2$  Gyr to all clusters. (Although an age spread of a few Gyr is known to exist in the Galactic GC system, at such an old average age this makes little difference in the population-synthesis colors and mass-to-light ratios; see Figs. 3 and 4.) The second and third columns of Table 8 list these ages and metallicities. Column 4 gives the observed  $(B-V)$  color of the cluster whenever such a measurement exists (taken either from the aperture-photometry sources in Table 3 above, or from Harris 1996, for the Milky Way globulars)). The rest of the two lines for each cluster list the intrinsic colors and  $M/L_V$  ratios obtained from each of six combinations of two population-synthesis codes and four stellar IMFs discussed in §3.1. It is column (6) of Table 8—the combination of Bruzual & Charlot (2003) model with Chabrier (2003) disk-star IMF—that we draw on for all cluster modeling that follows. All uncertainties on the population-synthesis quantities in Table 8 follow directly from uncertainties in the cluster ages and  $[\text{Fe}/\text{H}]$  values (for which errorbars are cited by MG03 or Harris 1996, but not reproduced here).

We are not aware of any previous, comprehensive calculation of theoretical mass-to-light ratios for Galactic globular clusters. In Fig. 7 we show the distribution of population-synthesis  $\Upsilon_V$  values for the Milky Way GC system, taken from Column (6) of Table 8. Note the strong concentration of clusters at  $\Upsilon_V^{\text{pop}} \simeq 1.9 M_\odot L_{\odot,V}^{-1}$ , which is to be compared to the average *dynamically determined* ( $\Upsilon_V^{\text{dyn}} = 1.45 M_\odot L_{\odot,V}^{-1}$ ) for a much smaller sample of clusters (McLaughlin 2000). The tail towards higher  $\Upsilon_V^{\text{pop}}$  values in Fig. 7 is a direct reflection of the metal-rich (bulge-cluster) tail in the distribution of GC metallicities in the Galaxy. A more detailed, cluster-by-cluster comparison of population-synthesis and dynamically-measured mass-to-light ratios is given in §5 below, following the bulk of our model fitting in §4.

In the top panel of Fig. 8, we compare our adopted population-synthesis mass-to-light ratios for the

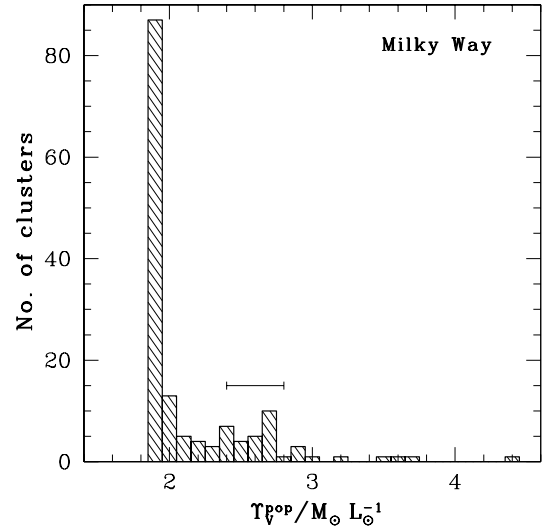


FIG. 7.—  $V$ -band mass-to-light ratios of 148 Galactic globular clusters as predicted by the population-synthesis code of Bruzual & Charlot (2003) using the disk-star IMF of Chabrier (2003). Values for individual objects are in Column (6) of Table 8. A common age of  $13 \pm 2$  Gyr has been assumed for all clusters, so that the spread in  $\Upsilon_V^{\text{pop}}$  directly reflects the metallicity distribution of Galactic GCs given  $[\text{Fe}/\text{H}]$  values taken from Harris (1996). The horizontal errorbar shows the rms uncertainty in the predicted  $\Upsilon_V^{\text{pop}}$ .

LMC+SMC+Fornax cluster sample, with those computed by Mackey & Gilmore (2003a,b,c). Ours are always lower than theirs, in part because of the much steeper stellar IMF that MG03 assumed—as discussed in §3.1—and in part because they appear not to have allowed for the loss of cluster mass through massive-star ejecta in their application of the PÉGASe model (a  $\sim 30\%$  cumulative effect over a Hubble time, in either the Bruzual-Charlot or Fioc & Rocca-Volmerange codes). Further still, MG03 give the ages of some of their oldest LMC clusters—the genuine globulars there—as greater than 13 Gyr, but we have fixed such ages at  $\tau = 13 \pm 2$  Gyr, resulting again in lower  $\Upsilon_V^{\text{pop}}$  ratios. We note in passing that the leftmost point in this plot—the cluster with the lowest mass-to-light ratio in MG03, and the largest errorbar in our own assessment—is R136=30 Doradus, which at  $\tau \simeq 3 \times 10^6$  yr is the youngest cluster in our entire sample and the one most susceptible to uncertainties in the current population-synthesis models.

Finally, the bottom panel of Fig. 8 plots the difference between our population-synthesis derived  $E(B-V) = [(B-V) - (B-V)_0]$ —that is, the difference of Columns (4) and (6) in Table 8—and the published reddenings for individual clusters in the LMC, SMC, Fornax, and the Milky Way. This plot is dominated by the Galactic GC sample, where the published  $E(B-V)$  are those from Harris (1996). These are generally in very good agreement with our model calculations; the strongest outliers are Palomar 6 and Terzan 5, which have large  $E(B-V) = 1.46$  and  $2.15$ , respectively. This reflects well both on the calibration of the population-synthesis models against old, single-burst stellar populations and on the quality of the reddening estimates in the Harris (1996) catalogue.



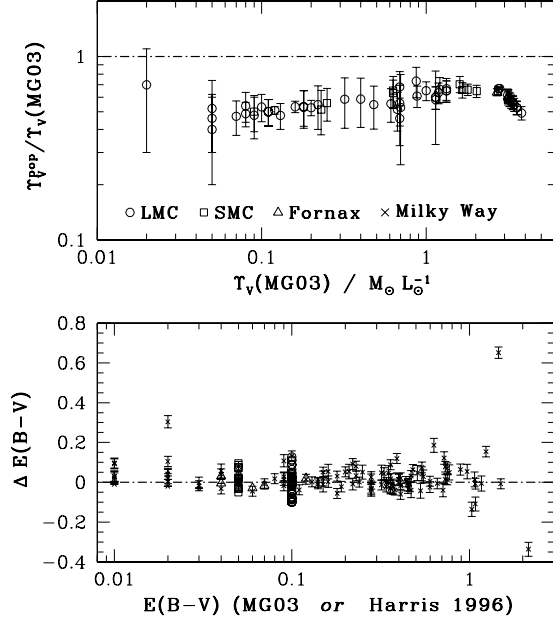


FIG. 8.— *Top panel:* Ratio of our computed population-synthesis  $V$ -band mass-to-light ratios for LMC, SMC, and Fornax clusters (from Column 6 of Table 8), to those calculated by Mackey & Gilmore (2003a,b,c). Our values are always lower because MG03 adopt a significantly steeper stellar IMF and do not account for gradual cluster mass loss from stellar-wind and supernova debris. *Bottom panel:* Difference of our computed population-synthesis reddening *minus* published reddenings for individual clusters in the LMC, SMC, Fornax, and the Milky Way. Reddenings of Fornax and Milky Way GCs are taken from the compilations of Mackey & Gilmore (2003c) and Harris (1996) and are largely based on CMD studies of individual clusters. Reddenings of LMC clusters are compared to an average  $\langle E(B-V) \rangle = 0.1$  assumed by Mackey & Gilmore (2003a), except for R136=30 Doradus. SMC reddenings are compared to an average  $\langle E(B-V) \rangle = 0.05$  assumed by Mackey & Gilmore (2003b).

The comparisons for the old Fornax globulars (with true measurements culled from the literature by Mackey & Gilmore 2003c) are likewise very favorable. In the LMC and SMC samples, the “published”  $E(B-V)$  used for comparison in Fig. 8 are generally the rough average values adopted by Mackey & Gilmore (2003a,b): a constant  $E(B-V) = 0.10$  mag in the LMC, and constant  $E(B-V) = 0.05$  mag in the SMC. It is encouraging that our more detailed modeling returns values clustered well around these reasonable averages. The one LMC cluster to which MG03 assign a non-average reddening is R136=30 Doradus, for which they quote  $E(B-V) = 0.38$  mag from the CMD analysis of Hunter et al. (1995). Our model value for 30 Dor is 0.407 mag.

In what follows, then, we make use of the population-synthesis  $E(B-V)$  values that we have derived for each LMC and SMC cluster to correct their observed surface brightnesses and magnitudes for extinction. There are two LMC clusters (SL-663 and SL-855) for which we were unable to find  $(B-V)$  colors in the literature to estimate their reddenings, so we simply assign to them the average (0.096) of the other LMC model  $E(B-V)$  values. This also happened for the SMC cluster NGC 361, to which we therefore assign the average (0.069) of the model results for the other SMC clusters. For the Fornax and Milky Way GC samples, we use the *measured*  $E(B-V)$  tabulated by Mackey & Gilmore (2003c) and Harris (1996) (see these papers for references to the orig-

inal determinations of the reddenings, most of which come from direct study of the cluster CMDs). For every cluster in all four galaxies we apply our population-synthesis  $T_V$  ratios whenever we need to convert between luminosity and mass.

#### 4. DYNAMICAL MODELS AND FITS

##### 4.1. Dynamical Models

We fit three types of model to each cluster:

First is the usual King (1966) single-mass, isotropic, modified isothermal sphere, which is defined by the stellar distribution function

$$f(E) \propto \begin{cases} \exp[-E/\sigma_0^2] - 1 & , E < 0 \\ 0 & , E \geq 0 \end{cases} \quad (1)$$

where  $E$  is the stellar energy. Under certain restrictive conditions, this formula roughly approximates a steady-state solution of the Fokker-Planck equation (e.g., King 1965). It has, of course, already been fit to all of the Galactic GCs in the surface-brightness profile database of Trager, King, & Djorgovski (1995), and more. These fits are the basis of the standard catalogues (Djorgovski 1993; Harris 1996) of globular cluster structural and dynamical properties. King (1966) models have also been fit to a number of old globular clusters in other galaxies, including the LMC, and a few younger Magellanic Cloud clusters; but a systematic and uniform comparison of these standard models against all of the high-quality profile data that we now have for the LMC, SMC, and Fornax clusters has not yet been made.

Second is a power law density profile with a core (also variously known as Moffat profiles, modified Hubble laws, or “Elson-Fall-Freeman” [EFF] profiles). With  $I(R)$  the luminosity surface density of a cluster, such that  $\mu = \text{constant} - 2.5 \log[I(R)/L_\odot \text{pc}^{-2}]$ , these models are defined by

$$I(R) = \frac{(\gamma-3)L_{\text{tot}}}{2\pi r_0^2} \left[ 1 + (R/r_0)^2 \right]^{-(\gamma-1)/2} \quad (2)$$

corresponding to a three-dimensional luminosity density profile  $j(r) \propto [1 + (r/r_0)^2]^{-\gamma/2}$ . Since the density is non-zero even as  $r \rightarrow \infty$ ,  $\gamma > 3$  is required if the integrated luminosity is to be finite. Equation (2) is strictly an ad hoc fitting function with no underlying basis in theory, but it is frequently fit to massive young clusters in the Magellanic Clouds and other galaxies, following the seminal work of Elson, Fall, & Freeman (1987) showing that King (1966) models cannot always account for the spatially extended halos of such objects. MG03 accordingly fit this model to all of the clusters in their sample—including the old globulars in the Clouds and the Fornax dwarf, and even a handful of Milky Way GCs (Mackey & Gilmore 2003c). However, equation (2) has not been fit to any modern surface-brightness data for large numbers of Galactic globulars such as we have at hand.

The physical parameters extracted for young massive clusters from fits of equation (2) by Elson, Fall, & Freeman (1987), MG03, and others (e.g., Larsen 2004) are generally confined to the central intensity  $I_0$ , the scale radius  $r_0$  (and perhaps an associated core radius  $R_c$  and/or effective radius  $R_h$ ), the power-law exponent  $\gamma$ , and the total luminosity  $L_{\text{tot}}$ . This small set of quantities falls well short of the wide array that has been calculated for King (1966) models, including relaxation times, central escape velocities, global binding energies, and more. A full comparison between the systemic properties of globular and other massive star clusters would

seem to require comparable levels of detail in the modeling of all objects, no matter what specific model is actually applied; and a clear understanding of how model-dependent are the values of the derived physical parameters is critical. These issues can only be tackled by completely fitting both of the model types just described to all of the clusters in all four galaxies of our sample.

Certainly a good reason why power-law models have not been fit systematically to Galactic globular clusters is that they lack the tidal cut-off radius so important to King (1966) models and obviously present in real GCs. We therefore expect a priori that the power-law models may provide poorer fits than King models to many globular cluster density profiles. Conversely, we already know for a fact (e.g., Elson, Fall, & Freeman 1987) that power laws provide better fits than King (1966) models to the outer envelopes of some young LMC clusters. We therefore wish also to fit all of our clusters with a third model which is intermediate between these two, one which can afford more extended halos than King (1966) models but still goes to zero density at a finite radius. Another reason to consider such an additional model is the original suggestion of Elson, Fall, & Freeman (1987) (see also the recent review of Schweizer 2004), that the power-law fits to some young LMC clusters represent unbound halos of stars around relatively recently formed systems that could be stripped away over Gyr timescales, leaving behind more standard King-type configurations. In assessing this idea, it is worthwhile to ask whether self-consistent, non-King models with extended but *bound* stellar halos are capable at all of describing these data.

The third model that we have fit is again based on a specified stellar distribution function, motivated by the work of Wilson (1975) on modeling elliptical galaxies:

$$f(E) \propto \begin{cases} \exp[-E/\sigma_0^2] - 1 + E/\sigma_0^2, & E < 0 \\ 0, & E \geq 0, \end{cases} \quad (3)$$

which is a different type of single-mass and isotropic modified isothermal sphere. Wilson (1975) included a multiplicative term in the distribution function depending on the angular momentum  $J_z$ , in order to create axisymmetric model galaxies. We have dropped this term from  $f(E)$  to make spherical and isotropic cluster models, but we still refer to equation (3) as Wilson's model. The connection with the King (1966) model in equation (1) is clear: the extra  $+E/\sigma_0^2$  in the first line of equation (3) is simply taking away the linear term in the Taylor series expansion of the fundamental  $\exp(-E/\sigma_0^2)$  near the zero-energy (tidal) boundary of the cluster. Although patently an ad hoc thing to do, the net effect of this more gradual lowering of the isothermal sphere is to produce clusters which are spatially more extended than King (1966) models, but still finite.

It will be noted that there is a slight asymmetry between equations (1) and (3) and equation (2): the former explicitly involve a velocity scale parameter  $\sigma_0$ , while the latter incorporates an explicit radial scale  $r_0$ . In the formulation of his model, King (1966) defined a radial scale associated with  $\sigma_0$ :

$$r_0^2 \equiv \frac{9\sigma_0^2}{4\pi G\rho_0}, \quad (4)$$

where  $\rho_0$  is the central mass density of the model. We adopt the same definition for our single-mass, isotropic Wilson models; and we use it also in our construction of power-law models to define a velocity scale  $\sigma_0$  in terms of  $r_0$  from

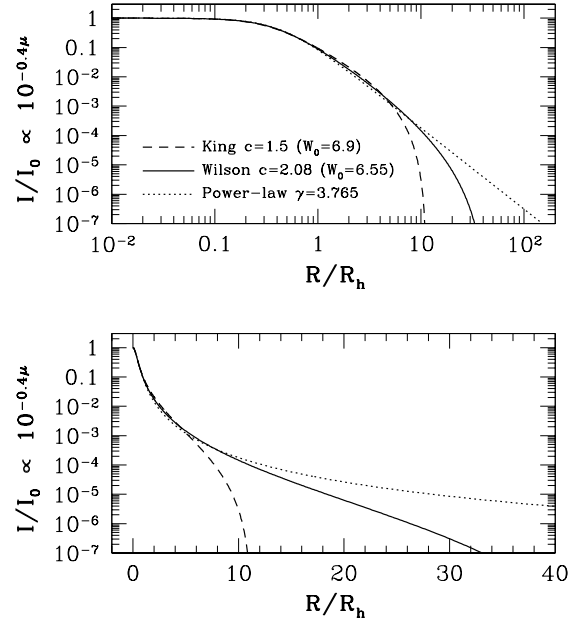


FIG. 9.— Comparison of the projected density/surface-brightness profiles of a single-mass King (1966) model cluster (dashed curves) defined by equation (1); a spherical and isotropic Wilson (1975) model (solid curves) defined by equation (3); and a cored power-law model (dotted curves) defined by equation (2). The three examples shown all have the same dimensionless total luminosity  $L_{\text{tot}}/I_0 R_h^2$ . *Top panel* is a log-log plot of the models highlighting their core structures; *bottom panel* is a log-linear representation emphasizing their halos. Structural differences between the models are most significant beyond a few projected half-light (effective) radii.

equation (2). It is important to recognize that  $r_0$  and  $\sigma_0$  are *not* equivalent, in general, to typically observed quantities such as a core (half-power) radius or central velocity dispersion—although the connections between the theoretical scales and these or other observables are straightforward to calculate for any member of these model families.

In their dimensionless form, King and Wilson models are characterized by the profiles of  $\rho/\rho_0$  and  $\sigma/\sigma_0$  as functions of  $r/r_0$ . Both profiles are fully specified by the value of the dimensionless central potential,  $W_0 \equiv -\phi(0)/\sigma_0^2 > 0$ . In principle  $W_0$  can take on any real value between 0 and  $\infty$ , with the latter limit corresponding to a regular isothermal sphere of infinite extent.  $W_0$  bears a one-to-one relationship with the more intuitive *concentration parameter*:  $c \equiv \log(r_t/r_0)$ , where  $r_t$  is the tidal radius of the model cluster [ $\rho(r_t) = 0$ ]. For more details of the relations between these model parameters, and of the construction of King models in general, see King (1966) or Binney & Tremaine (1987). We have essentially followed the prescription of Binney & Tremaine (1987)—with the obvious substitution of the distribution function  $f(E)$  in equation (3) for that in equation (1)—to compute Wilson models with arbitrary  $W_0$  or  $c$ . The result is normalized three-dimensional density and velocity-dispersion profiles, which are then projected onto the plane of the sky (using standard integrals that can also be found, e.g., in Binney & Tremaine 1987) for fitting to data.

Fixing  $W_0$  or  $c$  at some value essentially defines the overall shape of the internal density profile (and the velocity-dispersion profile) of a King or Wilson model. The anal-

ogous shape parameter for the cored power-law models of equation (2) is the index  $\gamma > 3$ , the exponent of the power law hypothesized to describe the asymptotic behavior of a cluster’s density distribution. Clearly in this case  $\gamma$  does not correspond to any measure of a tidal radius— $r_t$  is always infinite in these models—but it still has a one-to-one connection with the (finite) central potential of a cluster. Starting from equation (2) for the observable surface-density profile in these models, which is fitted directly to real cluster data, it is a simple matter to compute the deprojected volume density  $j(r)$  analytically and then solve the spherical Jeans equation (Binney & Tremaine 1987), assuming unit mass-to-light ratio and velocity isotropy, to obtain a normalized velocity-dispersion profile for any  $\gamma$ . The complete structural and dynamical details of power-law clusters are then known in full, and all of the derived physical parameters that we present in §4.2 can be evaluated equally well within any of the three models that we fit.

It is instructive first to consider how these different types of models compare with one another. Thus, in Figure 9 we show normalized surface-density profiles of one example each of a King, Wilson, and power-law model cluster. We first calculated a  $c = 1.5$  King (1966) model—representative of an average Galactic globular cluster—and found its dimensionless total luminosity,  $L_{\text{tot}}/I_0 R_h^2$ , in terms of an arbitrary central surface density  $I_0$  and projected half-light (effective) radius  $R_h$ . The surface-density profile  $I(R)$ , normalized by  $I_0$  and scaled in projected radius by  $R_h$  is shown as the dashed curves in both panels of Fig. 9. The top panel here is a log-log plot of the density vs. radius; the bottom panel is a log-linear plot, a representation which emphasizes the outer *halo* structure over the inner core regions.

We then sought the Wilson (1975) model with the same dimensionless  $L_{\text{tot}}/I_0 R_h^2$  as the  $c = 1.5$  King (1966) cluster. This turns out to be given by a Wilson  $c = 2.08$ , and the projection of this model onto the plane of the sky is shown as the solid curves in Fig. 9. Similarly, the  $\gamma = 3.765$  power-law model shown as the dotted curves has the same  $L_{\text{tot}}/I_0 R_h^2$  again. Thus, Fig. 9 illustrates the relative spatial extent predicted by these three models for a cluster with fixed total luminosity, central surface brightness, and projected half-light radius (all quantities that tend to be observationally well-determined in real clusters). Clearly apparent is the intermediacy of the Wilson model between the more sharply truncated King model and the infinite power law. Also evident is that the differences between these models are generally largest beyond a few effective radii, in the outer halos of clusters.

Figure 10 extends this comparison to general King (1966) cluster concentrations. [A more comprehensive discussion of the defining features of King models vs. Wilson models in particular can be found in Hunter (1977).] Here, we have calculated the dimensionless  $L_{\text{tot}}/I_0 R_h^2$  for each of a large number of King models with  $0.3 \leq c \leq 4$ , and then found the unique Wilson  $c$  and power-law  $\gamma$  that give the same dimensionless luminosity. Although we have done this formally without any restrictions on the parameter  $c$ , note that the majority of King-model fits to real GCs return  $c \lesssim 2$ , and indeed the model itself is unstable to the gravothermal catastrophe at concentrations higher than this.

It is noteworthy from this figure that, first, *low*-concentration King or Wilson models, which are characterized by a sharp decline in density beyond a dominant, nearly constant-density core, find their analogue in *high*- $\gamma$  power laws. Second, while the shape parameters  $c$  or  $\gamma$  are certainly

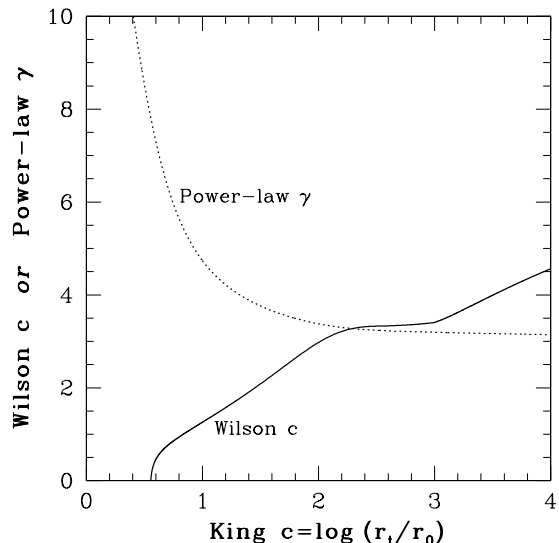


FIG. 10.— Relation between King-model concentration  $c \equiv \log(r_t/r_0)$ , Wilson-model  $c$ , and power-law exponent  $\gamma$  when a cluster is required to have the same total luminosity and effective radius and central surface-brightness in all three models. (Each  $c$  or  $\gamma$  corresponds to a unique value of  $L_{\text{tot}}/I_0 R_h^2$ .) King and Wilson models with  $c < 0$  exist in principle ( $c \rightarrow -\infty$  as the dimensionless central potential  $W_0 \rightarrow 0$ ) but are not shown here, as real clusters of such low concentration are rare. The same is true of power-law models with  $\gamma > 10$ .

useful indicators of a cluster’s global structure, their numerical values are highly model-dependent. This makes it of interest to consider a more generally applicable “concentration index” able to represent the spatial extent or potential depth of any cluster in a more model-independent way (so as to allow, e.g., for a combined analysis of clusters which may not all be described well by the same type of model). We return to this point below in §4.2, where we now present the fits of all models to our cluster sample.

#### 4.2. Surface-Brightness Fits and Cluster Physical Parameters

Our fitting procedure involves computing in full large numbers of King, Wilson, and power-law structural/dynamical models, spanning a wide range of fixed values of the appropriate shape parameter  $W_0$  or  $\gamma$ . Separately for each family in turn, we then fit every model on the appropriate  $W_0$ - or  $\gamma$ -grid to a cluster’s observed surface-brightness profile,  $\mu_V = \mu_{V,0} - 2.5 \log[I(R/r_0)/I_0]$ , finding the radial scale  $r_0$  and central SB  $\mu_{V,0}$  which minimize  $\chi^2$  for every given value of  $W_0$  or  $\gamma$ . The  $(W_0, r_0, \mu_{V,0})$  or  $(\gamma, r_0, \mu_{V,0})$  combination that yields the global minimum  $\chi_{\text{min}}^2$  over the grid used defines the best-fit model of that type. Estimates of the one-sigma uncertainties on these basic fit parameters, and those on all associated derived quantities, follow from their extreme values over the subgrid of fits with  $\chi^2 \leq \chi_{\text{min}}^2 + 1$ . For the most part, we calculate and minimize  $\chi^2$  as the weighted sum of squared differences between model and observed intensities  $I$  (in units of  $V$ -band  $L_\odot \text{pc}^{-2}$ ), rather than logarithmic surface-brightness units; although in a few cases more stable fits resulted from

defining  $\chi^2$  as the weighted sum of squared surface-brightness deviations. The vast majority of our fits are error-weighted, with the uncertainties on individual datapoints either taken from the original sources of HST and ground-based starcounts in the LMC, SMC, and Fornax clusters, or estimated by us from the Trager et al. (1995) catalogue data (§2.2 and Table 6).

#### 4.2.1. Fits to $\omega$ Centauri

As a detailed example, Figure 11 shows our best King, Wilson, and power-law fits to the well-studied Galactic globular cluster  $\omega$  Centauri = NGC 5139 (see also McLaughlin & Meylan 2003). The main parameters and minimum  $\chi^2$  values for the three fits are listed in Table 9. These are also given, along with many other derived structural and dynamical parameters, in our results below for the full cluster sample (Tables 10 through 14).

The upper panels of Figure 11 display the cluster’s model and observed surface-brightness profiles, while the lower panels show the predicted and observed internal velocity-dispersion profiles, which we consider in detail for this one object only. The V-band surface-brightness datapoints are those from Trager, King, & Djorgovski (1995) with our estimated errorbars attached. The radial scale is given in units of arcseconds along the lower horizontal axes and parsecs (for an assumed distance of 5.3 kpc taken from Harris 1996) along the upper axes. The left-hand upper panel is a log-log representation of density vs. radius, which focuses on the core structure of the cluster; the right-hand panel is in log-linear format to highlight its halo structure.

The main point to be taken from the top of Fig. 11 is that even among Milky Way globular clusters, where King (1966) models are generally taken as the best physical description, alternate models can fit even the most comprehensive data at least as well and sometimes, as in the case of the Wilson model here, better. To be sure, the single-mass and isotropic King models that we fit have long been known to be inadequate for many old GCs, a fact that is usually attributed *by hypothesis* to the influences of energy equipartition and mass segregation and/or velocity anisotropy in well-relaxed multimass stellar populations. Multimass and anisotropic models still based on the King distribution function (eq. [1]) have therefore been developed (Da Costa & Freeman 1976; Gunn & Griffin 1979) and fit to a good number of Galactic globulars—including  $\omega$  Centauri (e.g., Meylan et al. 1995)—with much better success. The case of  $\omega$  Cen is instructive, however, in that it is an *unrelaxed* cluster showing no evidence of advanced mass segregation (Anderson 1997), nor of velocity anisotropy (Merritt et al. 1997; van Leeuwen et al. 2000). Compensating for the shortcomings of the simple King (1966) model in Fig. 11 is therefore better done with entirely different single-mass and isotropic models—even if they are ad hoc to some degree—than with multimass and anisotropic variations on the King distribution function. This is an additional justification for our fitting of Wilson and power-law models to a full suite of Galactic globulars.  $\omega$  Cen is the most massive GC in the Milky Way, and an uncharacteristically diffuse one. It might therefore have been thought, justifiably, to be a rather special case; but as we shall see, our single-mass, isotropic Wilson models in particular do provide fits of quality comparable to or better than King models for a majority of GC surface-brightness profiles. We also note that the cluster tidal radius implied by the Wilson-model fit in  $\omega$  Cen is only 50% larger than that of the King model (see Table 11 below),

meaning that the generally greater extent of Wilson’s model relative to King’s need not imply severe inconsistencies with the expected sizes of GCs for a given Galactic tidal field.

The bottom panels of Fig. 11 show the observed velocity dispersion as a function of radius in  $\omega$  Cen (Meylan et al. 1995; Seitzer 1983), again with a logarithmic radial scale on the left and a linear radial scale on the right. The model curves now are the profiles predicted (after projection along the line of sight) by solving the spherical Jeans equation with the de-projections of the best-fit density profiles in the upper panels. The model predictions are inherently dimensionless in form, yielding  $\sigma_p/\sigma_0$  as a function of projected radius  $R$  where  $\sigma_0$  is the velocity scale defined by  $\sigma_0^2 \equiv (4\pi G \Upsilon_V j_0 r_0^2)/9$  (cf. eq. [4]). Knowing the radial scale  $r_0$  and the central three-dimensional luminosity density  $j_0$  from fitting to the cluster surface brightness, the theoretical velocity-dispersion curves are scaled to match the data essentially by fixing a (spatially constant) mass-to-light ratio  $\Upsilon_V$ . The value of  $\Upsilon_V$  that gives the best agreement with the velocity dispersions in  $\omega$  Cen is listed for each model type in the lower right-hand panel of Fig. 11. The main conclusion is that our different surface-brightness fits are, in general, associated with self-consistent internal dynamics that are closely similar both in relative terms (the shapes of the model velocity-dispersion profiles) and in an absolute sense (the implied value of  $\Upsilon_V$ ).

#### 4.2.2. Fits to All Clusters

Figure 12, which can be found at the end of the paper, displays the best-fit King, Wilson, and power-law models for the V-band surface-brightness profiles of our 53 LMC clusters, 10 SMC clusters, the 5 globulars in Fornax, and 84 Galactic GCs besides  $\omega$  Centauri (recall that we do not present fits to the entire database of Trager, King, & Djorgovski 1995, for reasons discussed in §2.2). Each cluster is presented in two panels formatted as in the top of Fig. 11, one with both axes on logarithmic scales and one in log-linear form. Along the top of every panel, projected radius is given in pc, obtained by assuming a distance of 50.1 kpc to all clusters in the LMC, 60.0 kpc to all clusters in the SMC, and 137 kpc to Fornax; heliocentric distances to individual Milky Way GCs are taken from the catalogue of Harris (1996). In all cases, dashed curves are the King-model fits; solid curves are Wilson models; and dotted lines are power laws with cores.

In the LMC, SMC, and Fornax cluster panels, the open circles correspond to surface-brightness data taken from Mackey & Gilmore (2003a,b,c), *after* applying the zeropoint corrections discussed in §2.1 (see Table 4) and correcting for the V-band extinction  $A_V = 3.1 [(B - V) - (B - V)_0]$  inferred from our population-synthesis modeling in §3.2 (see Table 8). There are generally two such points at each radius, one coming from the primary V-band counts of MG03 and the other from their secondary B or I profiles shifted by the color terms in Table 2. The open squares in the plots for LMC and SMC clusters denote the ground-based starcount data that we have collected and matched onto the re-zeropointed MG03 profiles. Asterisks refer to datapoints that we have not included in calculating and minimizing  $\chi^2$  to identify the best model fits (i.e., those with “fit flags” of 0 in Table 5).

In the Milky Way GC panels, the open circles are the datapoints from Trager, King, & Djorgovski (1995), taken exactly as published except for Palomar 10 and Terzan 7, which we have calibrated as described in §2.2. The errorbars on these points are our own estimates based on Table 6. The asterisks in these cases are surface-brightness measurements also pub-

TABLE 9  
MODEL FITS TO  $\omega$  CENTAURI = NGC 5139

Model (1)	Reduced $\chi^2_{\min}$ <sup>a</sup> (2)	$W_0/\gamma$ (3)	$c = \log(r_t/r_0)$ (4)	$\mu_{V,0}$ <sup>b</sup> (5)	$r_0$ [sec] (6)	$r_0$ [pc] <sup>c</sup> (7)
King	1.73	$W_0 = 6.20^{+0.20}_{-0.10}$	$1.31^{+0.05}_{-0.03}$	$16.44^{+0.06}_{-0.11}$	$141.20^{+6.50}_{-12.69}$	$3.63^{+0.17}_{-0.33}$
Wilson	0.47	$W_0 = 4.70^{+0.10}_{-0.10}$	$1.34^{+0.03}_{-0.03}$	$16.52^{+0.05}_{-0.05}$	$196.81^{+7.08}_{-7.01}$	$5.06^{+0.18}_{-0.18}$
Power-law	1.47	$\gamma = 5.55^{+0.10}_{-0.10}$	$\infty$	$16.65^{+0.05}_{-0.04}$	$327.58^{+11.48}_{-11.71}$	$8.42^{+0.29}_{-0.30}$

<sup>a</sup>There are 54 datapoints in the fitted profile, and we fit by finding the  $\mu_{V,0}$  and  $r_0$  which minimizes  $\chi^2$  over a large grid of fixed  $W_0$  or  $\gamma$  values. Thus, the reduced  $\chi^2_{\min}$  per degree of freedom is just  $\chi^2_{\min}/52$ .

<sup>b</sup>Corrected for extinction given in Harris (1996).

<sup>c</sup>Assumes a heliocentric distance of  $D = 5.3$  kpc (Harris 1996).

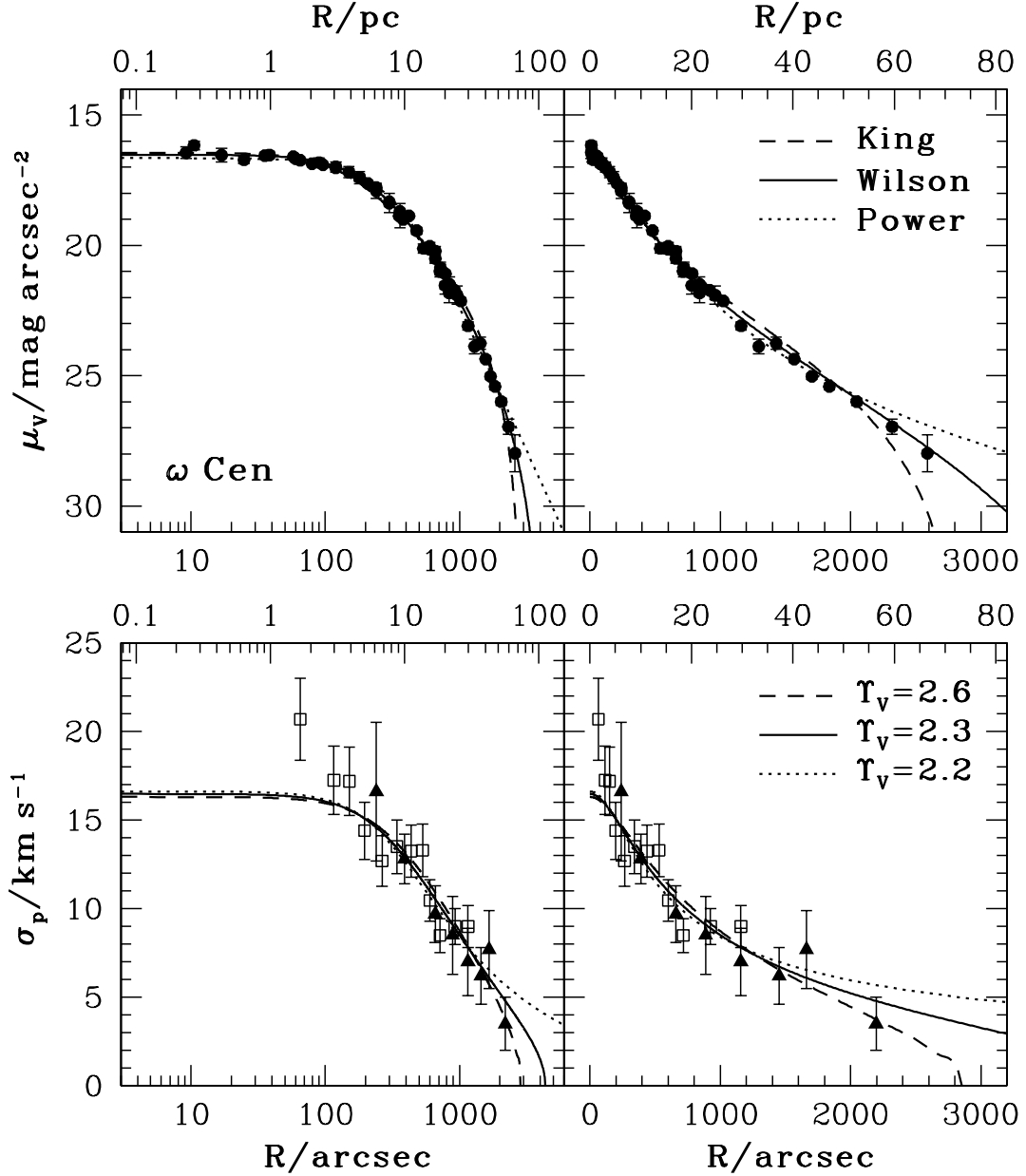


FIG. 11.— Detailed fitting of King (1966), Wilson (1975), and power-law models to the Galactic globular cluster  $\omega$  Centauri. *Top panels* show the surface-brightness profile as a function of logarithmic projected radius on the left, linear projected radius on the right. *Bottom panels* show the observed internal line-of-sight velocity-dispersion profile from Meylan et al. (1995, open squares) and Seitzer (1983, filled triangles), and the model profiles after normalization by the V-band mass-to-light ratios indicated.

lished by Trager et al. but given relative weightings  $w_i < 0.15$  by them; we did not include these points when fitting our models.

Table 10 (also at the end of the paper) gives a few important numbers for each cluster and lists the main parameters of every fit. The first column here is the cluster name with a short prefix identifying its parent galaxy. Column (2) is the zeropoint shift that we have applied to published surface-brightness magnitudes (copied directly from Table 4 for the MG03 cluster sample; 0 for all but Palomar 10 and Terzan 7 in the Milky Way GC sample). Column (3) is the estimated  $V$ -band extinction, derived as discussed in §3.2. Next are the assumed distance to the cluster, the number of datapoints ultimately included in fitting any model to the cluster, and a code for the weighting scheme used to minimize  $\chi^2$ .

Subsequent columns in Table 10 cover three lines for each cluster, one line for each type of model fit. Column (7) identifies the model; Column (8) gives the minimum *unreduced*  $\chi^2$  obtained for that class of model; Column (9) gives the appropriate “shape” parameter  $W_0$  or  $\gamma$  at which  $\chi^2$  is minimized; Column (10) gives the concentration  $c \equiv \log(r_t/r_0)$  of the best fit (this is related uniquely to  $W_0$  for King and Wilson models but is always  $\infty$  for power-law models); Column (11) gives the best-fit central surface brightness *after correction* for both extinction and any zeropoint change; Column (12) gives the best-fit model scale radius,  $r_0$ , in arcseconds; and Column (13) gives the value of  $r_0$  in parsecs. The uncertainties in  $W_0$ ,  $c$ ,  $\gamma$ , and  $r_0$  reflect their variations among model fits with  $\chi^2 \leq \chi^2_{\min} + 1$ . The errorbars on  $\mu_{V,0}$  derive from these formal fitting uncertainties combined in quadrature with the uncertainties in the zeropoint offsets  $\Delta\mu_V$  and extinctions  $A_V$  (the  $\chi^2$  of any fit is calculated using the published uncertainties in the individual SB datapoints before any systematic corrections are applied).

Table 11 (at the end of the paper) contains a number of other structural cluster properties derived from the basic fit parameters:

- $\log r_t = c + \log r_0$  is the model tidal radius.
- $\log R_c$  refers to the projected *core* radius of the model fitting a cluster. It is defined by  $I(R_c) = I_0/2$ , or  $\mu_V(R_c) \simeq \mu_{V,0} + 0.753$ , and is *not* the same in general as the radial scale  $r_0$  in Table 10. For King and Wilson models,  $r_0$  is simply a convenience defined by dimensional analysis of Poisson’s equation, although it does bear a unique relationship to the observable  $R_c$  through well-defined functions of  $W_0$  or  $c$ . For power-law models, the connection between  $r_0$  and  $R_c$  stems from the defining equation (2) above.
- $\log R_h$  refers to the half-light, or effective, radius of a model: that radius containing half the total luminosity in projection. It is related to  $r_0$  by one-to-one functions of  $W_0$  or  $\gamma$ .
- $\log(R_h/R_c)$  is a measure of cluster concentration that is relatively more model-independent than  $W_0$  or  $c$  or  $\gamma$ , in the sense that it is generically well defined and its physical meaning is always the same. We consider it a more suitable quantity to use when intercomparing the overall properties of clusters which may not all be fit by the same kind of model (cf. our earlier discussion around Fig. 10).

- $\log I_0 = 0.4(26.422 - \mu_{V,0})$  is the logarithm of the best-fit central luminosity surface density in the  $V$  band, in units of  $L_\odot \text{pc}^{-2}$ . The surface-brightness zeropoint of 26.422 corresponds to a solar absolute magnitude  $M_{V,\odot} = +4.85$  (e.g., Lang 1999).
- $\log j_0$  is the logarithmic central luminosity *volume* density in the  $V$  band, in units of  $L_\odot \text{pc}^{-3}$ . It is given by  $j_0 = \mathcal{J}I_0/r_0$ , where  $\mathcal{J}$  is a smooth, model-dependent function of  $W_0$  or  $\gamma$ , which we have calculated in detail for King, Wilson, and power-law models.
- $\log L_{\text{tot}}$  is the logarithm of the total integrated model luminosity in the  $V$  band. It is related to the product  $I_0 r_0^2$  by model-dependent functions of  $W_0$  or  $\gamma$ .
- $V_{\text{tot}} = 4.85 - 2.5 \log(L_{\text{tot}}/L_\odot) + 5 \log(D/10 \text{pc})$  is the total, *extinction-corrected* apparent magnitude of a model cluster.
- $\log I_h \equiv \log(L_{\text{tot}}/2\pi R_h^2)$  is the  $V$ -band luminosity surface density averaged over the half-light/effective radius, in units of  $L_\odot \text{pc}^{-2}$ .
- $\langle \mu_V \rangle_h \equiv 26.42 - 2.5 \log(I_h/L_\odot \text{pc}^{-2})$  is the average surface brightness inside the half-light radius, in  $V$ -band mag arcsec $^{-2}$ .

Again, the uncertainties on all of these derived parameters have been estimated (separately for each given model family) by calculating them in every model which yields  $\chi^2$  within 1 of the global minimum for a cluster, and then taking the differences between the extreme and best-fit values of the parameters.

Table 12 (see the end of the paper) next lists a number of cluster properties derived from the structural parameters already given *plus* a mass-to-light ratio. The first column of this table contains the cluster name, as usual. Column (2) shows the mass-to-light ratio, in solar units, that we have adopted for each object from the analysis in §3—that is, on the basis of population-synthesis modeling given individual ages and metallicities for the clusters, using the model code of Bruzual & Charlot (2003) and assuming the disk-star IMF of Chabrier (2003). The values of  $\Upsilon_V^{\text{pop}}$  in Table 12 have been copied directly from Column (6) of Table 8. The remaining entries in Table 12 are, for each type of model fit to each cluster:

- $\log M_{\text{tot}} = \log \Upsilon_V^{\text{pop}} + \log L_{\text{tot}}$ , the integrated model mass in solar units.
- $\log E_b$ , the integrated binding energy in ergs, defined through  $E_b \equiv -(1/2) \int_0^{r_t} 4\pi r^2 \rho \phi dr$ . Here the minus sign makes  $E_b$  positive for gravitationally bound objects, and  $\phi(r)$  is the potential generated (through Poisson’s equation) by the model mass-density distribution  $\rho(r)$ .  $E_b$  can be written in terms of the fitted central luminosity density  $j_0$ , scale radius  $r_0$ , a model-dependent function of  $W_0$  or  $\gamma$ , and  $\Upsilon_V^{\text{pop}}$ . A more detailed outline of this procedure for King models may be found in McLaughlin (2000), which we have followed closely to evaluate  $E_b$  for our Wilson and power-law fits as well.
- $\log \Sigma_0 = \log \Upsilon_V^{\text{pop}} + \log I_0$ , the central *mass* surface density of the model fit in  $M_\odot \text{pc}^{-2}$ .

- $\log \rho_0 = \log \Upsilon_V^{\text{pop}} + \log j_0$ , the central mass volume density in  $M_\odot \text{pc}^{-3}$ .
- $\log \Sigma_h = \log \Upsilon_V^{\text{pop}} + \log I_h$ , the model mass density averaged over the half-light radius  $R_h$  (which is equal to the half-mass radius under our assumption of single-mass stellar populations, i.e., spatially constant mass-to-light ratios).
- $\sigma_{p,0}$ , the predicted line-of-sight velocity dispersion at the cluster center, in  $\text{km s}^{-1}$ . As was already suggested above, the solution of Poisson’s and Jeans’ equations for any model yields a dimensionless  $\sigma_{p,0}/\sigma_0$ , and with  $\sigma_0$  given by the fitted  $r_0$  and  $\rho_0$  through equation (4), the predicted observable dispersion follows immediately.
- $v_{\text{esc},0}$ , the predicted central “escape” velocity in  $\text{km s}^{-1}$ . A star moving out from the center of a cluster with speed  $v_{\text{esc},0}$  will just come to rest at infinity. In general, then,  $v_{\text{esc},0}^2/\sigma_0^2 = 2 [W_0 + GM_{\text{tot}}/r_t\sigma_0^2]$ . Note that the second term on the right-hand side of this definition vanishes for power-law models, in which  $r_t \rightarrow \infty$ . In these models a (finite) dimensionless  $W_0$  is associated with every value of  $\gamma > 3$  by solving Poisson’s equation with  $\phi(\infty) = 0$ .
- $\log t_{\text{rh}}$ , the two-body relaxation time at the model projected half-mass radius. This is estimated as  $t_{\text{rh}}/\text{yr} = [2.06 \times 10^6 / \ln(0.4M_{\text{tot}}/m_*)] m_*^{-1} M_{\text{tot}}^{1/2} R_h^{3/2}$  (Binney & Tremaine 1987, eq. 8-72), if  $m_*$  (the average stellar mass in a cluster) and  $M_{\text{tot}}$  are both in solar units and  $R_h$  is in pc. We have evaluated this timescale assuming an average  $m_* = 0.5 M_\odot$  in all clusters.
- $\log f_0 \equiv \log [\rho_0/(2\pi\sigma_c^2)^{3/2}]$ , a measure of the model’s central phase-space density in units of  $M_\odot \text{pc}^{-3} (\text{kms}^{-1})^{-3}$ . In this expression,  $\sigma_c$  refers to the central one-dimensional velocity dispersion *without* projection along the line of sight. The ratio  $\sigma_c/\sigma_0$  is obtained in general from the solution of the Poisson and Jeans equations for given  $W_0$  or  $\gamma$ , and the fitted  $\sigma_0$  again is known from equation (4). With the central relaxation time  $t_{\text{rc}}$  of a cluster defined as in equation (8-71) of Binney & Tremaine (1987), taking an average stellar mass of  $m_* = 0.5 M_\odot$  and a typical Coulomb logarithm  $\ln \Lambda \approx 12$  leads to the approximate relation  $\log(t_{\text{rc}}/\text{yr}) \simeq 8.28 - \log f_0$ .

The uncertainties in these derived dynamical quantities are estimated from their variations around the minimum of  $\chi^2$  on the model grids we fit, as above, combined in quadrature with the population-synthesis model uncertainties in  $\Upsilon_V^{\text{pop}}$ , which in turn reflect the estimated uncertainties in published cluster ages and metallicities.

### 4.3. Fit Comparisons

#### 4.3.1. Our Fits vs. Published Catalogues

An important check on the array of cluster properties presented in §4.2 is provided by comparing our basic fit parameters against those in published catalogues for the Milky Way and LMC/SMC/Fornax clusters. We confine such comparisons to one between our power-law fit parameters and those reported by Mackey & Gilmore (2003a,b,c, MG03) for LMC, SMC, and Fornax clusters; and one between our King-model

fits to the Galactic GCs and the parameters in the catalogue of Harris (1996) (itself ultimately based in large part on the profile database of Trager, King, & Djorgovski 1995). The generally good results give us confidence that there are no problematic biases or any other procedural issues with our modeling or fitting techniques; thus, we have not searched the literature to compare with all other model fits that might have been performed on any of these clusters.

The left-hand panels of Fig. 13 show our power-law exponents  $\gamma$ , scale radii  $r_0$ , and central surface brightnesses  $\mu_{V,0}$  against those published by MG03 for their cluster sample. The overall agreement between our numbers and theirs is apparent—although note that the “Mackey & Gilmore” surface brightnesses we compare to in the bottom left panel have already been *corrected* for our extinctions and zeropoint offsets in Table 10. There is somewhat more scatter in the plots of  $\gamma$  and  $r_0$  values than in the  $\mu_{V,0}$  graph, for the simple reason that the latter parameters are more sensitive to the ground-based starcounts which we have added to about two-thirds of the MG03 cluster sample.

It is worth noting a frequent tendency for our power-law fits to return somewhat steeper  $\gamma$ , and correspondingly larger  $r_0$ , than those of MG03. This can also be traced to our inclusion of ground-based data, as the specific example of the LMC cluster NGC 2121 illustrates well. MG03 quote a value of  $\gamma = 3.25$  for this object, whereas we have obtained  $\gamma = 6.00$ ; it is clearly visible as an “outlier” in the upper left-hand panel of Fig. 13. Referring back to the plotted fits in Fig. 12, however, we see that the SB profile from Mackey & Gilmore (2003a) extends only to  $R \simeq 70'' = 17 \text{ pc}$  in this case—just barely outside the constant-density core region of NGC 2121—while our additional groundbased data reach to  $R \simeq 100'' \simeq 24 \text{ pc}$  and are critical to accurately constraining any model fit. Fortunately this example is the most extreme in our sample, but the point is made that when a model extrapolates significantly beyond the limit of the fitted data, care must be taken in using the results. This is of most concern for power-law models, which are innately the most spatially extensive of the ones we fit.

The right-hand panels of Fig. 13 show our fitted King-model concentrations, scale radii, and central surface brightnesses for 85 Galactic globular clusters, against those parameters taken from the Harris catalogue. For the most part, the agreement is again quite good; but there are a number of clusters for which we claim significantly different  $c$  values from those indicated by Harris (1996), and these differences propagate into the  $r_0$  and  $\mu_{V,0}$  plots (given the same data, a lower fitted  $c$  corresponds in general to a measurably larger  $r_0$  and somewhat fainter  $\mu_{V,0}$ ).

For the two GCs NGC 6101 and NGC 6496, we find King concentrations  $c \approx 0$  while Harris gives  $c \simeq 0.7\text{--}0.8$ . Looking at these objects in Fig. 12, they are unquestionably low-concentration clusters, with steep declines in surface brightness beyond relatively large cores. The exact details of any fit are heavily influenced by the outermost one or two datapoints in each case (and by irregular structure at the center of NGC 6496), and our errorbars on  $c$  (and  $r_0$  and  $\mu_{V,0}$ ) reflect this.

Somewhat similarly, we find  $c = 1.5 \pm 0.12$  for NGC 6528, whereas Harris (1996) states  $c = 2.3$ . There are many points from Trager, King, & Djorgovski (1995) for this cluster to which we assigned zero weight when doing our fits. The model parameters are apparently quite dependent on which of the data are taken into account for this relatively poorly defined brightness profile.

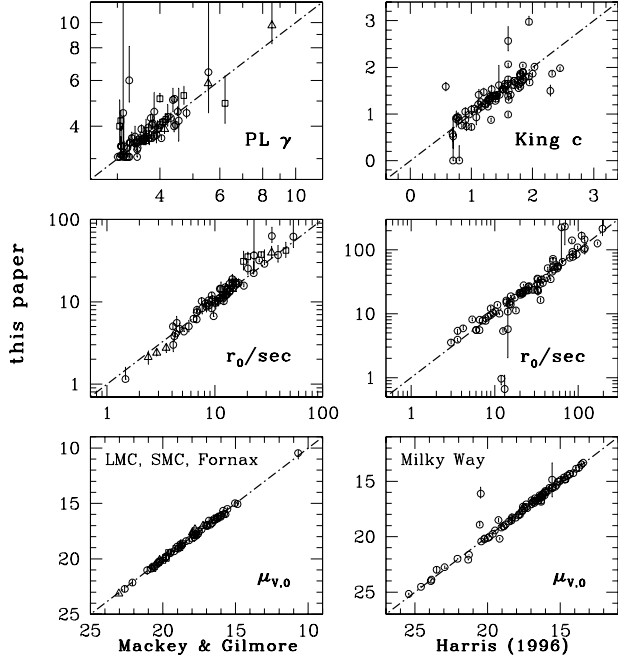


FIG. 13.— Comparison of our power-law fit parameters for LMC, SMC, and Fornax clusters (*left-hand panels*) against those from Mackey & Gilmore (2003a,b,c), and of our King-model fit parameters for Milky Way globular clusters (*right-hand panels*) against those catalogued by Harris (1996). Broken lines in all panels indicate equality. The comparison of our central surface brightnesses with the “Mackey & Gilmore” values in the lower left-hand panel uses their data *after correction* for both the zeropoint offsets  $\Delta\mu_V$  in Column (2) of Table 10 (also Table 4) and the  $V$ -band extinctions in Column (3) of Table 10. The Milky Way GC central surface brightnesses plotted in the bottom right panel are corrected for the  $A_V$  in Table 10, which are the same as those in Harris (1996).

The three points falling highest above the line of equality in the top right-hand panel of Fig. 13 correspond to Palomar 10 (Harris  $c = 0.58$ ; our  $c = 1.59$ ), Palomar 1 (Harris  $c = 1.6$ ; our  $c = 2.57$ ), and Palomar 12 (Harris  $c = 1.94$ ; our  $c = 2.98$ ). Inspection of these in Fig. 12 shows no obvious problem with any of our models for Pal 10, although clearly the range of fitted datapoints from Trager, King, & Djorgovski (1995) is less than ideal; in fact, Harris’ tabulated parameters are based on observations by Kaisler, Harris, & McLaughlin (1997) which supersede those of Trager et al. The data for Pal 1 do not show any clear evidence for an isothermal core in the first place, allowing this cluster to be fit by a high-concentration King model with a small predicted scale radius and bright central surface brightness that are in fact unobserved. Pal 12 shows what might be described as a double-core structure, and it is therefore also fit relatively best by high- $c$ , low- $r_0$  and bright- $\mu_{V,0}$  King and Wilson models—although the fits are certainly not “good” in an absolute  $\chi^2$  sense (see Table 10). Any catalogued fit parameters (including ours) for these three Palomar clusters are probably best viewed as only provisional.

#### 4.3.2. Goodness-of-Fit for Different Models

We next compare the  $\chi^2$  values of the different model fits to every cluster in our sample. We make this comparison relative to  $\chi^2$  of the best-fit King model in each case by computing  $\Delta \equiv (\chi^2 - \chi^2_{\text{King}})/(\chi^2 + \chi^2_{\text{King}})$  for the best Wilson and power-law fits. This index ranges from a minimum of  $\Delta = -1$  for an alternate model with  $\chi^2 \ll \chi^2_{\text{King}}$  to a maximum of  $\Delta = +1$

when  $\chi^2_{\text{King}} \ll \chi^2$ .

The top panels of Fig. 14 show the distribution of  $\Delta$  values for the Wilson (filled circles) and power-law (open squares) fits to the MG03 cluster sample in the LMC, SMC, and Fornax. The points for the Wilson and power-law fits of any one cluster are connected by a solid line. On the left we plot  $\Delta$  as a function of cluster dynamical age, i.e., the chronological age  $\tau$  in units of the King-model half-mass relaxation time  $t_{\text{rh}}$  from Table 12. On the right, we show  $\Delta$  as a function of the ratio  $R_{\text{last}}/R_h$ , where  $R_{\text{last}}$  is the clustercentric radius of the outermost surface-brightness datapoint observed in a cluster and  $R_h$  is the (King-model) half-mass radius.

It is immediately apparent that, in every LMC/SMC/Fornax cluster studied here, Wilson (1975) models fit at least as well as King (1966) models, and very often substantially better. Power-law models generally fit roughly as well as Wilson models, sometimes slightly better and sometimes somewhat worse. On one level, the top panels of Fig. 14 are therefore a re-statement of the appreciated fact that many clusters in the Magellanic Clouds are more extended than classic King models (e.g., Elson, Fall, & Freeman 1987; Mackey & Gilmore 2003a,b). New here is the demonstration that, although they are usually acceptable fits, untruncated power-law forms specifically are *not required* to describe the density distributions of these objects. We expect that the same is likely true of young massive clusters in other disk galaxies (Larsen 2004; Schweizer 2004, and references therein).

Also new is our quantification of the improvement in fit yielded by the more extended models as a function of cluster age. Elson, Fall, & Freeman (1987) originally suggested that power-law models fit *young* LMC clusters better than King models because of the presence of unbound stellar halos which are relics of the cluster formation process and simply have not had time to be stripped away by tides. The chronologically young clusters in the current sample (which includes that of Elson, Fall, & Freeman 1987) generally have  $\tau/t_{\text{rh}} \lesssim 1$  in the upper left panel of Fig. 14. Many of them have  $\Delta < 0$  and are undoubtedly fit better by Wilson or power-law models than by King models; but about as many have  $\Delta \approx 0$  and are equally well fit by any model type. Moreover, there is a comparable number of chronologically and dynamically *old* clusters (including the Magellanic Cloud globulars and those in Fornax) which, at  $\tau/t_{\text{rh}} \sim 10$ , also have  $\Delta < 0$  and are characterized by spatially extended halos not easily reproduced by King models. [Working from completely independent data, Rodgers & Roberts (1994) have already claimed this for three of the five globular clusters in Fornax.] Age appears not to be the main factor in determining whether or not any of these clusters can be well described by regular King models.

Instead, the upper right-hand panel of Fig. 14 shows simply that King models provide progressively less satisfactory fits as surface-brightness and starcount data extend farther and farther into cluster halos. All of the clusters here—young or old, in the disk or halo populations of any of these three small galaxies—are better fit by Wilson or power-law models if the models are forced to fit beyond  $\simeq 4$ – $5$  half-light radii in the clusters. (It will be recalled from Fig. 10 above that this is the point where the King, Wilson, and power-law model structures begin to differ appreciably.) We suggest that the halos of massive star clusters are *generically* more extensive than the stellar distribution function of King (1966) allows, and that the development of a physically motivated model accounting for this (one less ad hoc than a Wilson or power-law



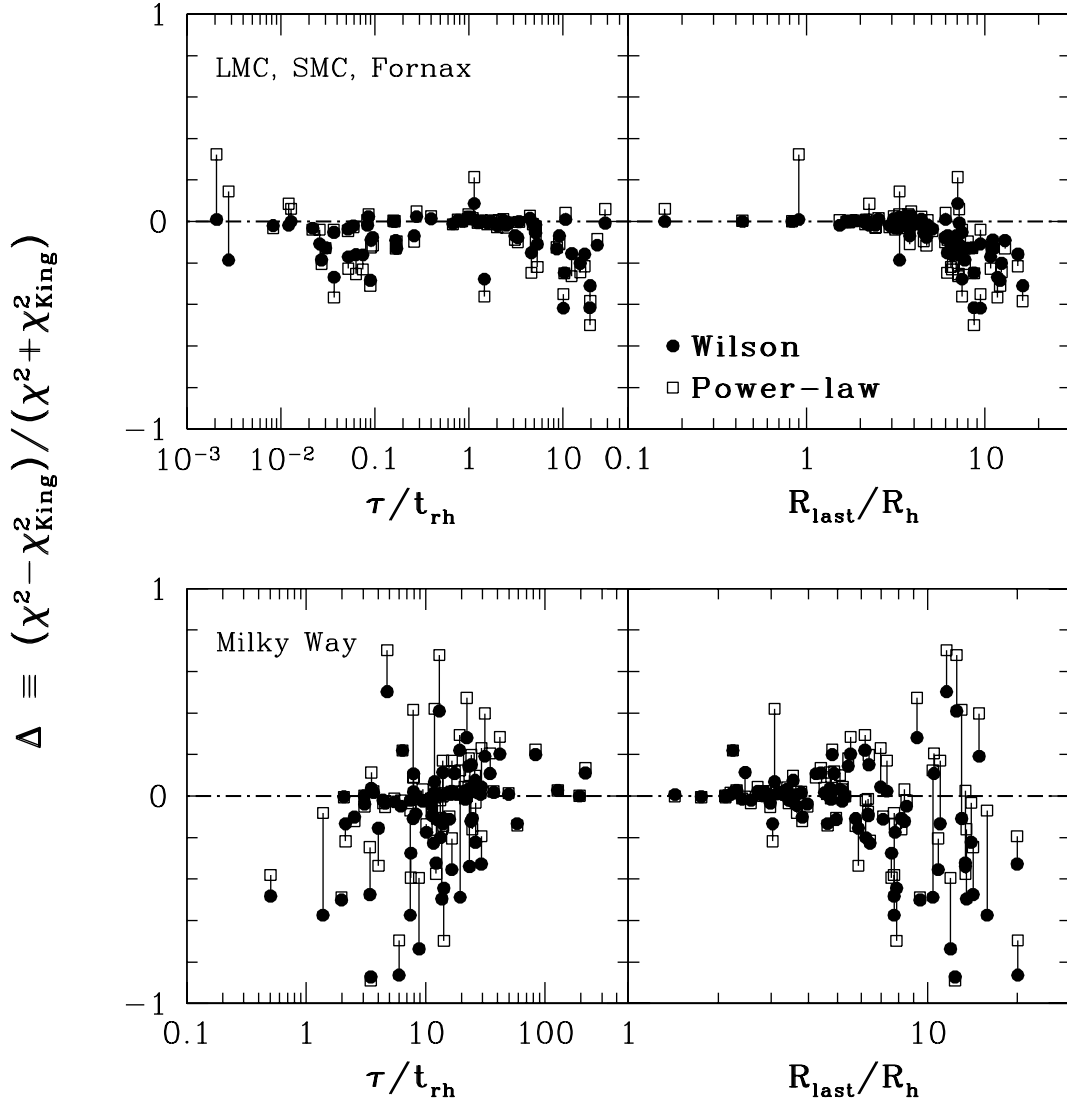


FIG. 14.— Goodness of fit of Wilson (1975) spheres and power-law models, relative to standard King (1966) models, for 68 clusters in the LMC, SMC, and Fornax (*top panels*) and for 85 globular clusters in the Milky Way (*bottom panels*). Solid points mark the relative  $\chi^2$  index,  $\Delta$ , for the Wilson-model fits; open squares denote  $\Delta$  for the power-law fits. Solid lines connect the Wilson and power-law  $\Delta$  values for each cluster.  $\Delta$  is shown as a function of cluster dynamical age in the left-hand panels, and as a function of the radial extent of the observed surface-brightness profiles in the right-hand panels. The inherently more extended Wilson model tends to fit clusters of any age better ( $\Delta < 0$ ) when their outer halos are better defined empirically.

prescription) could lend substantial new insight into questions of cluster formation and evolution.

The fundamental physical question remaining from Elson, Fall, & Freeman (1987) is whether the stars at the largest observed radii in the young clusters particularly are gravitationally bound in a model-independent sense: do these objects overflow the Roche lobes defined by the potentials of their parent galaxies? Simply fitting power laws to the clusters does not in fact address this issue, as equally good or better fits of spatially limited Wilson models can be found; but at the same time, it remains to be shown that the fitted  $r_t$  from the Wilson models actually correspond to the true tidal limits imposed by the galaxies. Moreover, the question now has to be extended to many old globulars. To properly answer it for any cluster requires *at a minimum* not only a highly precise empirical estimate of  $r_t$  itself, but also a detailed understanding of

the total mass distribution and gravitational field of the parent galaxy; good information on the present-day galactocentric position of the cluster; and knowledge of its orbital energy and pericenter. The interplay between these ingredients makes for a subtle problem, fraught with uncertainty even in the Milky Way (see, e.g., Innanen, Harris, & Webbink 1983), which is beyond the scope of this paper. However, we do touch briefly on a comparison between the fitted “tidal” radii in the King and Wilson models for our cluster sample, in Fig. 18 below.

The bottom panels of Fig. 14 are plots of the relative  $\chi^2$  index  $\Delta$  against both dynamical age and spatial extent of the SB data for the 85 Galactic GCs that we have modeled.<sup>4</sup> It is clear

<sup>4</sup> Note the absence of Milky Way globulars with  $R_{\text{last}}/R_h < 1$  in Fig. 14, contrasting with the presence of such objects in the LMC/SMC/Fornax cluster sample. As we discussed in §2.2, such large fitted  $R_h$  in the Galactic sample tend to be associated either with relatively poor data or with clusters iden-

that many globulars with well-observed halos ( $R_{\text{last}}/R_h \gtrsim 5$ ) are again relatively better fit by Wilson models than by single-mass, isotropic King models, regardless of their dynamical age  $\tau/t_{\text{th}}$ . In most of these cases power laws are worse fits than Wilson models, which likely reflects the inability of the former to describe tidal limits to a cluster. But now there are also about ten globulars with data extending beyond  $5R_h$ , which are better fit by King models than either Wilson or power-law spheres. A good example is NGC 104 = 47 Tucanae ( $\Delta = +0.5$  for the Wilson model fit), although in Fig. 12 this profile actually appears to prefer some kind of description *intermediate* to King (1966) and Wilson (1975).

The bottom left panel in this plot gives the visual impression that—unlike in the LMC, SMC, and Fornax cluster sample—there may be some correlation between our  $\Delta$  statistic and the dynamical age  $\tau/t_{\text{th}}$ . A test using the Spearman rank correlation coefficient for the Wilson-model fits specifically shows that these quantities are indeed correlated, with a formal confidence level of  $> 99\%$ . However, the correlation between  $\Delta$  and  $R_{\text{last}}/R_h$  for the Milky Way GCs is still stronger and more significant than any correlation with  $\tau/t_{\text{th}}$ . In any case, all of this is going on over a narrow range of extreme age relative to the rather larger spread in the LMC, SMC, and Fornax sample, where the situation is much clearer.

Some of these differences in the bottom panels of Fig. 14 relative to the upper panels may simply be a reflection of the more heterogeneous nature of the original data compiled by Trager, King, & Djorgovski (1995). It could also be indicative of the ultimate limitations of our assumptions of velocity isotropy and (probably more important) a single-mass stellar population in the clusters: NGC 104, for example, is known to exhibit mass segregation (e.g., Anderson 1997) and can be fit well with multimass King models (Meylan 1988, 1989). On the other hand, we find here that the cluster NGC 5272 = M 3, which was the original motivation for the development of multimass King models (Da Costa & Freeman 1976; Gunn & Griffin 1979), can be perfectly well fit by a single-mass and isotropic Wilson model; it is the filled circle at  $R_{\text{last}}/R_h = 12.4$  and  $\Delta = -0.87$  in the lower right panel of Fig. 14.

The totality of the results presented here still suggest to us that a fundamental alteration to the King (1966) distribution function is required to account for the halo structure and dynamics of massive star clusters in general. That the ad hoc, single-mass, and isotropic Wilson (1975) model is not the perfect solution should come as no surprise; but, as our discussion of  $\omega$  Centauri concluded (§4.2.1), neither can multimass and/or anisotropic variations on the standard King (1966) distribution function correctly explain the structure of all globular clusters.

This issue aside, we now turn to consider whether the observable, physical properties—core and half-light radii, total luminosities, and the like—that we have derived for our clusters are reasonably model-independent. In particular, we would like some assurance that they are robust enough to allow useful characterizations of parameter interdependences and trends between clusters.

#### 4.3.3. Physical Cluster Properties in Different Models

identified as core-collapsed by Trager, King, & Djorgovski (1995). These GCs are named in Table 7 but have been left out of Fig. 14 (and Tables 10–12) by construction.

Figure 15 compares the Wilson- and King-model values for a number of parameters of the LMC, SMC, and Fornax (MG03) clusters in our sample (see Tables 10–12). The overriding conclusion to be drawn is that these two types of model fits tend, with some understandable exceptions, to agree within  $\sim 5\%$  ( $\sim 0.02$  dex) on the values of basic cluster properties. We have plotted the differences in fitted and derived properties between the two models as functions of the relative  $\chi^2$  index  $\Delta \equiv (\chi^2_{\text{Wilson}} - \chi^2_{\text{King}})/(\chi^2_{\text{Wilson}} + \chi^2_{\text{King}})$ .

The upper left-hand panel of Fig. 15 shows that in most cases the central surface brightness  $\mu_{V,0}$  is very well determined, stable at the  $\sim 0.03$ -mag level on average no matter which model is fit. (Note, however, that when the Wilson model fits better, it tends to return a slightly fainter central brightness than a King-model fit.) One of the most obvious exceptions is the LMC cluster NGC 2005, which is the point enclosed in an open square; it in fact lies off the vertical scale at  $\mu_{V,0}(\text{W}) - \mu_{V,0}(\text{K}) = -5.01$ . Although the  $\chi^2$  of the two fits are essentially the same, the Wilson model for this cluster is of much higher concentration—and therefore brighter central surface brightness—than the King model, due to the influence of a single datapoint at  $R \simeq 1'' \simeq 0.24$  pc (see Fig. 12). [NGC 2005 is an old globular that has been cited by other authors as a core-collapsed object; e.g., Mateo (1987). See Mackey & Gilmore (2003a) for discussion of other possible core-collapse candidates in this sample of LMC GCs.] The other main outlier in this plot, with  $\mu_{V,0}(\text{W}) - \mu_{V,0}(\text{K}) = -1.09$ , is R 136 = 30 Doradus in the LMC. This very young object’s extremely compact configuration is not particularly well fit by any of our models (for further discussion, see, e.g., Mackey & Gilmore 2003a).

The upper middle panel shows a tendency for the projected core radius to be larger in the Wilson models for these clusters, by  $\sim 5\%$  on average but up to  $\sim 15\%$  when Wilson spheres fit very much better than King models. This might be viewed as a demonstration that fitting the “wrong” type of model to a cluster introduces possible error of this order in the fitted  $R_c$ . Note that NGC 2005 and R 136 are again outliers here, with their much *smaller* core radii in the Wilson fits corresponding to their much brighter  $\mu_{V,0}$ .

It can be seen in the upper right-hand panel of Fig. 15 that, when Wilson models fit better than King in the LMC/SMC/Fornax sample, the model half-light radius  $R_h$  is essentially the same—again to within about 5% on average—in either model. The reason is that observations out to  $R \gtrsim 5R_h$  are generally required (Fig. 14) in order to show a clear preference for one model or the other. In such cases  $R_h$  is very well constrained by the data themselves and must be reproduced by essentially *any* model fit. When Wilson- and King-model fits have comparable  $\chi^2$ , on the other hand, it occasionally happens that their  $R_h$  values differ by factors of 2.5–3. When this occurs, it is most often because  $R_{\text{last}}/R_h$  is of order 1 or smaller, meaning that few if any data are available at large cluster radii to constrain the very different extrapolations of the two types of model. It then becomes unclear which  $R_h$  is correct—although Fig. 15 shows that our estimated errorbars in these cases are also larger than average, properly signaling the problem.

The bottom panels of Fig. 15 are all very similar. The predicted central velocity dispersions for these clusters are (except for NGC 2005 and R 136) the same to within  $\sim 1\%$ , on average, whether Wilson or King models are fit (and regardless of which is the better fit); total cluster luminosities are

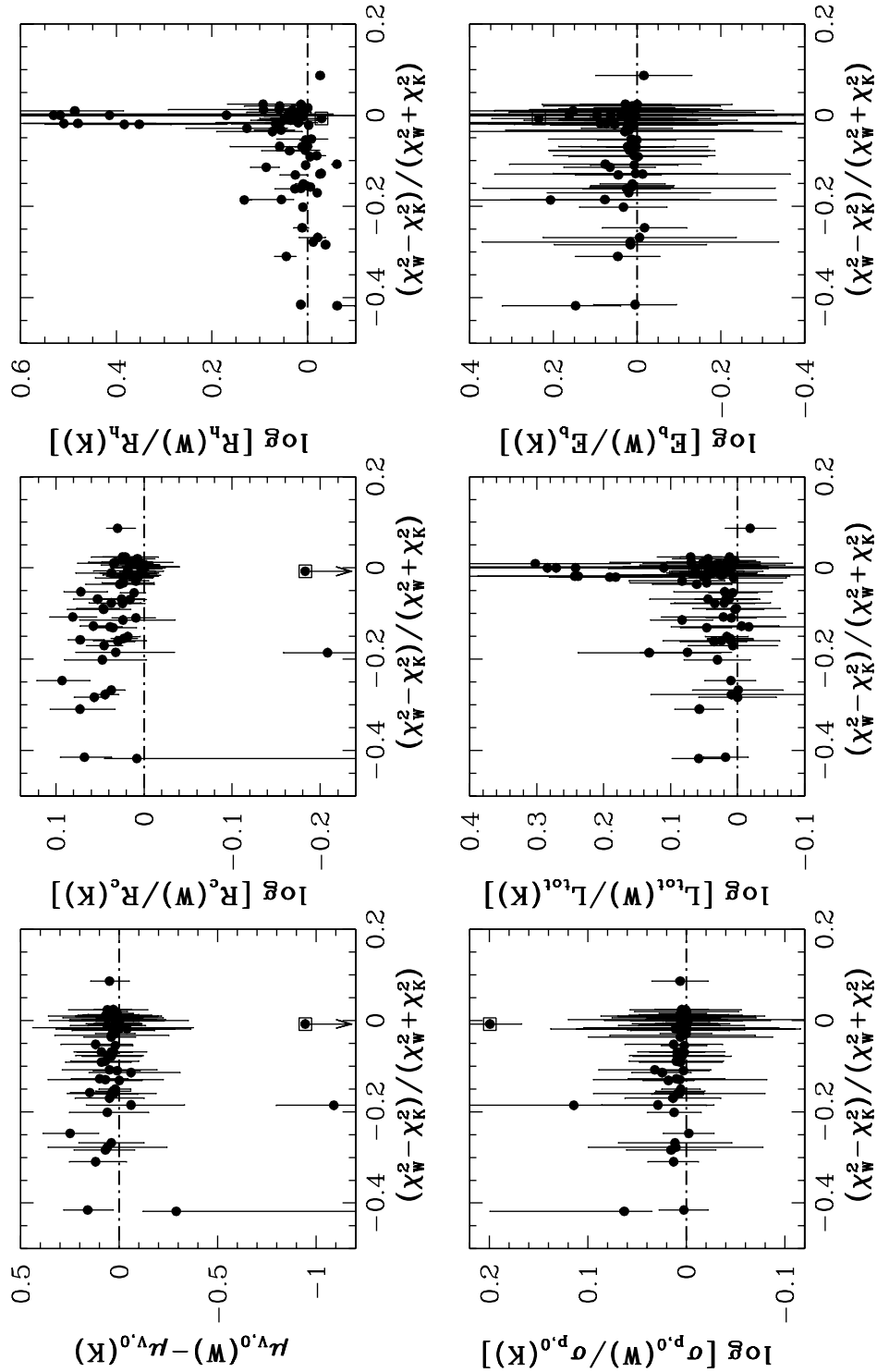


FIG. 15. — Comparison of physical cluster properties derived from Wilson-model fits to LMC, SMC, and Fornax clusters, vs. those derived from King-model fits. The point enclosed in a square in every panel is the LMC globular cluster NGC 205. See text for details.

about as well determined as the cluster half-light radii (with the same potential for some large Wilson–King discrepancies and large errorbars when the two models have comparable  $\chi^2$  values); and global cluster binding energies differ by  $< 5\%$  on average between the two models.

Figure 16 is analogous to Fig. 15 but compares the fits of power laws to those of Wilson models for the MG03 cluster set. NGC 205 is again enclosed by an open square in every panel, and the rightmost datapoint is R 136 = 30 Dor. Similar comments apply to these comparisons as to the previous

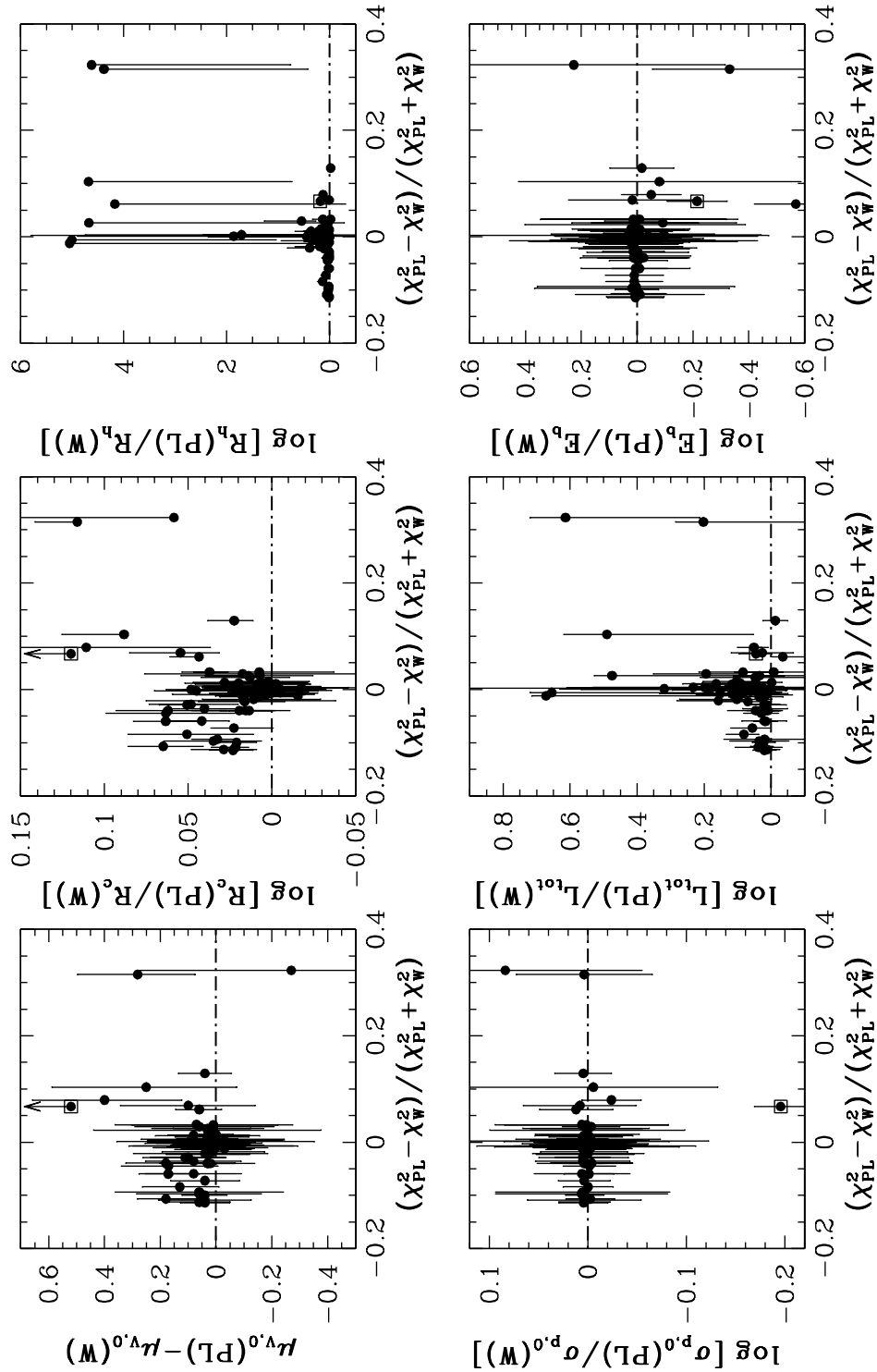


FIG. 16. — Comparison of physical cluster properties derived from power-law model fits to LMC, SMC, and Fornax clusters, vs. those derived from Wilson-model fits. The point enclosed in a square in every panel is the LMC globular cluster NGC 2005. See text for details.

ones, with the important exception that the half-light radii implied by power-law fits can sometimes be *orders of magnitude larger* than the  $R_h$  obtained from Wilson- or King-model fits. This reflects a fundamental difficulty with power-law models: extrapolation of a fit which happens to fall too near  $\gamma = 3$  over

some available (too small) range of data is barely convergent (see eq. [2]) and clearly unphysical. Nevertheless, our estimated errorbars on  $R_h$  (and on  $L_{\text{tot}}$ ) even for unrealistic power-law fits such as these do reasonably reflect the situation. And in many of the cases seen here, the power-law fit is, after all,

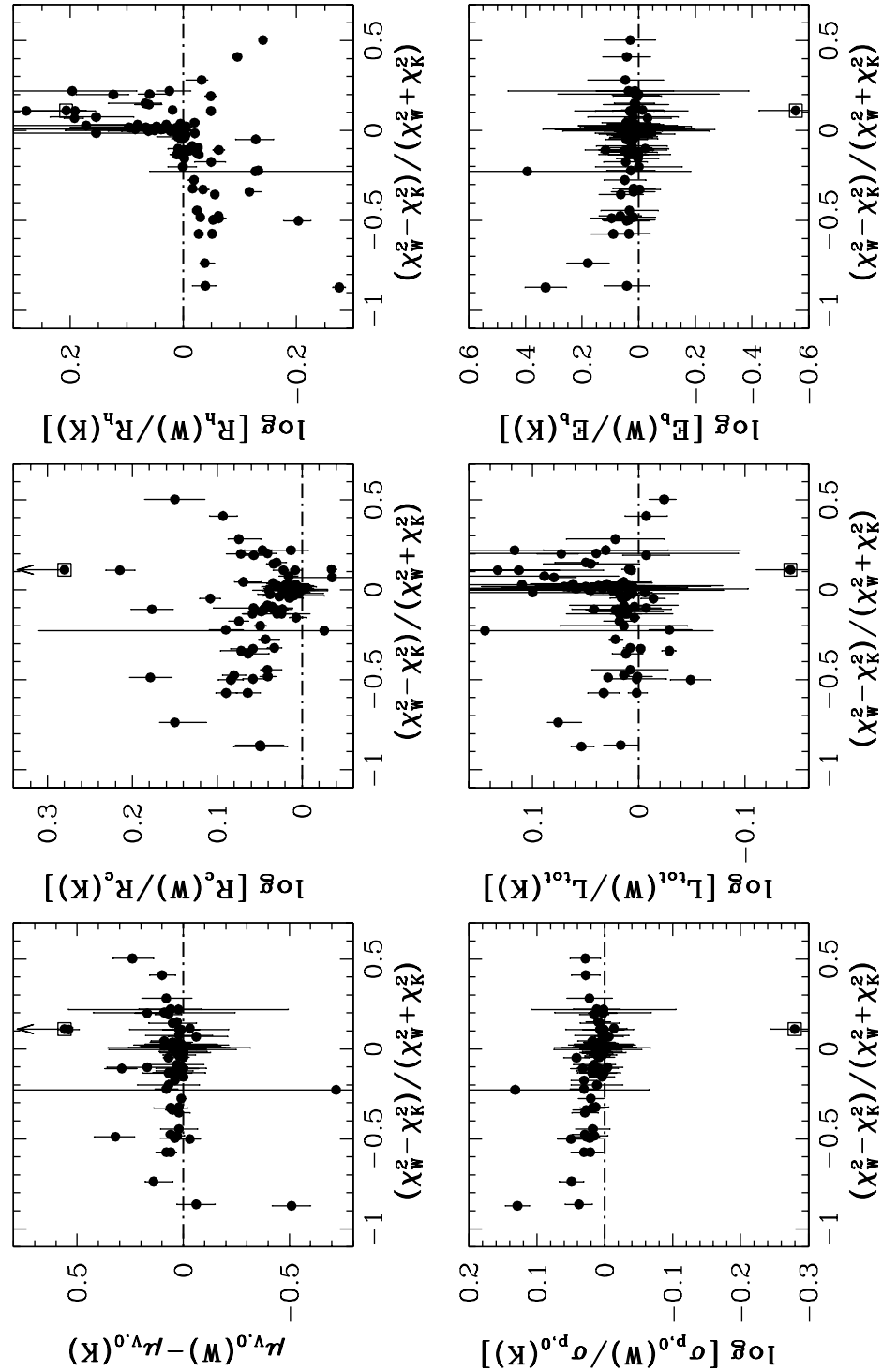


FIG. 17.— Comparison of physical cluster properties derived from Wilson-model fits to Galactic globular clusters, vs. those derived from King-model fits. The point enclosed in a square in every panel is Palomar 1. See text for details.

measurably worse ( $\Delta > 0$ ) than the best Wilson-model fit.

Figure 17 next compares the King and Wilson fit parameters for Galactic globular clusters. The point enclosed in an open square in every panel is Palomar 1, which has  $\mu_{V,0}(W) - \mu_{V,0}(K) = 5.81$  and  $\log[R_c(W)/R_c(K)] = 1.74$  as a

result of the much higher concentration of the King model fit in this case (see Fig. 12 and recall the discussion around Fig. 13 above). The other main outliers in the upper left-hand panel of Fig. 17 are NGC 5272 = M 3, at  $\Delta = -0.87$  and  $\mu_{V,0}(W) - \mu_{V,0}(K) = -0.51$ , and Palomar 2, at  $\Delta = -0.23$

and  $\mu_{V,0}(\text{W}) - \mu_{V,0}(\text{K}) = -0.72$  with a large errorbar. Aside from these objects, Wilson fits to Galactic GCs tend to imply central surface brightnesses slightly fainter than King-model fits, but by only 0.02 mag on average and less than  $\simeq 0.1$  mag in most cases. Wilson models are also associated with slightly larger projected half-intensity radii  $R_c$  and smaller half-light radii  $R_h$ , and thus relatively lower concentrations as measured by the ratio  $R_h/R_c$ . This is simply a result of the more extended cluster structure essentially assumed *ab initio* in the model. It is apparent again that the disagreement between King- and Wilson-model estimates of  $R_h$ , and subsequently  $L_{\text{tot}}$ , is potentially largest when the two models fit a given cluster about equally well. As above, equal-quality fits with disparate  $R_h$  typically occur when the available cluster data do not extend far enough in clustercentric radius to definitively constrain the large- $R$  extrapolation of either model; but our estimated uncertainties on the derived quantities generally reflect this. The predicted central velocity dispersion and global cluster binding energy are as well-behaved as in our LMC/SMC/Fornax cluster fits.

Finally, in Fig. 18 we compare the extrapolated tidal radii from King- and Wilson-model fits to 37 of the LMC, SMC, and Fornax clusters (top panel) and 43 Milky Way globulars (bottom panel). We have only included clusters in these graphs if they have  $R_{\text{last}}/R_h \geq 4$ —so that the extrapolations of the fits to  $r_t$  are constrained as well as possible—and  $\Delta = (\chi^2_{\text{Wilson}} - \chi^2_{\text{King}})/(\chi^2_{\text{Wilson}} + \chi^2_{\text{King}}) \leq 0.1$ —in which case Wilson (1975) spheres fit the surface-brightness data at least as well as King (1966) models.

What we have actually plotted in Fig. 18 is the mass-normalized tidal radius evaluated for each of these clusters within each of the two model fits:  $r_t M_{\text{tot}}^{-1/3}$ , the inverse cube root of the average cluster density. This quantity is related directly to the tidal field in which a cluster is embedded; most simply, in the case of a cluster at radius  $r_{\text{gc}}$  in a spherical galaxy,  $M_{\text{tot}}/r_t^3 \propto M_{\text{gal}}(r_{\text{gc}})/r_{\text{gc}}^3$ . Ideally, we would like to compare estimates of  $r_t M_{\text{tot}}^{-1/3}$  from fits of structural models, to the value expected for any cluster in a given galactic tidal field (in order, for example, to assess whether an extended cluster halo is “unbound;” cf. §4.3.2). However, to do this requires detailed knowledge of the parent galaxy mass profile  $M(r_{\text{gc}})$  (including dark matter); of the instantaneous three-dimensional position of the cluster,  $r_{\text{gc}}$ ; and of the shape and energy of the cluster orbit, which together set the coefficient connecting the mean cluster density to the average galaxy density at  $r_{\text{gc}}$  (e.g., King 1962; Innanen, Harris, & Webbink 1983). Estimating all of these quantities individually for each object in our sample is clearly out of the question, and even a statistical treatment of the cluster ensemble in each galaxy (such as in Innanen, Harris, & Webbink 1983) is beyond the scope of our analysis.

We simply point out that—as expected—the mass-normalized tidal radii implied by the Wilson-model fits to our clusters are systematically larger than those implied by King-model fits. The dotted line in each panel of Fig. 18 indicates equality between the Wilson and King values for  $r_t M_{\text{tot}}^{-1/3}$ , while the bolder, dash-dot lines show the median ratios of the two estimates:  $\simeq 2.9$  in the LMC/SMC/Fornax sample, and  $\simeq 2.5$  for the Milky Way globular clusters. We emphasize again that each of the points plotted represents a cluster which is fit *at least as well or better* by a Wilson sphere vs. a King model. But the question remains open as to whether the limiting radii (or mean densities) of the former models are quan-

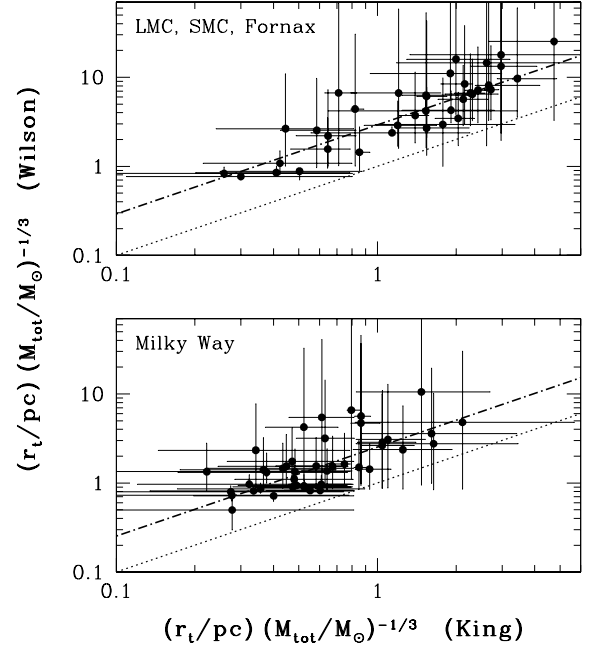


FIG. 18.— Mass-normalized tidal radii inferred from Wilson-model fits, vs. those from King-model fits, for 37 clusters in the LMC, SMC, and Fornax (top panel) and 43 globular clusters in the Milky Way (bottom panel). Only clusters with  $R_{\text{last}}/R_h \geq 4$  and  $\Delta = (\chi^2_{\text{Wilson}} - \chi^2_{\text{King}})/(\chi^2_{\text{Wilson}} + \chi^2_{\text{King}}) \leq 0.1$  are plotted. Dotted line in each panel indicates equality,  $r_t M_{\text{tot}}^{-1/3}(\text{Wilson}) = r_t M_{\text{tot}}^{-1/3}(\text{King})$ . Bolder, dash-dot lines are at the median ratios  $r_t M_{\text{tot}}^{-1/3}(\text{Wilson})/r_t M_{\text{tot}}^{-1/3}(\text{King}) = 2.9$  for the LMC/SMC/Fornax sample, and  $r_t M_{\text{tot}}^{-1/3}(\text{Wilson})/r_t M_{\text{tot}}^{-1/3}(\text{King}) = 2.5$  for the Milky Way globulars.

titatively consistent with a naive association of *fitted*  $r_t$  values with the *true* tidal radii of the real clusters. The large errorbars on both King and Wilson values of  $r_t M_{\text{tot}}^{-1/3}$  for all the clusters in Fig. 18 only stress further the difficulty of precision work along these lines. Even for these best-observed clusters,  $r_t$  is almost always inferred from extrapolation rather than measured directly; it is the most uncertain cluster parameter that we estimate.

##### 5. OBSERVED VELOCITY DISPERSIONS AND DYNAMICAL MASS-TO-LIGHT RATIOS

As we have described, the derivation of total cluster masses (and all the dependent quantities in Table 12 above) from our surface-brightness fits has been facilitated by adopting a mass-to-light ratio for each cluster based on the population-synthesis modeling of §3. This is a necessary step towards examining physical trends and dependences among the properties of star clusters spanning a wide range of ages. It remains to be shown, however, that the population-synthesis models we use predict mass-to-light ratios that are consistent with what can be inferred directly for the minority of clusters which have measured velocity dispersions. Such a demonstration is the purpose of this Section.

To make this check, we have compiled velocity-dispersion data for as many of our modeled LMC, SMC, Fornax, and Milky Way clusters as we could easily find in the published literature. We have not made an attempt at a comprehensive collection, but simply one including enough clusters to address meaningfully the question at hand (in fact, for Milky

Way globulars we have relied exclusively on the work of Pryor & Meylan 1993, which is itself a compilation of earlier studies). A drawback is that very few young Magellanic Cloud clusters have well-determined velocity dispersions: among those in our sample, we have found data only for NGC 1850, 1866, 2157, 2164, and 2214 in the LMC, and NGC 330 in the SMC. Although bright, these objects are usually of relatively low mass compared to the average old GC, and their velocity dispersions are intrinsically low and difficult to measure. Thus, our comparison of population-synthesis and dynamical mass-to-light ratios really speaks most clearly to the old-age limit of the models; but the good results in that limit are encouraging.

Our analysis is detailed in Table 13. After the cluster name, Column (2) of this table repeats the  $V$ -band mass-to-light ratio predicted by population-synthesis models [from Column (6) of Table 8 or Column (2) of Table 12]. Column (3) is the observed velocity dispersion in the cluster, as reported in the literature. Some of these dispersions are based on radial-velocity measurements of individual stars spread throughout the cluster; others, on integrated-light spectroscopy within a finite slit width. Either way, every  $\sigma_{p,obs}$  is in effect a weighted average of the cluster’s projected velocity-dispersion profile over some area on the sky. From the details of each observation in the original papers, we have estimated the effective radius of a circular aperture with roughly the appropriate area. [Note that this is always  $R_{ap} = 0$  for the Milky Way globular clusters, since the observed dispersions in this case have already been extrapolated to their central values by (Pryor & Meylan 1993).] This is reported in Column (4) of Table 13. Column (5) gives the reference to the source of the data.

Given a King, Wilson, or power-law model with fitted  $W_0$  (or  $\gamma$ ) and  $r_0$  for any cluster, solving Poisson’s and Jeans’ equations and projecting along the line of sight yields a dimensionless velocity-dispersion profile,  $\tilde{\sigma}_p = \sigma_p(R)/\sigma_p(R=0)$  as a function of projected clustercentric radius  $R$ . The weighted average  $S^2(R_{ap}) \equiv \left[ \int_0^{R_{ap}} R I(R) \tilde{\sigma}_p^2 dR \right] \left[ \int_0^{R_{ap}} R I(R) dR \right]^{-1}$  then gives the predicted mean-square velocity dispersion within any circular aperture of radius  $R_{ap}$ . We have calculated  $S$  for each of the model fits to each of the clusters in Table 13 given the aperture radii estimated in the table, and obtained the line-of-sight velocity dispersions at the cluster centers as  $\sigma_p(R=0) = \sigma_{p,obs}/S(R_{ap})$ . In general, the value of  $\sigma_p(R=0)$  depends on the model used to compute  $S$ , but the differences in our case are usually small and in Column (6) of Table 13 we report only the mean of our three determinations.

The observed  $\sigma_p(R=0)$  values are to be compared with the predicted  $\sigma_{p,0}$ , based on our population-synthesis  $M/L_V$  ratios for each cluster, in Table 12. As described above for the calculation of these predictions, our fitted models with known  $W_0$  or  $\gamma$  also provide the dimensionless ratio  $\sigma_p(R=0)/\sigma_0$ , for  $\sigma_0$  the theoretical scale velocity appearing in equation (4). We therefore compute  $\sigma_0$  and use our fitted  $r_0$  (Table 10) in equation (4) to compute the central mass density  $\rho(r=0)$  of every cluster in Table 13. A “dynamical” estimate of the  $V$ -band mass-to-light ratio follows immediately as  $\Upsilon_V^{dyn} \equiv \rho(r=0)/j_0$ , with the luminosity density  $j_0$  taken from Table 11. Our estimates of  $\Upsilon_V^{dyn}$  for every model fit, and the comparisons  $\Delta(\log \Upsilon_V) = \log(\Upsilon_V^{dyn}/\Upsilon_V^{pop})$ , constitute the rest of Table 13.

Inspection of Table 13 shows, first, that the dynamical esti-

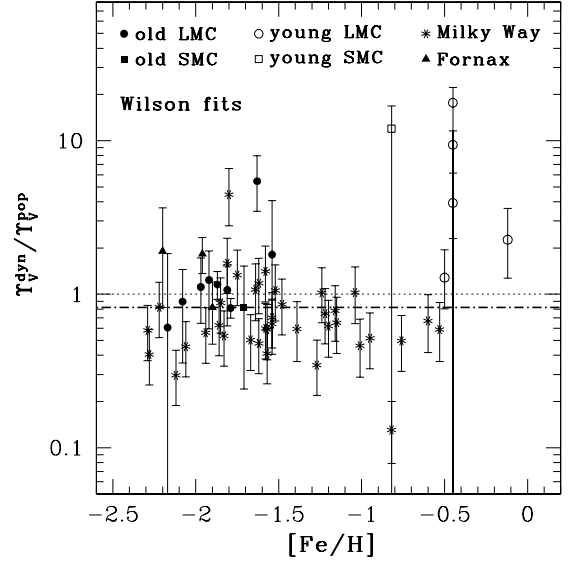


FIG. 19.— Ratio of dynamical  $V$ -band mass-to-light ratio to population-synthesis model prediction, as a function of cluster metallicity, for all clusters with measured central velocity dispersions in Table 13. The dynamical  $\Upsilon_V$  used are those calculated from  $\sigma_{p,obs}$  using Wilson-model structural fits to each cluster. Population-synthesis mass-to-light ratios are those predicted by the model of Bruzual & Charlot (2003) using the disk-star IMF of Chabrier (2003). The bold, dash-dot line indicates the median  $\Upsilon_V^{dyn}/\Upsilon_V^{pop} = 0.82$ , which has a standard error of  $\simeq \pm 0.07$ .

mates of  $\Upsilon_V$  are generally very model-independent. The single greatest exception is NGC 2005 in the LMC, the cluster for which our Wilson-model fit has a much higher central surface brightness and smaller scale radius, and thus a smaller inferred mass-to-light ratio, than the King- or power-law model fits (see Fig. 15 and Fig. 12). Second, the comparison between  $\Upsilon_V^{dyn}$  and  $\Upsilon_V^{pop}$  is favorable. Figure 19 shows this graphically, with the ratio of the two mass-to-light values plotted as a function of cluster metallicity (from Table 8 above). For definiteness, the results for  $\Upsilon_V^{dyn}$  from our Wilson modeling have been used in this plot, but it makes no significant difference if the King- or power-law model numbers are used instead. In all cases, the median  $\Upsilon_V^{dyn}/\Upsilon_V^{pop} \simeq 0.82 \pm 0.07$ .

The few young massive clusters in the LMC and SMC for which we have obtained dynamical mass-to-light estimates are shown as open symbols in Fig. 19. Although these tend to fall nominally above the line  $\Upsilon_V^{dyn} = \Upsilon_V^{pop}$ , their measured  $\sigma_{p,obs}$  in Table 13 are relatively uncertain, as our associated errorbars attest. In fact, in three of the six cases only *upper limits* to  $\sigma_{p,obs}$  are given by the original authors. All other points in Fig. 19 refer to old ( $\tau > 10^{10}$  yr) globular-type clusters and, as mentioned above, provide a direct check only on that extreme of the population-synthesis models. Overall, however, we feel confident that our use of  $\Upsilon_V^{pop}$  in general to infer mass-based cluster properties from simple surface-brightness modeling is well justified.

## 6. $\kappa$ -SPACE PARAMETERS AND GALACTOCENTRIC DISTANCES

We anticipate a main use of our results in Tables 10, 11, and 12 above to be in the definition and interpretation of correla-

tions between the primary physical properties of star clusters. Ultimately, such correlations can constrain theories of cluster formation and evolution. They have been identified and discussed in many forms in the literature for old, globular clusters in the Milky Way and a few other galaxies. So far as we are aware, our work here is the first to allow for systematic investigation of the effects of fitting GCs with models other than that of King (1966). It is also the first to put a significant number of young massive clusters on a completely equal footing with the old globulars.

Correlations among GCs are typically couched in terms of a structural “fundamental plane” analogous to that originally defined by Djorgovski & Davis (1987) and Dressler et al. (1987) for dynamically hot galaxies. There are at least three *equivalent* formulations of the globular cluster fundamental plane in the literature:

First, Djorgovski (1995) presents strong bivariate correlations involving  $\sigma_{p,0}$ ,  $r_0$ ,  $\mu_{V,0}$ ,  $R_h$ , and  $\langle\mu_V\rangle_h$ , showing Galactic GCs to be an essentially two-parameter family.

Second, McLaughlin (2000) works with  $\Upsilon_V$ ,  $L_{\text{tot}}$ , King-model  $c$ , and global binding energy  $E_b$  to arrive, in different form and with different physical emphasis, at the same basic conclusion. McLaughlin shows explicitly the equivalence between his and Djorgovski’s formulations of the GC fundamental plane. In either, the Galactocentric positions  $R_{\text{gc}}$  of the globulars are an important external influence; it is well known, for example, that GC half-mass radii and binding energies correlate significantly with their location in the Galaxy ( $R_h \propto R_{\text{gc}}^{0.4}$  and  $E_b \propto R_{\text{gc}}^{0.4}$ ; van den Bergh, Morbey, & Pazder 1991; McLaughlin 2000).

To bring young massive clusters, such as those we have modeled in the LMC and SMC, into analyses along these lines, it is preferable to work in terms of  $M_{\text{tot}}$ ,  $\Sigma_0$ , and  $\Sigma_h$ —rather than their luminosity or surface-brightness equivalents—so as to avoid purely age-related effects. All but one of the required fundamental-plane variables for our full cluster sample are then given in Tables 10 through 12 above. The last—cluster positions within their parent galaxies—is listed in Table 14, discussed below.

A third equivalent formulation of the fundamental plane is that of Bender, Burstein, & Faber (1992) and Burstein et al. (1997), who manipulate the basic observables of velocity dispersion, surface density, and half-mass radius to define an orthonormal set of derived parameters,

$$\begin{aligned}\kappa_1 &\equiv (\log \sigma_{p,0}^2 + \log R_h) / \sqrt{2} \\ \kappa_2 &\equiv (\log \sigma_{p,0}^2 + 2 \log \Sigma_h - \log R_h) / \sqrt{6} \\ \kappa_3 &\equiv (\log \sigma_{p,0}^2 - \log \Sigma_h - \log R_h) / \sqrt{3}\end{aligned}\quad (5)$$

and find tight distributions in  $\kappa_3$  vs.  $\kappa_1$  for early-type galaxies and (separately) for globular clusters. Bender, Burstein, & Faber (1992) and Burstein et al. (1997) actually define this “ $\kappa$  space” using the luminosity intensity  $I_h$  averaged over the half-light radius  $R_h$ ; but in order to remove the influence of age from comparisons of cluster structures, we instead use the average mass density  $\Sigma_h = \Upsilon_V I_h = M_{\text{tot}} / 2\pi R_h^2$ . Then  $\kappa_1 \leftrightarrow \log(\sigma_{p,0}^2 R_h)$  is related to the total mass of a system, and  $\kappa_3 \leftrightarrow \log(\sigma_{p,0}^2 R_h / M_{\text{tot}})$  contains the exact details of this relationship—that is, information on the internal density profile. In fact, the mass-based  $\kappa_3$  of equation (5) can be viewed as a replacement for King- or Wilson-model concentrations  $c$  or power-law indices  $\gamma$ , or any other model-specific shape parameter. As such, any trends involving  $\kappa_3$  are directly of relevance to questions

concerning cluster (non)homology. The definition of  $\kappa_2$  is chosen simply to make the three  $\kappa$  parameters mutually orthogonal; it results in the correspondence  $\kappa_2 \leftrightarrow \log(\Sigma_h^3)$  (see Bender, Burstein, & Faber 1992, for further discussion).

Table 14 gives the values of  $\kappa_1$ ,  $\kappa_2$ , and  $\kappa_3$  for all the young and globular clusters that we fit with structural models in §4.2. In calculating these parameters, we have used the  $\sigma_{p,0}$  and  $\Sigma_h$  values as predicted in Table 12 by our adoption of population-synthesis mass-to-light ratios. Equations (5) are evaluated for  $\sigma_{p,0}$  in units of  $\text{km s}^{-1}$ ,  $\Sigma_h$  in  $M_\odot \text{pc}^{-2}$ , and  $R_h$  in kpc (following Bender et al. and Burstein et al., who originally had galaxies in mind).

Table 14 also contains the observed distance, in kpc, of each cluster from the center of its parent galaxy. These are projected galactocentric radii for the LMC, SMC, and Fornax clusters, and three-dimensional radii for the Milky Way globular clusters. For the Galactic GCs, we have simply copied  $R_{\text{gc}}$  directly from the catalogue of Harris (1996). For the LMC, SMC, and Fornax clusters, we have computed  $R_{\text{gc}}$  ourselves, using the right ascensions and declinations of the clusters as given by Mackey & Gilmore (2003a,b,c) and taking the galaxy centers to be

$$\begin{aligned}\alpha_{2000} &= 5^{\text{h}}25^{\text{m}}6^{\text{s}} & \delta_{2000} &= -69^\circ47' & (\text{LMC}) \\ \alpha_{2000} &= 0^{\text{h}}52^{\text{m}}45^{\text{s}} & \delta_{2000} &= -72^\circ49'43'' & (\text{SMC}) \\ \alpha_{2000} &= 2^{\text{h}}39^{\text{m}}59^{\text{s}}.3 & \delta_{2000} &= -34^\circ26'57'' & (\text{Fornax}).\end{aligned}\quad (6)$$

The HI and optical centers of the LMC are offset from each other, and here we have more or less arbitrarily adopted the optical center of the bar from van der Marel (2001). The SMC center is taken from Westerlund (1997), and the Fornax center from SIMBAD. In converting angular distances to kpc, we assume a constant distance of 50.1 kpc to all clusters in the LMC; 60.0 kpc to the SMC; and 137 kpc to Fornax.

## 7. SUMMARY

We have fit three distinct dynamical models to V-band surface-brightness profiles for each of 68 massive star clusters (50 of which have young ages, between several Myr and a few Gyr) in the LMC, SMC, and Fornax dwarf spheroidal, and to 85 old globular clusters in the Milky Way. We have also applied publicly available population-synthesis models to infer the expected intrinsic  $(B-V)_0$  colors (and thus reddenings) and V-band mass-to-light ratios for all of these clusters plus another 63 Galactic globulars. Combining these with the surface-brightness model fits, we have calculated a wide range of structural and dynamical parameters characterizing the clusters. Our main results are contained in Tables 8, 10, 11, 12, and 14 above. We have also taken velocity-dispersion measurements from the literature for a subset of the full cluster sample and calculated dynamical mass-to-light ratios for comparison with the predicted population-synthesis values. The results of this are in Table 13, which shows quite good agreement in general.

The V-band surface-brightness data we have employed for LMC, SMC, and Fornax star clusters derive primarily from HST-based starcounts made in the inner regions by Mackey & Gilmore (2003a,b,c, collectively MG03). We have supplemented these wherever possible with ground-based starcounts and  $BV$  aperture photometry from the literature, both to extend the MG03 cluster profiles to larger projected radii and to re-calibrate the V-band magnitude scale of MG03. This re-calibration turns out to be rather significant, amounting to several tenths of a magnitude (in the sense that the surface brightnesses published in MG03 are generally too faint)



in many cases. Full details of our analyses on the 68 MG03 clusters are in §2.1; the re-calibrated surface-brightness profiles, with all ground-based data properly incorporated, are given in Table 5. All surface-brightness profiles for Milky Way globular clusters were taken from the database constructed by Trager, King, & Djorgovski (1995), with only minor modifications described in §2.2.

Our population-synthesis modeling, which includes a comparison of results from two separate codes (Bruzual & Charlot 2003; Fioc & Rocca-Volmerange 1997) using a variety of assumed stellar IMFs, is described in §3. Table 8 lists intrinsic cluster colors and theoretical mass-to-light ratios obtained with six different code+IMF combinations, although for our subsequent modeling (requiring estimates of cluster *V*-band extinctions and conversions between luminosity and mass) we adopted numbers from the code of Bruzual & Charlot (2003) using the disk-star IMF of Chabrier (2003). As described in §3.2, we have thus obtained systematically lower predicted mass-to-light ratios, at any age, than MG03 inferred for their LMC/SMC/Fornax clusters. Our values nevertheless compare well with the dynamical mass-to-light ratios calculated directly from velocity-dispersion measurements for 57 clusters (mostly old globulars) in §5. Additionally, our model-based extinctions agree very well with direct measurements for the old globular clusters in the Galaxy and the Fornax dwarf.

The three models that we fit to each cluster are described in some detail in §4, which also contains the fits themselves and the bulk of our derived structural and dynamical parameters. The models are: (1) the single-mass, isotropic, modified isothermal sphere of King (1966); (2) an asymptotic power law with a constant-density core; and (3) an alternate modification of the isothermal sphere (still single-mass and isotropic) based on the stellar distribution function developed by Wilson (1975). For otherwise similar clusters (e.g., given a fixed total luminosity, central surface brightness, and effective radius), Wilson (1975) spheres are spatially more extended than King (1966) models, although both have finite tidal radii; the untruncated power-law models we fit are formally infinite in extent and, in some cases, barely convergent in their integrated properties. Even so, the structural differences between these models are most important at relatively large cluster-centric distances, in the outer halos beyond a few effective radii. As a result, we have verified (§4.3) that for *most* clusters, *most* of the physical properties we have calculated are reasonably well constrained no matter which particular model is taken to fit the surface-brightness data.

We have looked with particular interest at the question of which of the three fits—the spatially limited King model; a more extended but still finite Wilson sphere; or an infinite power-law model—provides the best description of these clusters in a  $\chi^2$  sense (see §4.3.2). *All* of the 68 LMC, SMC, and Fornax clusters from MG03 are fit *at least* as well, and in several cases significantly better, by the larger envelopes of Wilson (1975) models rather than the more compact King (1966) models. This is true for the 18 old globular clusters

as well as of the 50 younger objects in this sample. It also holds for the majority ( $\approx 70/85$ ) of the old Galactic globulars to which we have fit all three models; a particularly clear example is provided by  $\omega$  Centauri (§4.2.1). In all cases, asymptotic power laws are not vast improvements over the Wilson-model fits; in fact, they are somewhat worse for many clusters.

In the LMC, SMC, and Fornax sample especially (where the surface-brightness data are most homogeneous), there is no correlation between cluster age and the relative quality of fit for King vs. Wilson or power-law models. Instead, we have shown that the primary factor in determining whether an extended-halo model describes a cluster better than a King (1966) model is simply the spatial extent of the available surface-brightness data being fit. Specifically, it is only when a cluster’s observed density profile reaches to more than  $\sim 4$ –5 effective radii that it becomes possible to decide conclusively whether or not it has a non-King envelope structure; and when such data do exist, a more distended but finite Wilson model is most often the better option of the three we have examined—whatever the cluster age.

Thus, we conclude that the extended halos which are known to surround many young massive star clusters in the Magellanic Clouds and other galaxies *do not require* description by untruncated power laws which would necessarily have all the clusters overfill the Roche lobes defined by their parent galaxies (see Elson, Fall, & Freeman 1987; Larsen 2004; Schweizer 2004)—although whether or not this does happen in individual cases is a complicated question that we have not undertaken to address here. More generally, despite the ad hoc nature of the Wilson and power-law models that we have fit, it is a clear fact that self-gravitating clusters *commonly* have envelope structures which do not match the extrapolations of simple King (1966) models fitting the cluster cores. This phenomenon is not confined exclusively to young clusters and is not obviously only transient; it may point instead to generic, internal cluster physics not captured by King’s stellar distribution function.

This interesting issue aside, the work we have presented provides the basic information required to define and compare physical parameter correlations and the fundamental plane(s) of young and old massive star clusters in the Milky Way, LMC, SMC, and Fornax. It also offers a starting point for careful examination of potential model-dependent artifacts in these correlations, and ultimately it should allow for direct contact to be made with the well-established fundamental plane of elliptical galaxies and bulges. We plan to address these issues in future work.

We thank Dougal Mackey for providing his LMC, SMC, and Fornax cluster data to us in electronic form, and for helpful discussions. Support for this work was provided by NASA through a grant associated with HST project 10323, awarded by STScI, which is operated by AURA, Inc., under NASA contract NAS 5-26555.

## REFERENCES

- Anderson, A. J. 1997, PhD Thesis, University of California at Berkeley  
 Barmby, P., Holland, S., & Huchra, J. P. 2002, *AJ*, 123, 1937  
 Bellazzini, M. 1998, *New A*, 3, 219  
 Bender, R., Burstein, D., & Faber, S. M. 1992, *ApJ*, 399, 462  
 Bernard, A. 1975, *A&A*, 40, 199  
 Bernard, A., & Bigay, J. H. 1974, *A&A*, 33, 123  
 Bica, E., Claria, J. J., Dottori, H., Santos, J. F. C., & Piatti, A. E. 1996, *ApJS*, 102, 57  
 Binney, J., & Tremaine, S. 1987, *Galactic Dynamics* (Princeton:Princeton University Press)  
 Böker, T., Sarzi, M., McLaughlin, D. E., van der Marel, R. P., Rix, H.-W., Ho, L. C., & Shields, J. C. 2004, *AJ*, 127, 105  
 Bruzual, G., & Charlot, S. 2003, *MNRAS*, 344, 1000  
 Burstein, D., Bender, R., Faber, S., & Nolthenius, R. 1997, *AJ*, 114, 1365  
 Chabrier, G. 2003, *PASP*, 115, 763  
 Chrysovergis, M., Kontizas, M., & Kontizas, E. 1989, *A&AS*, 77, 357

- Da Costa, G. S., & Freeman, K. C. 1976, *ApJ*, 206, 128
- de Vaucouleurs, G., & Ables, H. D. 1970, *ApJ*, 159, 425
- Djorgovski, S. 1993, in *Structure and Dynamics of Globular Clusters*, ASP Conf. Ser. 50, ed. S. G. Djorgovski and G. Meylan (San Francisco:ASP), p. 373
- Djorgovski, S. 1995, *ApJ*, 438, 29
- Djorgovski, S., & Davis, M. 1987, *ApJ*, 313, 59
- Djorgovski, S., & Meylan, G. 1994, *AJ*, 108, 1292
- Djorgovski, S. G., Gal, R. R., McCarthy, J. K., Cohen, J. G., de Carvalho, R. R., Meylan, G., Bendinelli, O., & Parmeggiani, G. 1997, *ApJ*, 474, L19
- Dressler, A., Lynden-Bell, D., Burstein, D., Davies, R. L., Faber, S. M., Terlevich, R., & Wegner, G. 1987, *ApJ*, 313, 42
- Dubath, P., & Grillmair, C. J. 1997, *A&A*, 321, 379
- Dubath, P., Meylan, G., & Mayor, M. 1992, *ApJ*, 400, 510
- Dubath, P., Meylan, G., & Mayor, M. 1997, *A&A*, 324, 505
- Elson, R. A. W., Fall, S. M., & Freeman, K. C. 1987, *ApJ*, 323, 54
- Feast, M. W., & Black, C. 1980, *MNRAS*, 191, 285
- Fioc, M., & Rocca-Volmerange, B. 1997, *A&A*, 326, 950
- Fischer, P., Welch, D. L., & Mateo, M. 1993, *AJ*, 105, 938
- Fischer, P., Welch, D. L., Côté, P., Mateo, M., & Madore, B. F. 1992, *AJ*, 103, 857
- Gordon, K. C., & Kron, G. E. 1983, *PASP*, 95, 461
- Gunn, J. E., & Griffin, R. F. 1979, *AJ*, 84, 752
- Harris, W. E. 1996, *AJ*, 112, 1487
- Harris, W. E., Harris, G. L. H., Holland, S. T., & McLaughlin, D. E. 2002, *AJ*, 124, 1435
- Hodge, P. W. 1965, *ApJ*, 141, 308
- Hodge, P. W. 1969, *PASP*, 81, 875
- Holland, S., Côté, P., & Hesser, J. E. 1999, *A&A*, 348, 418
- Hunter, C. 1977, *AJ*, 82, 271
- Hunter, D. A., Shaya, E. J., Holtzman, J. A., Light, R. M., O'Neil, E. J., & Lynds, R. 1995, *ApJ*, 448, 179
- Innanen, K. A., Harris, W. E., & Webbink, R. F. 1983, *AJ*, 88, 338
- Kaisler, D., Harris, W. E., & McLaughlin, D. E. 1997, *PASP*, 109, 920
- King, I. R. 1962, *AJ*, 67, 471
- King, I. R. 1965, *AJ*, 70, 376
- King, I. R. 1966, *AJ*, 71, 64
- King, I. R. 1988, *PASP*, 100, 999
- Kontizas, E., & Kontizas, M. 1983, *A&AS*, 52, 143
- Kontizas, M., Chrysovergis, M., & Kontizas, E. 1987, *A&AS*, 68, 147
- Kontizas, M., Danezis, E., & Kontizas, E. 1982, *A&AS*, 49, 1
- Kontizas, M., Hadjidimitriou, D., & Kontizas, E. 1987, *A&AS*, 68, 493
- Kroupa, P., Tout, C. A., & Gilmore, G. 1993, *MNRAS*, 262, 545
- Lang, K. R. 1999, *Astrophysical Formulae* (Berlin:Springer-Verlag)
- Larsen, S. S. 2002, *A&A*, 416, 537
- Larsen, S. S., Brodie, J. P., Sarajedini, A., & Huchra, J. P. 2002, *AJ*, 124, 2615
- Lupton, R. H., Fall, S. M., Freeman, K. C., & Elson, R. A. W. 1989, *ApJ*, 347, 201
- Mackey, A. D., & Gilmore, G. F. 2003a, *MNRAS*, 338, 85 (MG03)
- Mackey, A. D., & Gilmore, G. F. 2003b, *MNRAS*, 338, 120 (MG03)
- Mackey, A. D., & Gilmore, G. F. 2003c, *MNRAS*, 340, 175 (MG03)
- Martini, P., & Ho, L. C. 2004, *ApJ*, 610, 233
- Mateo, M. 1987, *ApJ*, 323, 41
- Mateo, M., Welch, D. L., & Fischer, P. 1991, in *The Magellanic Clouds*, IAU Symposium 148, ed. R. Haynes and D. Milne (Dordrecht:Kluwer), p. 191
- McLaughlin, D. E. 2000, *ApJ*, 539, 618
- McLaughlin, D. E., & Meylan, G. 2003, in *New Horizons in Globular Cluster Astronomy*, ASP Conf. Ser. 296, ed. G. Piotto, G. Meylan, G. Djorgovski, and M. Riello (San Francisco:ASP), p. 153
- Merritt, D., Meylan, G., & Mayor, M. 1997, *AJ*, 114, 1074
- Meylan, G. 1988, *A&A*, 191, 215
- Meylan, G. 1989, *A&A*, 214, 106
- Meylan, G., Mayor, M., Duquenois, A., & Dubath, P. 1995, *A&A*, 303, 761
- Pryor, C., & Meylan, G. 1993, in *Structure and Dynamics of Globular Clusters*, ASP Conf. Ser. 50, ed. S. G. Djorgovski and G. Meylan (San Francisco:ASP), p. 357
- Rodgers, A. W., & Roberts, W. H. 1994, *AJ*, 107, 1737
- Salpeter, E. E. 1955, *ApJ*, 121, 161
- Seitzer, P. O. 1983, PhD Thesis, University of Virginia
- Schweizer, F. 2004, preprint ([astro-ph/0404395](http://arxiv.org/abs/astro-ph/0404395))
- Trager, S. C., King, I. R., & Djorgovski, S. 1995, *AJ*, 109, 218
- van den Bergh, S. 1981, *A&AS*, 46, 79
- van den Bergh, S., Morbey, C., & Pazder, J. 1991, *ApJ*, 375, 594
- van der Marel, R. P. 2001, *AJ*, 122, 1827
- van Leeuwen, F., Le Poole, R. S., Reijns, R. A., Freeman, K. C., & de Zeeuw, P. T. 2000, *A&A*, 360, 472
- Walcher, C. J., van der Marel, R. P., McLaughlin, D., Rix, H.-W., Böker, T., Haering, N., Ho, L. C., Sarzi, M., & Shields, J. C. 2004, *ApJ*, 618, 237
- Webbink, R. F. 1985, in *Dynamics of Star Clusters*, ed. J. Goodman and P. Hut (Dordrecht:Reidel), p. 541
- Westerlund, B. E. 1997, *The Magellanic Clouds* (Cambridge:Cambridge University Press)
- Wilson, C. P. 1975, *AJ*, 80, 175
- Zepf, S. E., Ashman, K. M., English, J., Freeman, K. C., & Sharples, R. M. 1999, *AJ*, 118, 752

#### ONLINE MATERIAL AND FIGURE 12

The next seven pages show extracts from Table 8 and Tables 10–14, which are discussed in §3.2, §4.2.2, §5, and §6. Each of these tables can be downloaded in its entirety, in machine-readable format, from the online edition of the *Astrophysical Journal Supplement Series*, where this paper is published as

McLaughlin, D. E., & van der Marel, R. P. 2005, *ApJS*, 161, 304.

Following the tables is Figure 12 (§4.2.2), which shows the full set of fits to each of the LMC, SMC, Fornax, and Milky Way star clusters that we have modeled in detail. The full-resolution versions of these plots are available on the ApJ website, and also from <http://www.astro.le.ac.uk/~dm131/clusters.html>.

TABLE 8  
POPULATION-SYNTHESIS COLORS AND MASS-TO-LIGHT RATIOS

Cluster (1)	Published Data <sup>a</sup>				SSP Model Code/IMF <sup>b</sup>					
	age (2)	[Fe/H] (3)	(B−V) (4)	Property (5)	BC/ChD (6)	BC/Salp (7)	PEG/ChD (8)	PEG/Salp (9)	PEG/ChGC (10)	PEG/KTG (11)
LMC-HODGE11	10.11	−2.06	0.64	(B−V) <sub>0</sub>	0.594 ± 0.015	0.616 ± 0.014	0.609 ± 0.017	0.626 ± 0.016	0.606 ± 0.017	0.610 ± 0.017
SMC-KRON3	9.78	−1.16	0.68	$\Upsilon_V^{\text{pop}}$	1.893 ± 0.160	3.133 ± 0.226	2.013 ± 0.166	3.279 ± 0.237	1.778 ± 0.126	1.923 ± 0.146
				(B−V) <sub>0</sub>	0.664 ± 0.017	0.675 ± 0.017	0.700 ± 0.021	0.706 ± 0.021	0.699 ± 0.020	0.698 ± 0.021
FORNAX1	10.11	−2.20	0.65	$\Upsilon_V^{\text{pop}}$	1.129 ± 0.113	2.018 ± 0.194	1.281 ± 0.140	2.269 ± 0.240	1.236 ± 0.130	1.312 ± 0.127
				(B−V) <sub>0</sub>	0.579 ± 0.015	0.601 ± 0.015	0.589 ± 0.017	0.608 ± 0.016	0.586 ± 0.017	0.590 ± 0.017
MW-1636-283	10.11	−1.50	...	$\Upsilon_V^{\text{pop}}$	1.915 ± 0.163	3.155 ± 0.228	2.004 ± 0.167	3.249 ± 0.239	1.763 ± 0.127	1.911 ± 0.147
				(B−V) <sub>0</sub>	0.659 ± 0.016	0.678 ± 0.016	0.698 ± 0.025	0.710 ± 0.024	0.694 ± 0.025	0.698 ± 0.025
				$\Upsilon_V^{\text{pop}}$	1.888 ± 0.155	3.169 ± 0.224	2.134 ± 0.187	3.542 ± 0.286	1.914 ± 0.149	2.058 ± 0.170

NOTE. — A machine-readable version of Table 8 is published in its entirety in the electronic edition of the *Astrophysical Journal Supplement Series*; only a portion is shown here, for guidance regarding its form and content.

<sup>a</sup>Column (2) is the logarithm of cluster age in years. Ages, metallicities, and their uncertainties for LMC, SMC, and Fornax clusters are taken from the compilation and analysis by Mackey & Gilmore (2003a,b,c). All ages given as greater than 13 Gyr by Mackey & Gilmore have been re-set here to  $13 \pm 2$  Gyr ( $\log \tau = 10.11 \pm 0.07$ ). Aperture (B−V) colors for LMC, SMC, and Fornax clusters are from the literature summarized in Table 3. Milky Way globular cluster ages are set to a uniform  $13 \pm 2$  Gyr ( $\log \tau = 10.11 \pm 0.07$ ); their metallicities are taken from the catalogue of Harris (1996) and assigned uncertainties of  $\pm 0.2$  dex. (B−V) colors are also from Harris (1996), where available.

<sup>b</sup>Key to the combinations of population-synthesis codes and assumed stellar IMFs: BC/ChD—code of Bruzual & Charlot (2003) using the disk IMF of Chabrier (2003); BC/Salp—code of Bruzual & Charlot (2003) using the Salpeter (1955) IMF; PEG/ChD—PÉGASE v. 2.0 code of Fioc & Rocca-Volmerange (1997) using the disk IMF of Chabrier (2003); PEG/Salp—PÉGASE code using the Salpeter (1955) IMF; PEG/ChGC—PÉGASE code using the Globular Cluster IMF of Chabrier (2003); PEG/KTG—PÉGASE code using the IMF of Kroupa, Tout, & Gilmore (1993).

TABLE 10  
BASIC MODEL FIT PARAMETERS

Cluster (1)	$\Delta\mu_V$ (2)	$A_V$ (3)	$D$ [kpc] (4)	$N_{\text{pts}}$ (5)	weight (6)	model (7)	$\chi^2$ (8)	$W_0 / \gamma$ (9)	$c$ (10)	$\mu_{V,0}$ (11)	$r_0$ [sec] (12)	$r_0$ [pc] (13)
LMC-HODGE11	$-0.23^{+0.05}_{-0.05}$	$0.14^{+0.08}_{-0.08}$	50.1	50	1	K	17.62	$6.0^{+0.6}_{-0.6}$	$1.25^{+0.16}_{-0.14}$	$19.30^{+0.10}_{-0.09}$	$14.42^{+1.17}_{-0.94}$	$3.50^{+0.28}_{-0.23}$
						W	17.06	$6.1^{+0.8}_{-0.7}$	$1.84^{+0.47}_{-0.28}$	$19.32^{+0.09}_{-0.10}$	$15.21^{+1.30}_{-1.24}$	$3.69^{+0.32}_{-0.30}$
						PL	16.73	$3.65^{+0.35}_{-0.25}$	$\infty$	$19.32^{+0.10}_{-0.10}$	$16.52^{+2.40}_{-1.83}$	$4.01^{+0.58}_{-0.44}$
SMC-KRON3	$-0.15^{+0.05}_{-0.05}$	$0.05^{+0.08}_{-0.08}$	60.0	72	1	K	56.99	$5.5^{+0.2}_{-0.2}$	$1.14^{+0.05}_{-0.04}$	$20.04^{+0.10}_{-0.10}$	$23.24^{+1.26}_{-1.31}$	$6.76^{+0.37}_{-0.38}$
						W	67.83	$4.4^{+0.3}_{-0.2}$	$1.27^{+0.08}_{-0.05}$	$20.09^{+0.09}_{-0.10}$	$28.15^{+1.32}_{-1.94}$	$8.19^{+0.38}_{-0.56}$
						PL	87.98	$5.10^{+0.25}_{-0.15}$	$\infty$	$20.13^{+0.09}_{-0.09}$	$37.46^{+2.76}_{-1.75}$	$10.90^{+0.80}_{-0.51}$
FORNAX1	0	$0.22^{+0.08}_{-0.08}$	137.0	51	1	K	31.25	$2.6^{+0.5}_{-0.6}$	$0.61^{+0.08}_{-0.10}$	$23.06^{+0.10}_{-0.10}$	$21.50^{+4.07}_{-2.61}$	$14.28^{+2.70}_{-1.73}$
						W	32.26	$0.1^{+0.7}_{-0.0}$	$0.01^{+0.49}_{-0.00}$	$23.07^{+0.08}_{-0.08}$	$116.30^{+0.00}_{-76.0}$	$77.24^{+0.00}_{-50.5}$
						PL	33.12	$9.75^{+2.45}_{-1.45}$	$\infty$	$23.15^{+0.09}_{-0.09}$	$39.61^{+7.62}_{-5.21}$	$26.31^{+5.06}_{-3.46}$
MW-AM1	0	0	121.9	43	1	K	44.00	$6.6^{+0.4}_{-0.5}$	$1.41^{+0.12}_{-0.13}$	$23.88^{+0.04}_{-0.03}$	$12.11^{+1.16}_{-0.82}$	$7.16^{+0.69}_{-0.49}$
						W	45.52	$6.6^{+0.6}_{-0.7}$	$2.11^{+0.43}_{-0.36}$	$23.90^{+0.04}_{-0.03}$	$12.92^{+1.47}_{-1.13}$	$7.64^{+0.87}_{-0.67}$
						PL	46.16	$3.45^{+0.30}_{-0.20}$	$\infty$	$23.89^{+0.04}_{-0.03}$	$13.43^{+2.35}_{-1.66}$	$7.94^{+1.39}_{-0.98}$

NOTE. — A machine-readable version of Table 10 is published in its entirety in the electronic edition of the *Astrophysical Journal Supplement Series*; only a portion is shown here, for guidance regarding its form and content. Key to columns:

**Column (1)**—Cluster name.

**Column (2)**—Zeropoint correction applied to published  $V$ -band surface brightnesses; see §2 for details.

**Column (3)**— $V$ -band extinction, from population-synthesis modeling for LMC and SMC clusters (Table 8, with  $A_V \equiv 0$  enforced for clusters with observed  $(B - V)$  bluer than model  $(B - V)_0$ ); from Mackey & Gilmore (2003c) for Fornax globular clusters; from Harris (1996) for Galactic GCs.

**Column (4)**—Heliocentric distance

**Column (5)**—Number of surface-brightness datapoints constraining model fits

**Column (6)**—Weighting scheme for model fitting: “l” denotes weighted least-squares fit to surface-brightness data in linear units ( $L_\odot \text{ pc}^{-2}$ ); “s” denotes weighted least-squares fit to surface brightness data in mag arcsec $^{-2}$ ; “u” denotes unweighted least-squares fit to surface brightness data in mag arcsec $^{-2}$ .

**Column (7)**—Identification of fitted model: K=King (1966) model, defined by equation (1); W=isotropic Wilson (1975) model defined by equation (3); PL=power-law with core, defined by equation (2).

**Column (8)**—Minimum  $\chi^2$  for best model fit. For weighting schemes “l” and “s,” this is the unreduced  $\chi^2$  of the best-fitting model; the value per degree of freedom is given by  $\chi^2 / (N_{\text{pts}} - 2)$  with  $N_{\text{pts}}$  in Column (5). For unweighted fits “u,”  $\chi^2$  is actually the rms deviation of observed surface brightness (in  $V$  mag arcsec $^{-2}$ ) from the model profile.

**Column (9)**—For King- and Wilson-model fits, entry is the dimensionless central potential  $W_0$ ; for power-law models, entry is the exponent  $\gamma$  of the asymptotic *three-dimensional* density profile (see eq. [2]).

**Column (10)**—Concentration parameter  $c \equiv \log(r_i / r_0)$  (undefined for power-law models, which have infinite spatial extent).

**Column (11)**—Best-fit central  $V$ -band surface brightness, *after* correction for any zeropoint change in Column (2) and extinction in Column (3).

**Column (12)**—Best-fit model scale radius  $r_0$  in arcsec.

**Column (13)**—Best-fit model scale radius  $r_0$  in pc.

TABLE 11  
DERIVED STRUCTURAL PARAMETERS

Cluster	mod	$\log r_t$ [pc]	$\log R_c$ [pc]	$\log R_h$ [pc]	$\log (R_h/R_c)$	$\log I_0$ [ $L_\odot \text{ pc}^{-2}$ ]	$\log j_0$ [ $L_\odot \text{ pc}^{-3}$ ]	$\log L_{\text{tot}}$ [ $L_\odot$ ]	$V_{\text{tot}}$	$\log I_h$ [ $L_\odot \text{ pc}^{-2}$ ]	$\langle \mu_V \rangle_h$
(1)	(2)	(3)	(4)	(5)	(6)	(7)	(8)	(9)	(10)	(11)	(12)
LMC-HODGE11	K	$1.80^{+0.13}_{-0.11}$	$0.510^{+0.023}_{-0.021}$	$0.843^{+0.063}_{-0.042}$	$0.333^{+0.083}_{-0.065}$	$2.85^{+0.04}_{-0.02}$	$2.03^{+0.05}_{-0.06}$	$4.89^{+0.06}_{-0.05}$	$11.12^{+0.12}_{-0.15}$	$2.41^{+0.06}_{-0.09}$	$20.40^{+0.22}_{-0.15}$
	W	$2.41^{+0.43}_{-0.25}$	$0.518^{+0.020}_{-0.023}$	$0.900^{+0.135}_{-0.063}$	$0.381^{+0.158}_{-0.083}$	$2.84^{+0.04}_{-0.02}$	$2.01^{+0.05}_{-0.05}$	$4.94^{+0.10}_{-0.06}$	$11.00^{+0.15}_{-0.24}$	$2.34^{+0.09}_{-0.19}$	$20.57^{+0.46}_{-0.22}$
	PL	$\infty$	$0.522^{+0.025}_{-0.023}$	$1.039^{+0.259}_{-0.138}$	$0.517^{+0.282}_{-0.163}$	$2.84^{+0.04}_{-0.02}$	$2.01^{+0.05}_{-0.06}$	$5.03^{+0.13}_{-0.10}$	$10.77^{+0.24}_{-0.32}$	$2.16^{+0.19}_{-0.40}$	$21.03^{+0.99}_{-0.48}$
SMC-KRON3	K	$1.97^{+0.02}_{-0.02}$	$0.787^{+0.019}_{-0.021}$	$1.065^{+0.000}_{-0.001}$	$0.278^{+0.021}_{-0.019}$	$2.55^{+0.04}_{-0.02}$	$1.46^{+0.05}_{-0.05}$	$5.10^{+0.04}_{-0.04}$	$11.00^{+0.10}_{-0.09}$	$2.17^{+0.04}_{-0.04}$	$21.00^{+0.10}_{-0.09}$
	W	$2.18^{+0.05}_{-0.03}$	$0.817^{+0.012}_{-0.020}$	$1.039^{+0.000}_{-0.001}$	$0.222^{+0.020}_{-0.012}$	$2.53^{+0.04}_{-0.02}$	$1.40^{+0.05}_{-0.04}$	$5.08^{+0.04}_{-0.04}$	$11.04^{+0.09}_{-0.09}$	$2.20^{+0.04}_{-0.04}$	$20.91^{+0.09}_{-0.09}$
	PL	$\infty$	$0.840^{+0.016}_{-0.011}$	$1.023^{+0.001}_{-0.002}$	$0.183^{+0.013}_{-0.018}$	$2.52^{+0.04}_{-0.02}$	$1.36^{+0.04}_{-0.04}$	$5.07^{+0.04}_{-0.04}$	$11.07^{+0.09}_{-0.09}$	$2.22^{+0.04}_{-0.04}$	$20.86^{+0.09}_{-0.09}$
FORNAX1	K	$1.76^{+0.03}_{-0.03}$	$0.999^{+0.026}_{-0.025}$	$1.094^{+0.005}_{-0.004}$	$0.095^{+0.021}_{-0.021}$	$1.34^{+0.04}_{-0.02}$	$0.03^{+0.06}_{-0.06}$	$4.12^{+0.03}_{-0.03}$	$15.24^{+0.08}_{-0.08}$	$1.13^{+0.03}_{-0.03}$	$23.60^{+0.08}_{-0.08}$
	W	$1.89^{+0.03}_{-0.00}$	$1.009^{+0.000}_{-0.014}$	$1.093^{+0.000}_{-0.002}$	$0.084^{+0.012}_{-0.000}$	$1.34^{+0.03}_{-0.02}$	$0.01^{+0.04}_{-0.03}$	$4.12^{+0.03}_{-0.03}$	$15.23^{+0.08}_{-0.08}$	$1.13^{+0.03}_{-0.03}$	$23.58^{+0.08}_{-0.08}$
	PL	$\infty$	$1.037^{+0.019}_{-0.018}$	$1.099^{+0.003}_{-0.002}$	$0.062^{+0.016}_{-0.016}$	$1.31^{+0.04}_{-0.02}$	$-0.05^{+0.05}_{-0.05}$	$4.12^{+0.03}_{-0.03}$	$15.24^{+0.08}_{-0.08}$	$1.12^{+0.03}_{-0.03}$	$23.62^{+0.08}_{-0.08}$
MW-AM1	K	$2.27^{+0.08}_{-0.09}$	$0.829^{+0.033}_{-0.026}$	$1.245^{+0.044}_{-0.038}$	$0.416^{+0.070}_{-0.071}$	$1.02^{+0.01}_{-0.01}$	$-0.12^{+0.04}_{-0.05}$	$3.77^{+0.02}_{-0.01}$	$15.85^{+0.03}_{-0.04}$	$0.48^{+0.06}_{-0.07}$	$25.21^{+0.18}_{-0.16}$
	W	$2.99^{+0.39}_{-0.31}$	$0.843^{+0.034}_{-0.031}$	$1.311^{+0.134}_{-0.081}$	$0.468^{+0.164}_{-0.114}$	$1.01^{+0.01}_{-0.01}$	$-0.14^{+0.04}_{-0.05}$	$3.82^{+0.06}_{-0.04}$	$15.72^{+0.10}_{-0.16}$	$0.40^{+0.12}_{-0.20}$	$25.41^{+0.51}_{-0.30}$
	PL	$\infty$	$0.840^{+0.038}_{-0.033}$	$1.558^{+0.488}_{-0.224}$	$0.718^{+0.521}_{-0.262}$	$1.01^{+0.01}_{-0.01}$	$-0.13^{+0.05}_{-0.06}$	$3.96^{+0.15}_{-0.10}$	$15.39^{+0.25}_{-0.38}$	$0.04^{+0.35}_{-0.82}$	$26.32^{+2.06}_{-0.88}$

NOTE. — A machine-readable version of Table 11 is published in its entirety in the electronic edition of the *Astrophysical Journal Supplement Series*; only a portion is shown here, for guidance regarding its form and content. Key to columns:

**Column (1)**—Cluster name.

**Column (2)**—Model fit.

**Column (3)**—Logarithm of cluster tidal radius in pc:  $\log r_t = c + \log r_0$ . By construction,  $r_t = \infty$  for power-law models.

**Column (4)**—Logarithm of projected core (half-power) radius at which  $I(R_c) = I(0)/2$ , in pc.

**Column (5)**—Logarithm of projected half-light (effective radius) in pc. Half of the total cluster luminosity is emitted from within  $R_h$ .

**Column (6)**—Logarithm of ratio  $R_h/R_c$ , a measure of cluster concentration.

**Column (7)**—Logarithm of central luminosity surface density in V-band  $L_\odot \text{ pc}^{-2}$ .

**Column (8)**—Logarithm of central luminosity volume density in V-band  $L_\odot \text{ pc}^{-3}$ .

**Column (9)**—Total V-band luminosity of fitted model.

**Column (10)**—Apparent V-band magnitude of model cluster, corrected for extinction:  $V_{\text{tot}} = 4.85 - 2.5 \log(L_{\text{tot}}/L_\odot) + 5 \log(D/10 \text{ kpc})$ .

**Column (11)**—Logarithm of V-band luminosity surface density averaged inside the half-light radius:  $I_h \equiv L_{\text{tot}}/2\pi R_h^2$ .

**Column (12)**—V-band surface brightness corresponding to average projected luminosity density in Column (11):  $\langle \mu_V \rangle_h \equiv 26.422 - 2.5 \log(I_h/L_\odot \text{ pc}^{-2})$ .

TABLE 12  
DERIVED DYNAMICAL PARAMETERS

Cluster	$\Upsilon_V^{\text{pop}}$ [ $M_\odot L_\odot^{-1}$ ]	mod	$\log M_{\text{tot}}$ [ $M_\odot$ ]	$\log E_b$ [erg]	$\log \Sigma_0$ [ $M_\odot \text{pc}^{-2}$ ]	$\log \rho_0$ [ $M_\odot \text{pc}^{-3}$ ]	$\log \Sigma_h$ [ $M_\odot \text{pc}^{-2}$ ]	$\sigma_{p,0}$ [ $\text{km s}^{-1}$ ]	$v_{\text{esc},0}$ [ $\text{km s}^{-1}$ ]	$\log t_{\text{rh}}$ [yr]	$\log f_0$
(1)	(2)	(3)	(4)	(5)	(6)	(7)	(8)	(9)	(10)	(11)	(12)
LMC-HODGE11	$1.893^{+0.160}_{-0.160}$	K	$5.17^{+0.07}_{-0.06}$	$49.91^{+0.11}_{-0.11}$	$3.13^{+0.05}_{-0.05}$	$2.31^{+0.06}_{-0.07}$	$2.69^{+0.07}_{-0.10}$	$3.63^{+0.22}_{-0.21}$	$14.14^{+0.87}_{-0.83}$	$9.40^{+0.12}_{-0.08}$	$-0.605^{+0.062}_{-0.064}$
		W	$5.22^{+0.07}_{-0.13}$	$49.92^{+0.11}_{-0.11}$	$3.12^{+0.05}_{-0.05}$	$2.29^{+0.06}_{-0.06}$	$2.62^{+0.10}_{-0.19}$	$3.63^{+0.22}_{-0.21}$	$14.17^{+0.83}_{-0.82}$	$9.50^{+0.23}_{-0.12}$	$-0.629^{+0.067}_{-0.060}$
		PL	$5.31^{+0.13}_{-0.10}$	$49.95^{+0.11}_{-0.11}$	$3.12^{+0.05}_{-0.05}$	$2.29^{+0.07}_{-0.07}$	$2.43^{+0.19}_{-0.40}$	$3.64^{+0.22}_{-0.21}$	$14.27^{+0.89}_{-0.85}$	$9.75^{+0.45}_{-0.25}$	$-0.642^{+0.070}_{-0.074}$
SMC-KRON3	$1.129^{+0.113}_{-0.113}$	K	$5.15^{+0.06}_{-0.06}$	$49.65^{+0.12}_{-0.12}$	$2.61^{+0.06}_{-0.06}$	$1.51^{+0.07}_{-0.07}$	$2.22^{+0.06}_{-0.06}$	$2.74^{+0.19}_{-0.18}$	$10.51^{+0.71}_{-0.67}$	$9.72^{+0.03}_{-0.03}$	$-1.045^{+0.059}_{-0.052}$
		W	$5.13^{+0.06}_{-0.06}$	$49.63^{+0.12}_{-0.12}$	$2.59^{+0.06}_{-0.06}$	$1.46^{+0.07}_{-0.06}$	$2.26^{+0.06}_{-0.06}$	$2.78^{+0.19}_{-0.18}$	$10.42^{+0.71}_{-0.66}$	$9.67^{+0.03}_{-0.03}$	$-1.137^{+0.056}_{-0.041}$
		PL	$5.12^{+0.06}_{-0.06}$	$49.62^{+0.12}_{-0.12}$	$2.57^{+0.06}_{-0.06}$	$1.41^{+0.06}_{-0.06}$	$2.28^{+0.06}_{-0.06}$	$2.81^{+0.19}_{-0.18}$	$10.33^{+0.70}_{-0.66}$	$9.64^{+0.03}_{-0.03}$	$-1.213^{+0.040}_{-0.050}$
FORNAX1	$1.915^{+0.163}_{-0.163}$	K	$4.40^{+0.05}_{-0.05}$	$48.14^{+0.10}_{-0.10}$	$1.63^{+0.06}_{-0.06}$	$0.31^{+0.07}_{-0.07}$	$1.41^{+0.05}_{-0.05}$	$1.15^{+0.06}_{-0.06}$	$4.09^{+0.24}_{-0.22}$	$9.46^{+0.02}_{-0.02}$	$-1.150^{+0.065}_{-0.069}$
		W	$4.40^{+0.05}_{-0.05}$	$48.15^{+0.10}_{-0.10}$	$1.62^{+0.05}_{-0.05}$	$0.29^{+0.05}_{-0.05}$	$1.42^{+0.05}_{-0.05}$	$1.16^{+0.07}_{-0.06}$	$4.10^{+0.23}_{-0.22}$	$9.46^{+0.02}_{-0.02}$	$-1.191^{+0.042}_{-0.024}$
		PL	$4.40^{+0.05}_{-0.05}$	$48.14^{+0.10}_{-0.10}$	$1.59^{+0.05}_{-0.05}$	$0.23^{+0.06}_{-0.06}$	$1.40^{+0.05}_{-0.05}$	$1.15^{+0.07}_{-0.06}$	$4.05^{+0.23}_{-0.22}$	$9.47^{+0.02}_{-0.02}$	$-1.266^{+0.050}_{-0.052}$
MW-AM1	$1.868^{+0.156}_{-0.156}$	K	$4.04^{+0.04}_{-0.04}$	$47.25^{+0.07}_{-0.07}$	$1.29^{+0.04}_{-0.04}$	$0.15^{+0.05}_{-0.05}$	$0.76^{+0.07}_{-0.08}$	$0.63^{+0.03}_{-0.03}$	$2.51^{+0.11}_{-0.10}$	$9.55^{+0.08}_{-0.07}$	$-0.473^{+0.067}_{-0.084}$
		W	$4.10^{+0.07}_{-0.05}$	$47.27^{+0.07}_{-0.07}$	$1.28^{+0.04}_{-0.04}$	$0.13^{+0.06}_{-0.06}$	$0.67^{+0.13}_{-0.21}$	$0.63^{+0.03}_{-0.03}$	$2.52^{+0.11}_{-0.10}$	$9.66^{+0.23}_{-0.14}$	$-0.513^{+0.082}_{-0.088}$
		PL	$4.23^{+0.16}_{-0.11}$	$47.29^{+0.07}_{-0.07}$	$1.28^{+0.04}_{-0.04}$	$0.14^{+0.06}_{-0.07}$	$0.31^{+0.35}_{-0.82}$	$0.63^{+0.03}_{-0.03}$	$2.53^{+0.11}_{-0.10}$	$10.09^{+0.81}_{-0.39}$	$-0.508^{+0.093}_{-0.106}$

NOTE. — A machine-readable version of Table 12 is published in its entirety in the electronic edition of the *Astrophysical Journal Supplement Series*; only a portion is shown here, for guidance regarding its form and content. Key to columns:

**Column (1)**—Cluster name.

**Column (2)**—Population-synthesis  $V$ -band mass-to-light ratio, from Column (6) of Table 8.

**Column (3)**—Model fit.

**Column (4)**—Total cluster mass from extrapolation of fitted model density profile.

**Column (5)**—Total cluster binding energy.

**Column (6)**—Logarithm of central mass surface density.

**Column (7)**—Logarithm of central mass volume density.

**Column (8)**—Logarithm of mass surface density averaged over the projected half-light/half-mass radius:  $\Sigma_h \equiv M_{\text{tot}}/2\pi R_h^2$ .

**Column (9)**—Predicted line-of-sight velocity dispersion at cluster center ( $\sigma_{p,0}^2 \propto \Upsilon_V^{\text{pop}}$ ).

**Column (10)**—Predicted velocity of escape (to infinity) at cluster center ( $v_{\text{esc},0}^2 \propto \Upsilon_V^{\text{pop}}$ ).

**Column (11)**—Median two-body relaxation timescale, evaluated at the half-light radius; see text.

**Column (12)**—Central phase-space density  $f_0 \equiv \rho_0/(2\pi\sigma_c^2)^{3/2}$ , where  $\sigma_c$  is the unprojected, one-dimensional velocity dispersion at  $r=0$  in the model. Units are  $M_\odot \text{pc}^{-3} \text{km}^{-3} \text{s}^3$ , in which case the core relaxation time is given roughly by  $\log(t_{\text{rc}}/\text{yr}) \simeq 8.28 - \log f_0$ .

TABLE 13  
POPULATION VS. DYNAMICAL MASS-TO-LIGHT RATIOS

Cluster	$\Upsilon_V^{\text{pop}}$ [ $M_\odot L_\odot^{-1}$ ]	$\sigma_{p,\text{obs}}$ [ $\text{km s}^{-1}$ ]	$R_{\text{ap}}$ [sec]	Ref.	$\sigma_p(R=0)$ [ $\text{km s}^{-1}$ ]	King fits		Wilson fits		Power-Law fits	
						$\Upsilon_V^{\text{dyn}}$ [ $M_\odot L_\odot^{-1}$ ]	$\Delta(\log \Upsilon_V)$	$\Upsilon_V^{\text{dyn}}$ [ $M_\odot L_\odot^{-1}$ ]	$\Delta(\log \Upsilon_V)$	$\Upsilon_V^{\text{dyn}}$ [ $M_\odot L_\odot^{-1}$ ]	$\Delta(\log \Upsilon_V)$
(1)	(2)	(3)	(4)	(5)	(6)	(7)	(8)	(9)	(10)	(11)	(12)
LMC-NGC1466	$1.88 \pm 0.03$	$3.80^{+2.80}_{-3.80}$	2.8	1	$3.81^{+2.81}_{-3.81}$	$1.15^{+2.48}_{-1.15}$	$-0.213^{+0.506}_{-0.99}$	$1.14^{+2.45}_{-1.14}$	$-0.217^{+0.509}_{-0.99}$	$1.13^{+2.44}_{-1.13}$	$-0.221^{+0.512}_{-0.99}$
LMC-NGC1754	$1.88 \pm 0.15$	$7.80^{+3.80}_{-2.20}$	2.8	1	$7.91^{+3.81}_{-2.24}$	$3.79^{+3.81}_{-2.04}$	$0.304^{+0.413}_{-0.369}$	$3.41^{+3.79}_{-1.80}$	$0.258^{+0.440}_{-0.360}$	$3.48^{+3.80}_{-1.82}$	$0.267^{+0.435}_{-0.355}$
LMC-NGC1786	$1.87 \pm 0.16$	$8.30^{+1.50}_{-1.50}$	2.8	1	$8.36^{+1.51}_{-1.51}$	$1.78^{+0.89}_{-0.68}$	$-0.023^{+0.214}_{-0.244}$	$1.80^{+0.86}_{-0.66}$	$-0.017^{+0.212}_{-0.234}$	$1.85^{+0.85}_{-0.66}$	$-0.005^{+0.208}_{-0.227}$
		$9.90^{+3.00}_{-3.00}$	1.1	2	$9.91^{+3.01}_{-3.00}$	$2.50^{+2.07}_{-1.38}$	$0.125^{+0.300}_{-0.285}$	$2.53^{+2.03}_{-1.37}$	$0.130^{+0.298}_{-0.375}$	$2.60^{+2.02}_{-1.39}$	$0.143^{+0.292}_{-0.367}$
				ave.	$9.17^{+0.74}_{-0.81}$	$2.14^{+0.36}_{-0.36}$	$0.058^{+0.106}_{-0.116}$	$2.16^{+0.36}_{-0.36}$	$0.063^{+0.106}_{-0.115}$	$2.22^{+0.37}_{-0.37}$	$0.075^{+0.106}_{-0.115}$
LMC-NGC1835	$1.87 \pm 0.16$	$10.40^{+1.40}_{-1.40}$	2.8	1	$10.52^{+1.43}_{-1.42}$	$1.42^{+0.30}_{-0.41}$	$-0.119^{+0.170}_{-0.181}$	$1.38^{+0.30}_{-0.39}$	$-0.132^{+0.173}_{-0.179}$	$1.42^{+0.33}_{-0.41}$	$-0.120^{+0.170}_{-0.182}$
		$11.50^{+2.50}_{-2.50}$	1.1	2	$11.52^{+2.51}_{-2.51}$	$1.71^{+0.96}_{-0.73}$	$-0.039^{+0.231}_{-0.249}$	$1.65^{+0.94}_{-0.73}$	$-0.053^{+0.237}_{-0.249}$	$1.69^{+0.85}_{-0.73}$	$-0.043^{+0.233}_{-0.249}$
				ave.	$11.04^{+0.49}_{-0.51}$	$1.56^{+0.14}_{-0.14}$	$-0.077^{+0.076}_{-0.077}$	$1.51^{+0.14}_{-0.14}$	$-0.091^{+0.076}_{-0.076}$	$1.56^{+0.14}_{-0.14}$	$-0.080^{+0.075}_{-0.075}$
LMC-NGC1850	$0.05 \pm 0.01$	$3.00^{+0.70}_{-0.70}$	40.0	3	$3.19^{+0.70}_{-0.75}$	$0.12^{+0.07}_{-0.05}$	$0.354^{+0.291}_{-0.322}$	$0.12^{+0.07}_{-0.05}$	$0.356^{+0.290}_{-0.325}$	$0.12^{+0.07}_{-0.06}$	$0.356^{+0.289}_{-0.342}$
LMC-NGC1866	$0.10 \pm 0.02$	$2.30^{+0.40}_{-0.40}$	100.0	4	$2.67^{+0.40}_{-0.47}$	$0.13^{+0.07}_{-0.05}$	$0.117^{+0.259}_{-0.310}$	$0.12^{+0.07}_{-0.05}$	$0.108^{+0.303}_{-0.303}$	$0.12^{+0.07}_{-0.05}$	$0.110^{+0.302}_{-0.311}$
LMC-NGC1916	$1.90 \pm 0.16$	$8.20^{+1.10}_{-1.20}$	2.8	1	$8.32^{+1.12}_{-1.22}$	$0.68^{+0.24}_{-0.21}$	$-0.443^{+0.171}_{-0.194}$	$0.68^{+0.24}_{-0.21}$	$-0.446^{+0.172}_{-0.193}$	$0.69^{+0.25}_{-0.21}$	$-0.438^{+0.170}_{-0.191}$
		$16.60^{+4.00}_{-4.00}$	1.1	2	$16.64^{+4.01}_{-4.01}$	$2.75^{+1.72}_{-1.03}$	$0.161^{+0.250}_{-0.293}$	$2.71^{+1.67}_{-1.02}$	$0.156^{+0.252}_{-0.296}$	$2.76^{+1.75}_{-1.03}$	$0.163^{+0.249}_{-0.242}$
				ave.	$13.16^{+4.84}_{-4.84}$	$1.72^{+1.03}_{-1.03}$	$-0.044^{+0.434}_{-0.434}$	$1.70^{+1.02}_{-1.02}$	$-0.048^{+0.433}_{-0.433}$	$1.72^{+1.03}_{-1.03}$	$-0.041^{+0.432}_{-0.432}$
LMC-NGC2005	$1.88 \pm 0.16$	$8.10^{+1.30}_{-1.30}$	2.8	1	$8.60^{+1.42}_{-1.40}$	$2.18^{+0.93}_{-0.73}$	$0.065^{+0.193}_{-0.213}$	$1.16^{+0.52}_{-0.38}$	$-0.207^{+0.293}_{-0.206}$	$2.16^{+0.90}_{-0.71}$	$0.062^{+0.193}_{-0.207}$
		$15.30^{+4.30}_{-4.30}$	1.1	2	$15.71^{+4.44}_{-4.44}$	$7.61^{+5.64}_{-3.72}$	$0.608^{+0.279}_{-0.340}$	$3.58^{+2.78}_{-1.83}$	$0.281^{+0.449}_{-0.215}$	$7.52^{+5.48}_{-3.81}$	$0.603^{+0.281}_{-0.245}$
				ave.	$12.67^{+3.04}_{-4.06}$	$4.89^{+3.72}_{-2.72}$	$0.416^{+0.230}_{-0.387}$	$2.37^{+1.83}_{-1.21}$	$0.102^{+0.215}_{-0.344}$	$4.84^{+2.68}_{-2.68}$	$0.412^{+0.245}_{-0.385}$
LMC-NGC2019	$1.87 \pm 0.16$	$11.70^{+3.00}_{-3.00}$	1.1	2	$11.73^{+3.01}_{-3.01}$	$2.97^{+1.97}_{-1.41}$	$0.202^{+0.259}_{-0.314}$	$2.80^{+1.82}_{-1.33}$	$0.176^{+0.270}_{-0.315}$	$2.82^{+1.81}_{-1.31}$	$0.178^{+0.269}_{-0.308}$
		$7.50^{+1.30}_{-1.30}$	2.8	1	$7.61^{+1.33}_{-1.33}$	$1.25^{+0.56}_{-0.56}$	$-0.176^{+0.199}_{-0.199}$	$1.18^{+0.51}_{-0.43}$	$-0.200^{+0.207}_{-0.222}$	$1.19^{+0.51}_{-0.43}$	$-0.197^{+0.206}_{-0.215}$
				ave.	$9.89^{+1.84}_{-2.28}$	$2.11^{+0.86}_{-0.86}$	$0.053^{+0.187}_{-0.263}$	$1.99^{+0.81}_{-0.81}$	$0.027^{+0.186}_{-0.262}$	$2.00^{+0.81}_{-0.81}$	$0.030^{+0.186}_{-0.262}$
LMC-NGC2157	$0.05 \pm 0.01$	$2.80^{+0.60}_{-0.60}$	40.0	2	$3.16^{+0.68}_{-0.68}$	$0.22^{+0.14}_{-0.10}$	$0.606^{+0.290}_{-0.316}$	$0.22^{+0.14}_{-0.10}$	$0.593^{+0.295}_{-0.324}$	$0.22^{+0.13}_{-0.10}$	$0.601^{+0.292}_{-0.336}$
LMC-NGC2164	$0.06 \pm 0.01$	$4.30^{+0.60}_{-0.60}$	15.0	5	$4.55^{+0.60}_{-0.60}$	$0.61^{+0.06}_{-0.61}$	$0.992^{+0.116}_{-0.99}$	$0.58^{+0.06}_{-0.58}$	$0.973^{+0.117}_{-0.99}$	$0.58^{+0.06}_{-0.58}$	$0.974^{+0.117}_{-0.99}$
LMC-NGC2210	$1.88 \pm 0.16$	$7.30^{+1.70}_{-1.70}$	2.8	1	$7.33^{+1.71}_{-1.71}$	$2.16^{+1.28}_{-0.94}$	$0.059^{+0.241}_{-0.286}$	$2.10^{+1.25}_{-0.92}$	$0.047^{+0.245}_{-0.285}$	$2.09^{+1.24}_{-0.94}$	$0.046^{+0.246}_{-0.296}$
LMC-NGC2214	$0.05 \pm 0.01$	$3.90^{+0.60}_{-0.60}$	25.0	5	$4.15^{+0.61}_{-0.61}$	$1.00^{+0.11}_{-0.11}$	$1.260^{+0.121}_{-0.121}$	$0.97^{+0.12}_{-0.12}$	$1.246^{+0.123}_{-0.123}$	$0.97^{+0.10}_{-0.10}$	$1.245^{+0.123}_{-0.123}$
LMC-NGC2257	$1.87 \pm 0.15$	$5.50^{+1.00}_{-1.00}$	40.0	2	$5.81^{+1.00}_{-1.14}$	$10.19^{+3.65}_{-3.65}$	$0.736^{+0.201}_{-0.227}$	$10.20^{+3.65}_{-3.65}$	$0.737^{+0.200}_{-0.227}$	$10.25^{+3.65}_{-3.65}$	$0.738^{+0.200}_{-0.225}$
SMC- NGC121	$1.77 \pm 0.10$	$5.90^{+2.10}_{-2.70}$	3.4	1	$5.92^{+2.11}_{-2.71}$	$1.50^{+1.35}_{-1.08}$	$-0.074^{+0.304}_{-0.575}$	$1.46^{+1.35}_{-1.05}$	$-0.085^{+0.309}_{-0.572}$	$1.41^{+1.30}_{-1.01}$	$-0.099^{+0.316}_{-0.566}$
SMC- NGC330	$0.04 \pm 0.01$	$6.00^{+0.00}_{-6.00}$	40.0	6	$6.73^{+0.01}_{-0.73}$	$0.54^{+0.12}_{-0.54}$	$1.080^{+0.194}_{-0.194}$	$0.54^{+0.13}_{-0.54}$	$1.078^{+0.194}_{-0.194}$	$0.54^{+0.12}_{-0.54}$	$1.080^{+0.194}_{-0.194}$
FORNAX3	$1.88 \pm 0.16$	$8.80^{+1.00}_{-1.10}$	1.5	7	$8.89^{+1.01}_{-1.11}$	$3.71^{+1.08}_{-0.96}$	$0.296^{+0.150}_{-0.165}$	$3.43^{+1.02}_{-0.91}$	$0.262^{+0.158}_{-0.169}$	$3.37^{+0.97}_{-0.97}$	$0.253^{+0.160}_{-0.165}$
FORNAX4	$1.72 \pm 0.08$	$5.10^{+1.00}_{-1.20}$	1.5	7	$5.17^{+1.02}_{-1.22}$	$1.48^{+0.80}_{-0.69}$	$-0.064^{+0.206}_{-0.290}$	$1.41^{+0.76}_{-0.64}$	$-0.086^{+0.214}_{-0.283}$	$1.43^{+0.80}_{-0.64}$	$-0.081^{+0.212}_{-0.279}$
FORNAX5	$1.92 \pm 0.16$	$7.00^{+1.70}_{-1.70}$	1.5	7	$7.10^{+2.05}_{-1.73}$	$4.81^{+3.08}_{-2.66}$	$0.400^{+0.253}_{-0.311}$	$3.65^{+2.38}_{-1.21}$	$0.280^{+0.304}_{-0.445}$	$4.07^{+2.72}_{-1.91}$	$0.328^{+0.283}_{-0.310}$
MW-NGC104	$2.35 \pm 0.24$	$11.50^{+2.30}_{-2.30}$	0.0	8	$11.50^{+2.30}_{-2.30}$	$1.33^{+0.48}_{-0.48}$	$-0.247^{+0.206}_{-0.236}$	$1.17^{+0.52}_{-0.43}$	$-0.304^{+0.241}_{-0.241}$	$1.17^{+0.53}_{-0.42}$	$-0.303^{+0.234}_{-0.236}$
MW-NGC1851	$1.98 \pm 0.17$	$10.40^{+2.08}_{-2.08}$	0.0	8	$10.40^{+2.08}_{-2.08}$	$1.61^{+0.71}_{-0.58}$	$-0.090^{+0.196}_{-0.196}$	$1.48^{+0.68}_{-0.55}$	$-0.127^{+0.208}_{-0.208}$	$1.49^{+0.67}_{-0.54}$	$-0.125^{+0.207}_{-0.230}$
MW-NGC1904	$1.88 \pm 0.15$	$5.20^{+1.04}_{-1.04}$	0.0	8	$5.20^{+1.04}_{-1.04}$	$1.16^{+0.42}_{-0.42}$	$-0.210^{+0.190}_{-0.190}$	$1.11^{+0.41}_{-0.41}$	$-0.230^{+0.206}_{-0.232}$	$1.12^{+0.41}_{-0.41}$	$-0.223^{+0.203}_{-0.234}$
MW-NGC2419	$1.90 \pm 0.16$	$3.00^{+0.60}_{-0.60}$	0.0	8	$3.00^{+0.60}_{-0.60}$	$0.61^{+0.27}_{-0.22}$	$-0.497^{+0.201}_{-0.232}$	$0.56^{+0.26}_{-0.21}$	$-0.528^{+0.210}_{-0.234}$	$0.53^{+0.26}_{-0.19}$	$-0.554^{+0.219}_{-0.229}$
MW-NGC2808	$2.02 \pm 0.17$	$13.40^{+2.68}_{-2.68}$	0.0	8	$13.40^{+2.68}_{-2.68}$	$1.46^{+0.72}_{-0.58}$	$-0.142^{+0.214}_{-0.250}$	$1.31^{+0.65}_{-0.50}$	$-0.186^{+0.229}_{-0.244}$	$1.23^{+0.59}_{-0.48}$	$-0.215^{+0.239}_{-0.258}$
MW-NGC288	$1.97 \pm 0.16$	$2.91^{+0.58}_{-0.58}$	0.0	8	$2.91^{+0.58}_{-0.58}$	$2.15^{+0.88}_{-0.80}$	$0.038^{+0.236}_{-0.236}$	$2.02^{+0.74}_{-0.74}$	$0.010^{+0.234}_{-0.234}$	$1.92^{+0.72}_{-0.72}$	$-0.012^{+0.240}_{-0.240}$
MW-NGC3201	$1.88 \pm 0.15$	$5.20^{+1.04}_{-1.04}$	0.0	8	$5.20^{+1.04}_{-1.04}$	$2.87^{+1.33}_{-1.06}$	$0.184^{+0.202}_{-0.235}$	$2.64^{+1.22}_{-1.00}$	$0.149^{+0.214}_{-0.240}$	$2.53^{+1.15}_{-0.97}$	$0.130^{+0.220}_{-0.245}$
MW-NGC4147	$1.87 \pm 0.16$	$2.60^{+0.52}_{-0.52}$	0.0	8	$2.60^{+0.52}_{-0.52}$	$1.01^{+0.47}_{-0.37}$	$-0.269^{+0.205}_{-0.231}$	$1.00^{+0.45}_{-0.37}$	$-0.272^{+0.206}_{-0.231}$	$1.00^{+0.45}_{-0.37}$	$-0.271^{+0.206}_{-0.229}$
MW-NGC4590	$1.89 \pm 0.16$	$2.50^{+0.50}_{-0.50}$	0.0	8	$2.50^{+0.50}_{-0.50}$	$0.92^{+0.41}_{-0.33}$	$-0.315^{+0.198}_{-0.230}$	$0.86^{+0.38}_{-0.31}$	$-0.341^{+0.206}_{-0.229}$	$0.83^{+0.37}_{-0.31}$	$-0.358^{+0.211}_{-0.236}$
MW-NGC5053	$1.93 \pm 0.16$	$1.40^{+0.28}_{-0.28}$	0.0	8	$1.40^{+0.28}_{-0.28}$	$1.18^{+0.53}_{-0.44}$	$-0.214^{+0.200}_{-0.237}$	$1.12^{+0.51}_{-0.41}$	$-0.236^{+0.207}_{-0.234}$	$1.10^{+0.49}_{-0.41}$	$-0.246^{+0.210}_{-0.238}$
MW-NGC5139	$1.87 \pm 0.15$	$16.00^{+3.20}_{-3.20}$	0.0	8	$16.00^{+3.20}_{-3.20}$	$2.54^{+1.17}_{-0.93}$	$0.132^{+0.205}_{-0.232}$	$2.20^{+1.82}_{-0.82}$	$0.070^{+0.222}_{-0.258}$	$2.05^{+0.97}_{-0.72}$	$0.040^{+0.233}_{-0.234}$
MW-NGC5272	$1.88 \pm 0.15$	$5.60^{+1.12}_{-1.12}$	0.0	8	$5.60^{+1.12}_{-1.12}$	$1.39^{+0.63}_{-0.50}$	$-0.130^{+0.199}_{-0.228}$	$0.77^{+0.35}_{-0.28}$	$-0.387^{+0.296}_{-0.232}$	$0.71^{+0.33}_{-0.27}$	$-0.425^{+0.313}_{-0.239}$
MW-NGC5286	$1.87 \pm 0.16$	$8.00^{+1.60}_{-1.60}$	0.0	8	$8.00^{+1.60}_{-1.60}$	$0.99^{+0.49}_{-0.39}$	$-0.275^{+0.211}_{-0.250}$	$0.94^{+0.47}_{-0.37}$	$-0.298^{+0.219}_{-0.252}$	$0.91^{+0.47}_{-0.35}$	$-0.313^{+0.224}_{-0.245}$
MW-NGC5466	$1.92 \pm 0.16$	$1.70^{+0.34}_{-0.34}$	0.0	8	$1.70^{+0.34}_{-0.34}$	$1.61^{+0.60}_{-0.59}$	$-0.077^{+0.203}_{-0.239}$	$1.58^{+0.66}_{-0.59}$	$-0.086^{+0.206}_{-0.237}$	$1.50^{+0.66}_{-0.59}$	$-0.107^{+0.212}_{-0.234}$
MW-NGC5694	$1.87 \pm 0.16$	$5.50^{+1.10}_{-1.10}$	0.0	8	$5.50^{+1.10}_{-1.10}$	$1.35^{+0.59}_{-0.49}$	$-0.142^{+0.197}_{-0.229}$	$1.17^{+0.52}_{-0.42}$	$-0.202^{+0.216}_{-0.229}$	$1.17^{+0.52}_{-0.42}$	$-0.205^{+0.217}_{-0.230}$

TABLE 13 — *Continued*

Cluster (1)	$\Upsilon_V^{\text{pop}}$ [ $M_\odot L_\odot^{-1}$ ] (2)	$\sigma_{p,\text{obs}}$ [km s $^{-1}$ ] (3)	$R_{\text{ap}}$ [sec] (4)	Ref. (5)	$\sigma_p(R=0)$ [km s $^{-1}$ ] (6)	King fits		Wilson fits		Power-Law fits	
						$\Upsilon_V^{\text{dyn}}$ [ $M_\odot L_\odot^{-1}$ ] (7)	$\Delta(\log \Upsilon_V)$ (8)	$\Upsilon_V^{\text{dyn}}$ [ $M_\odot L_\odot^{-1}$ ] (9)	$\Delta(\log \Upsilon_V)$ (10)	$\Upsilon_V^{\text{dyn}}$ [ $M_\odot L_\odot^{-1}$ ] (11)	$\Delta(\log \Upsilon_V)$ (12)
MW-NGC5824	1.87 $\pm$ 0.16	11.60 $^{+2.32}_{-2.32}$	0.0	8	11.60 $^{+2.32}_{-2.32}$	1.96 $^{+0.93}_{-0.71}$	0.020 $^{+0.206}_{-0.197}$	1.64 $^{+0.76}_{-0.61}$	-0.057 $^{+0.232}_{-0.236}$	1.64 $^{+0.74}_{-0.63}$	-0.057 $^{+0.233}_{-0.245}$
MW-NGC5904	1.96 $\pm$ 0.16	5.70 $^{+1.14}_{-1.14}$	0.0	8	5.70 $^{+1.14}_{-1.14}$	0.78 $^{+0.35}_{-0.28}$	-0.398 $^{+0.197}_{-0.229}$	0.67 $^{+0.31}_{-0.25}$	-0.463 $^{+0.218}_{-0.231}$	0.69 $^{+0.30}_{-0.26}$	-0.451 $^{+0.215}_{-0.234}$
MW-NGC6093	1.87 $\pm$ 0.16	12.40 $^{+2.48}_{-2.48}$	0.0	8	12.40 $^{+2.48}_{-2.48}$	2.67 $^{+1.26}_{-0.99}$	0.155 $^{+0.205}_{-0.237}$	2.48 $^{+1.19}_{-0.94}$	0.124 $^{+0.215}_{-0.241}$	2.43 $^{+1.17}_{-0.92}$	0.115 $^{+0.219}_{-0.240}$
MW-NGC6121	1.99 $\pm$ 0.17	4.20 $^{+0.84}_{-0.84}$	0.0	8	4.20 $^{+0.84}_{-0.84}$	1.27 $^{+0.71}_{-0.52}$	-0.194 $^{+0.231}_{-0.262}$	1.23 $^{+0.70}_{-0.51}$	-0.208 $^{+0.236}_{-0.265}$	1.26 $^{+0.70}_{-0.51}$	-0.199 $^{+0.233}_{-0.261}$
MW-NGC6171	2.09 $\pm$ 0.19	4.10 $^{+0.82}_{-0.82}$	0.0	8	4.10 $^{+0.82}_{-0.82}$	2.20 $^{+1.22}_{-0.87}$	0.023 $^{+0.232}_{-0.256}$	2.14 $^{+1.16}_{-0.86}$	0.010 $^{+0.237}_{-0.261}$	2.17 $^{+1.14}_{-0.88}$	0.016 $^{+0.235}_{-0.264}$
MW-NGC6205	1.88 $\pm$ 0.15	7.10 $^{+1.42}_{-1.42}$	0.0	8	7.10 $^{+1.42}_{-1.42}$	1.51 $^{+0.70}_{-0.55}$	-0.097 $^{+0.203}_{-0.231}$	1.20 $^{+0.54}_{-0.44}$	-0.195 $^{+0.236}_{-0.239}$	1.08 $^{+0.47}_{-0.39}$	-0.242 $^{+0.254}_{-0.229}$
MW-NGC6218	1.89 $\pm$ 0.16	4.50 $^{+0.90}_{-0.90}$	0.0	8	4.50 $^{+0.90}_{-0.90}$	1.77 $^{+0.84}_{-0.64}$	-0.030 $^{+0.206}_{-0.231}$	1.62 $^{+0.80}_{-0.60}$	-0.066 $^{+0.218}_{-0.235}$	1.58 $^{+0.76}_{-0.60}$	-0.079 $^{+0.223}_{-0.242}$
MW-NGC6254	1.88 $\pm$ 0.15	6.60 $^{+1.32}_{-1.32}$	0.0	8	6.60 $^{+1.32}_{-1.32}$	2.16 $^{+1.11}_{-0.84}$	0.059 $^{+0.217}_{-0.249}$	2.00 $^{+1.05}_{-0.79}$	0.025 $^{+0.229}_{-0.253}$	1.91 $^{+0.97}_{-0.74}$	0.006 $^{+0.236}_{-0.247}$
MW-NGC6341	1.93 $\pm$ 0.16	5.90 $^{+1.18}_{-1.18}$	0.0	8	5.90 $^{+1.18}_{-1.18}$	0.88 $^{+0.41}_{-0.33}$	-0.339 $^{+0.205}_{-0.236}$	0.78 $^{+0.38}_{-0.29}$	-0.393 $^{+0.223}_{-0.240}$	0.81 $^{+0.38}_{-0.31}$	-0.379 $^{+0.219}_{-0.243}$
MW-NGC6362	2.16 $\pm$ 0.20	2.80 $^{+0.56}_{-0.56}$	0.0	8	2.80 $^{+0.56}_{-0.56}$	1.16 $^{+0.51}_{-0.43}$	-0.271 $^{+0.201}_{-0.239}$	1.12 $^{+0.51}_{-0.41}$	-0.287 $^{+0.206}_{-0.236}$	1.10 $^{+0.49}_{-0.42}$	-0.291 $^{+0.207}_{-0.243}$
MW-NGC6366	2.28 $\pm$ 0.22	1.30 $^{+0.26}_{-0.26}$	0.0	8	1.30 $^{+0.26}_{-0.26}$	0.30 $^{+0.20}_{-0.13}$	-0.878 $^{+0.265}_{-0.295}$	0.30 $^{+0.19}_{-0.13}$	-0.885 $^{+0.268}_{-0.298}$	0.29 $^{+0.20}_{-0.13}$	-0.895 $^{+0.272}_{-0.296}$
MW-NGC6388	2.55 $\pm$ 0.28	18.90 $^{+3.78}_{-3.78}$	0.0	8	18.90 $^{+3.78}_{-3.78}$	1.89 $^{+1.03}_{-0.76}$	-0.130 $^{+0.239}_{-0.270}$	1.71 $^{+0.93}_{-0.67}$	-0.174 $^{+0.256}_{-0.261}$	1.68 $^{+0.93}_{-0.68}$	-0.182 $^{+0.258}_{-0.271}$
MW-NGC6402	1.92 $\pm$ 0.16	8.20 $^{+1.64}_{-1.64}$	0.0	8	8.20 $^{+1.64}_{-1.64}$	1.16 $^{+0.76}_{-0.51}$	-0.217 $^{+0.257}_{-0.289}$	1.13 $^{+0.75}_{-0.51}$	-0.227 $^{+0.261}_{-0.294}$	1.10 $^{+0.73}_{-0.50}$	-0.241 $^{+0.267}_{-0.300}$
MW-NGC6441	2.66 $\pm$ 0.30	18.00 $^{+3.60}_{-3.60}$	0.0	8	18.00 $^{+3.60}_{-3.60}$	1.65 $^{+1.00}_{-0.70}$	-0.207 $^{+0.259}_{-0.289}$	1.56 $^{+0.97}_{-0.69}$	-0.230 $^{+0.267}_{-0.292}$	1.56 $^{+0.96}_{-0.65}$	-0.231 $^{+0.268}_{-0.279}$
MW-NGC6535	1.87 $\pm$ 0.16	2.40 $^{+0.48}_{-0.48}$	0.0	8	2.40 $^{+0.48}_{-0.48}$	8.53 $^{+4.00}_{-3.24}$	0.660 $^{+0.305}_{-0.242}$	8.33 $^{+3.92}_{-3.14}$	0.649 $^{+0.208}_{-0.240}$	8.29 $^{+3.87}_{-2.99}$	0.647 $^{+0.209}_{-0.229}$
MW-NGC6656	1.87 $\pm$ 0.15	9.00 $^{+1.80}_{-1.80}$	0.0	8	9.00 $^{+1.80}_{-1.80}$	2.07 $^{+1.15}_{-0.82}$	0.043 $^{+0.230}_{-0.255}$	2.00 $^{+1.09}_{-0.81}$	0.030 $^{+0.235}_{-0.259}$	1.96 $^{+1.07}_{-0.78}$	0.020 $^{+0.238}_{-0.257}$
MW-NGC6712	2.11 $\pm$ 0.19	4.30 $^{+0.86}_{-0.86}$	0.0	8	4.30 $^{+0.86}_{-0.86}$	0.99 $^{+0.55}_{-0.40}$	-0.331 $^{+0.234}_{-0.264}$	0.98 $^{+0.55}_{-0.40}$	-0.335 $^{+0.235}_{-0.268}$	0.97 $^{+0.55}_{-0.40}$	-0.339 $^{+0.237}_{-0.266}$
MW-NGC6715	1.88 $\pm$ 0.15	14.20 $^{+2.84}_{-2.84}$	0.0	8	14.20 $^{+2.84}_{-2.84}$	1.41 $^{+0.63}_{-0.52}$	-0.124 $^{+0.197}_{-0.233}$	1.12 $^{+0.52}_{-0.41}$	-0.223 $^{+0.231}_{-0.234}$	1.09 $^{+0.50}_{-0.40}$	-0.237 $^{+0.236}_{-0.233}$
MW-NGC6779	1.88 $\pm$ 0.16	4.00 $^{+0.80}_{-0.80}$	0.0	8	4.00 $^{+0.80}_{-0.80}$	1.05 $^{+0.50}_{-0.40}$	-0.251 $^{+0.207}_{-0.242}$	1.05 $^{+0.51}_{-0.40}$	-0.252 $^{+0.207}_{-0.242}$	1.06 $^{+0.49}_{-0.40}$	-0.250 $^{+0.206}_{-0.240}$
MW-NGC6809	1.87 $\pm$ 0.16	4.90 $^{+0.98}_{-0.98}$	0.0	8	4.90 $^{+0.98}_{-0.98}$	3.23 $^{+1.42}_{-1.18}$	0.238 $^{+0.196}_{-0.232}$	2.97 $^{+1.34}_{-1.07}$	0.202 $^{+0.208}_{-0.229}$	2.83 $^{+1.25}_{-1.02}$	0.181 $^{+0.215}_{-0.229}$
MW-NGC6864	2.01 $\pm$ 0.17	10.30 $^{+2.06}_{-2.06}$	0.0	8	10.30 $^{+2.06}_{-2.06}$	1.78 $^{+0.83}_{-0.66}$	-0.053 $^{+0.204}_{-0.236}$	1.57 $^{+0.73}_{-0.58}$	-0.109 $^{+0.223}_{-0.238}$	1.52 $^{+0.71}_{-0.56}$	-0.122 $^{+0.227}_{-0.237}$
MW-NGC6934	1.88 $\pm$ 0.15	5.10 $^{+1.02}_{-1.02}$	0.0	8	5.10 $^{+1.02}_{-1.02}$	1.51 $^{+0.67}_{-0.54}$	-0.095 $^{+0.196}_{-0.228}$	1.32 $^{+0.59}_{-0.48}$	-0.153 $^{+0.215}_{-0.218}$	1.27 $^{+0.56}_{-0.49}$	-0.171 $^{+0.221}_{-0.245}$
MW-NGC7089	1.87 $\pm$ 0.15	8.20 $^{+1.64}_{-1.64}$	0.0	8	8.20 $^{+1.64}_{-1.64}$	0.98 $^{+0.44}_{-0.36}$	-0.279 $^{+0.198}_{-0.230}$	0.89 $^{+0.52}_{-0.32}$	-0.321 $^{+0.212}_{-0.228}$	0.83 $^{+0.43}_{-0.31}$	-0.352 $^{+0.222}_{-0.234}$

REFERENCES. — (1)—Dubath, Meylan, & Mayor (1997); (2)—Mateo, Welch, & Fischer (1991); (3)—Fischer, Welch, & Mateo (1993); (4)—Fischer et al. (1992); (5)—Lupton et al. (1989); (6)—Feast & Black (1980); (7)—Dubath, Meylan, & Mayor (1992); (8)—Pryor & Meylan (1993).

NOTE. — The electronic edition of *Astrophysical Journal Supplement Series* also includes a machine-readable version of Table 13. Key to columns:

**Column (1)**—Cluster name.

**Column (2)**—Population-synthesis  $V$ -band mass-to-light ratio, from Column (6) of Table 8.

**Column (3)**—Observed stellar velocity dispersion from literature.

**Column (4)**—Radius of effective circular aperture corresponding to velocity-dispersion measurement in Column (3).

**Column (5)**—Source of  $\sigma_{p,\text{obs}}$  and  $R_{\text{ap}}$  estimates (see below).

**Column (6)**—Aperture-corrected line-of-sight velocity dispersion at cluster center (mean of separate results using King, Wilson, and power-law structural models).

**Column (7)**—Dynamical mass-to-light ratio calculated within King-model fit to cluster surface-brightness profile.

**Column (8)**—King-model  $\Delta(\log \Upsilon_V) \equiv \log(\Upsilon_V^{\text{dyn}}/\Upsilon_V^{\text{pop}})$ .

**Column (9)**—Dynamical mass-to-light ratio calculated within Wilson-model fit to cluster surface-brightness profile.

**Column (10)**—Wilson-model  $\Delta(\log \Upsilon_V) \equiv \log(\Upsilon_V^{\text{dyn}}/\Upsilon_V^{\text{pop}})$ .

**Column (11)**—Dynamical mass-to-light ratio calculated within power-law model fit to cluster surface-brightness profile.

**Column (12)**—Power-law model  $\Delta(\log \Upsilon_V) \equiv \log(\Upsilon_V^{\text{dyn}}/\Upsilon_V^{\text{pop}})$ .



TABLE 14  
GALACTOCENTRIC RADII AND  $\kappa$ -SPACE PARAMETERS

Cluster (1)	$R_{gc}$ [kpc] (2)	model (3)	$\kappa_1$ (4)	$\kappa_2$ (5)	$\kappa_3$ (6)
LMC-HODGE11	3.71	K	$-0.734^{+0.052}_{-0.045}$	$3.305^{+0.074}_{-0.107}$	$0.500^{+0.022}_{-0.021}$
		W	$-0.694^{+0.056}_{-0.053}$	$3.225^{+0.106}_{-0.212}$	$0.507^{+0.030}_{-0.022}$
		PL	$-0.593^{+0.181}_{-0.100}$	$3.020^{+0.217}_{-0.433}$	$0.535^{+0.075}_{-0.032}$
SMC-KRON3	2.16	K	$-0.749^{+0.040}_{-0.041}$	$2.919^{+0.049}_{-0.050}$	$0.370^{+0.025}_{-0.025}$
		W	$-0.759^{+0.041}_{-0.041}$	$2.962^{+0.049}_{-0.049}$	$0.373^{+0.025}_{-0.025}$
		PL	$-0.764^{+0.041}_{-0.040}$	$2.989^{+0.050}_{-0.049}$	$0.376^{+0.025}_{-0.025}$
FORNAX1	1.59	K	$-1.264^{+0.034}_{-0.034}$	$1.749^{+0.042}_{-0.042}$	$0.517^{+0.022}_{-0.022}$
		W	$-1.259^{+0.034}_{-0.034}$	$1.757^{+0.041}_{-0.041}$	$0.518^{+0.021}_{-0.021}$
		PL	$-1.256^{+0.034}_{-0.034}$	$1.743^{+0.042}_{-0.042}$	$0.522^{+0.022}_{-0.022}$
MW-AM1	123.28	K	$-1.525^{+0.033}_{-0.029}$	$0.947^{+0.076}_{-0.083}$	$0.502^{+0.022}_{-0.021}$
		W	$-1.474^{+0.084}_{-0.051}$	$0.857^{+0.140}_{-0.231}$	$0.514^{+0.036}_{-0.024}$
		PL	$-1.299^{+0.330}_{-0.144}$	$0.462^{+0.388}_{-0.880}$	$0.580^{+0.182}_{-0.063}$

NOTE. — A machine-readable version of Table 14 is published in its entirety in the electronic edition of the *Astrophysical Journal Supplement Series*; only a portion is shown here, for guidance regarding its form and content. Key to columns:

**Column (1)**—Cluster name.

**Column (2)**—Distance from center of parent galaxy, in kpc. For LMC, SMC, and Fornax-dwarf clusters,  $R_{gc}$  is a projected distance (with galaxy centers given in eq. [6] of the text); for Milky Way globulars,  $R_{gc}$  is the three-dimensional Galactocentric distance, taken from Harris (1996).

**Column (3)**—Model fit.

**Column (4)**— $\kappa_1 \equiv (\log \sigma_{p,0}^2 + \log R_h) / \sqrt{2}$ , for  $\sigma_{p,0}$  from Table 12 in  $\text{km s}^{-1}$  and  $R_h$  from Table 11 in kpc.

**Column (5)**— $\kappa_2 \equiv (\log \sigma_{p,0}^2 + 2 \log \Sigma_h - \log R_h) / \sqrt{6}$ , for  $\sigma_{p,0}$  from Table 12 in  $\text{km s}^{-1}$ ,  $\Sigma_h$  from Table 12 in  $M_\odot \text{pc}^{-2}$ , and  $R_h$  from Table 11 in kpc.

**Column (6)**— $\kappa_3 \equiv (\log \sigma_{p,0}^2 - \log \Sigma_h - \log R_h) / \sqrt{3}$ , for  $\sigma_{p,0}$  from Table 12 in  $\text{km s}^{-1}$ ,  $\Sigma_h$  from Table 12 in  $M_\odot \text{pc}^{-2}$ , and  $R_h$  from Table 11 in kpc.

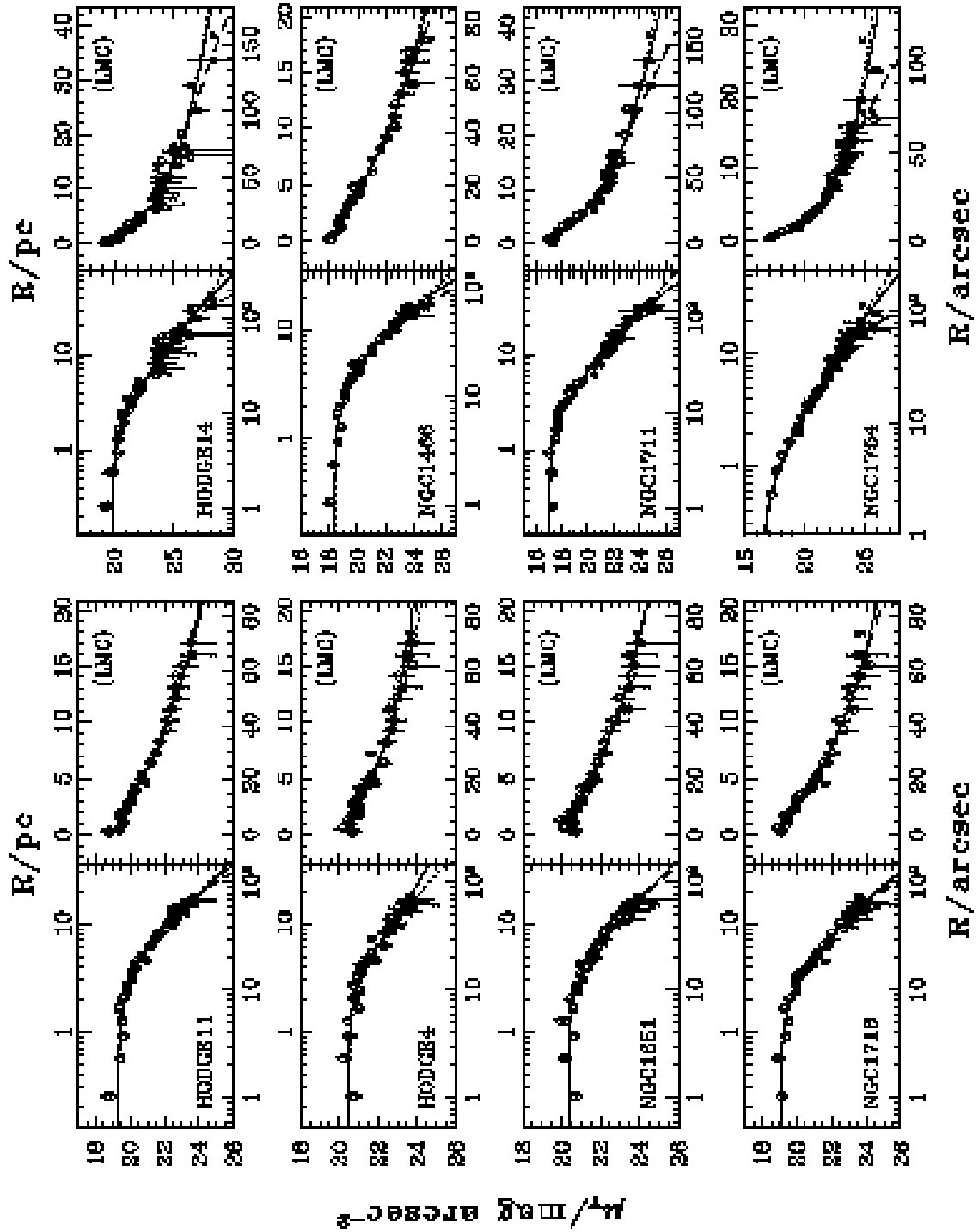


FIG. 12. — Fits of King (1966) models, isotropic Wilson (1975) models, and power-law models (eq. [2]) to the surface-brightness profiles of 53 LMC clusters and 10 SMC clusters spanning a wide range of ages; 5 globular clusters in the Fornax dwarf spheroidal; and 84 Galactic globular clusters besides  $\omega$  Centauri. In all panels, *solid* lines correspond to the Wilson-model fits; *dashed* lines, to King-model fits; and *dotted* lines, to power-law fits. All SB data are plotted with corrections for zeropoint changes and V-band extinction *included* (Columns 2 and 3 of Table 10). Radial scales are in arcsec along the lower horizontal axes of all panels, and in pc along the upper horizontal axes. Numerical details of every fit are given in Table 10, and derived cluster parameters are in Tables 11 and 12.

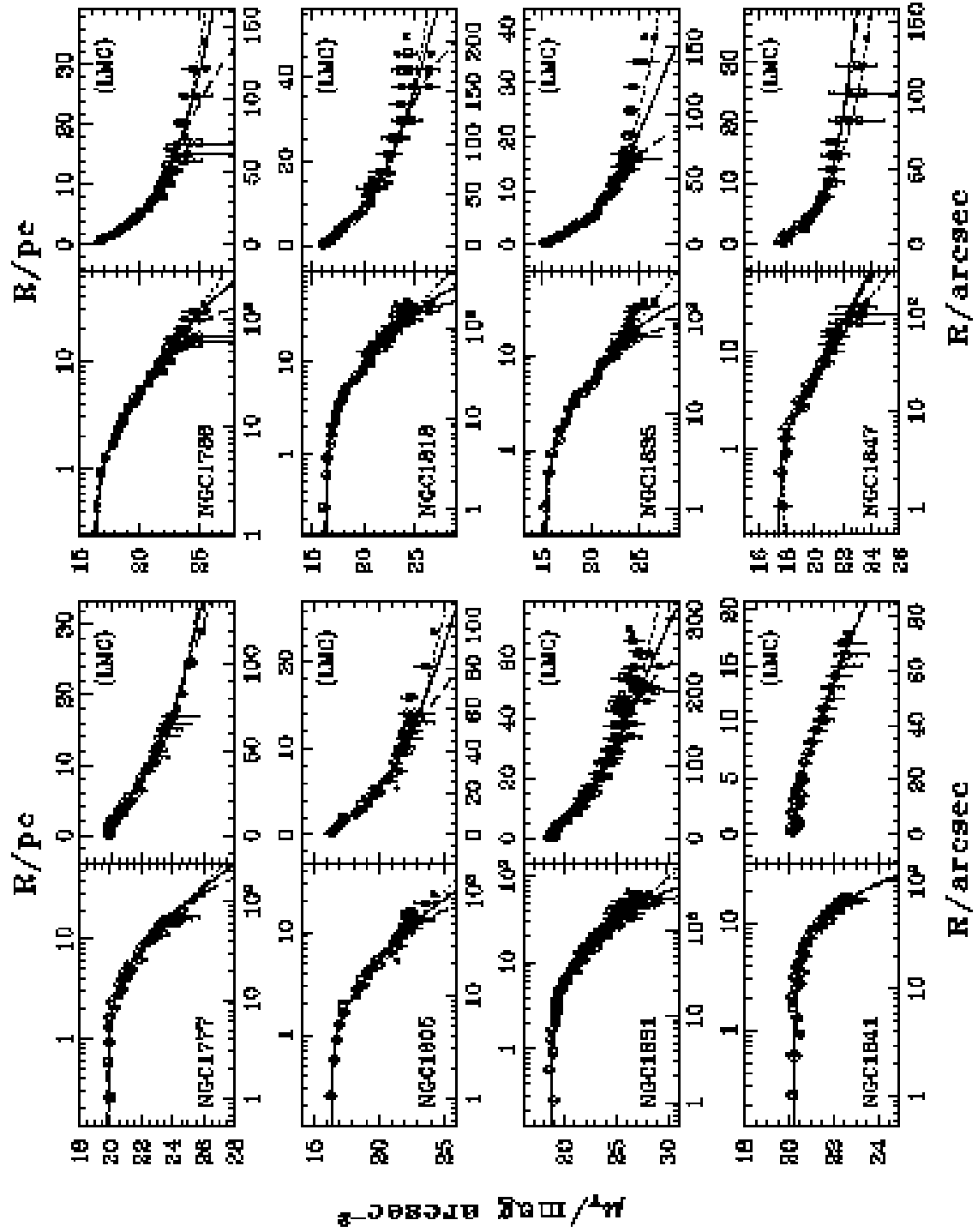


FIG. 12 [CONTINUED].—

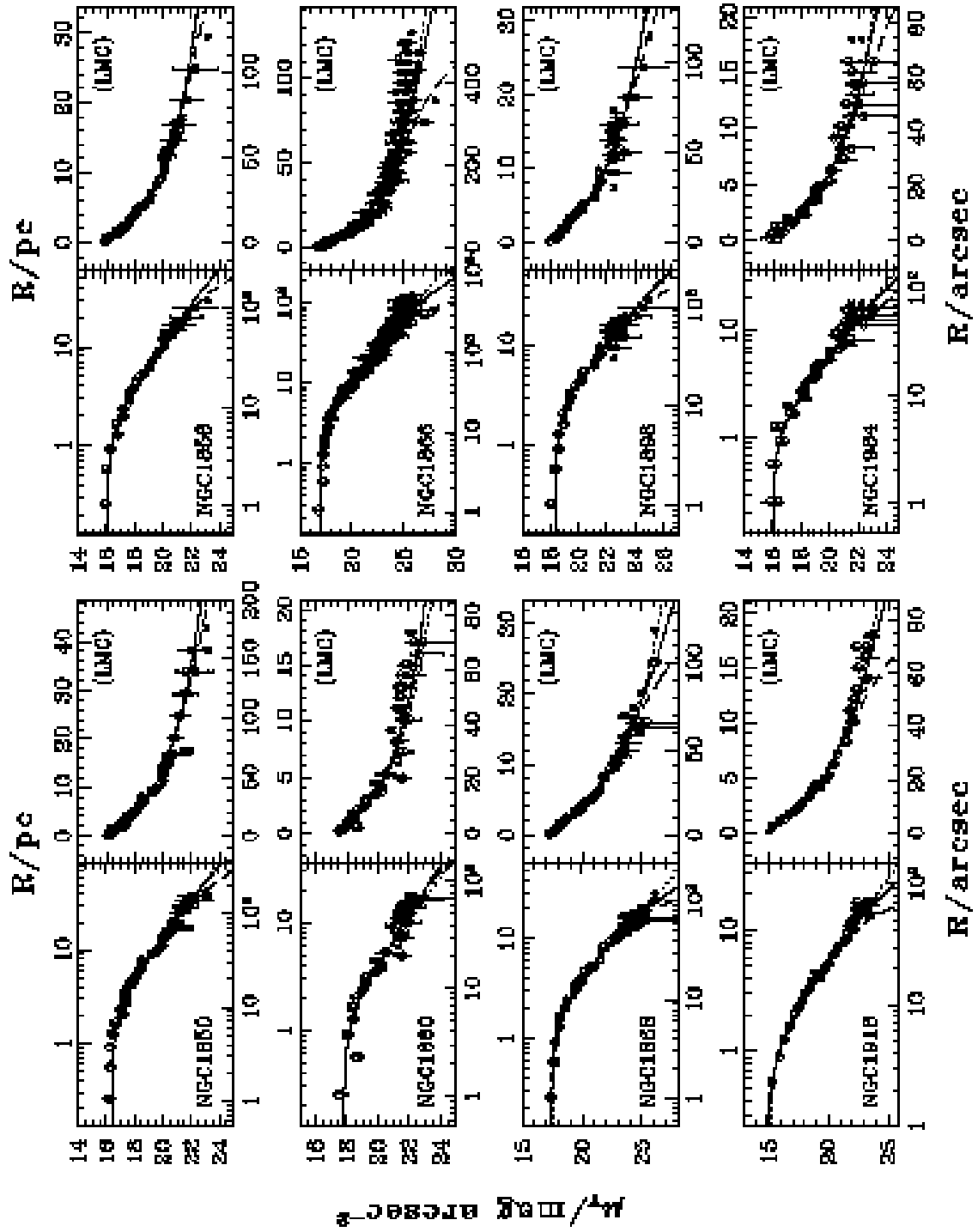


FIG. 12 [CONTINUED].—

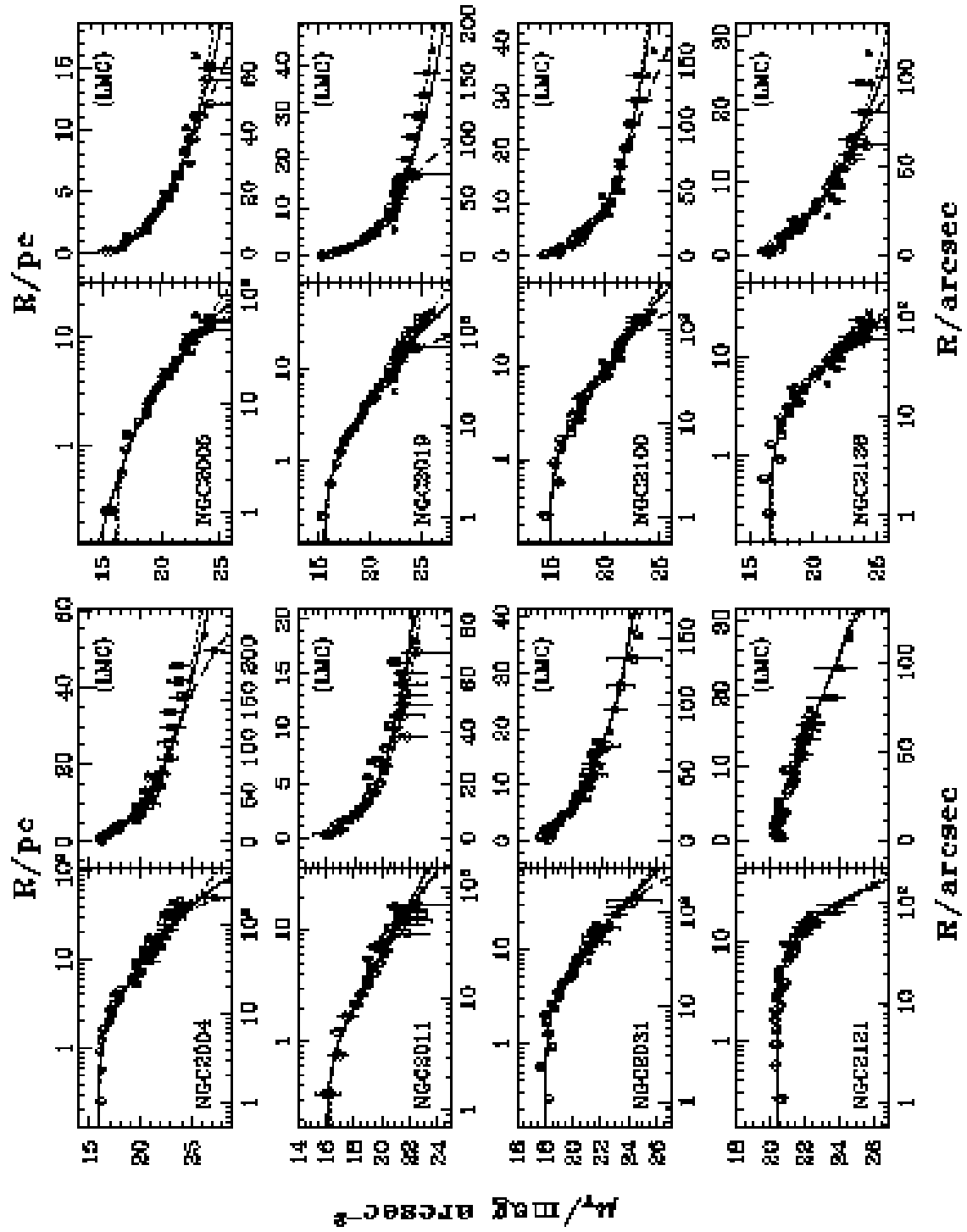


FIG. 12 [CONTINUED].—

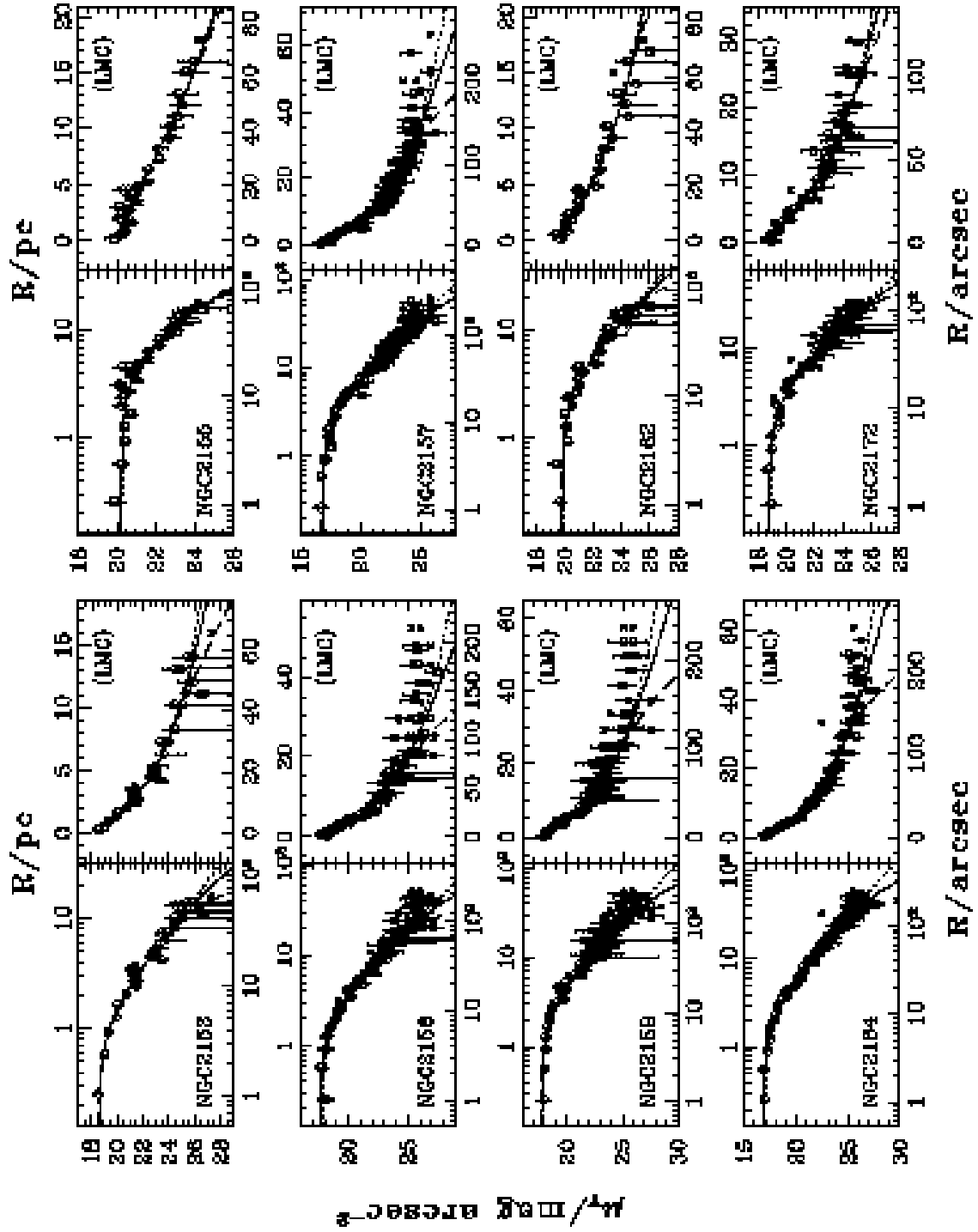


FIG. 12 [CONTINUED].—

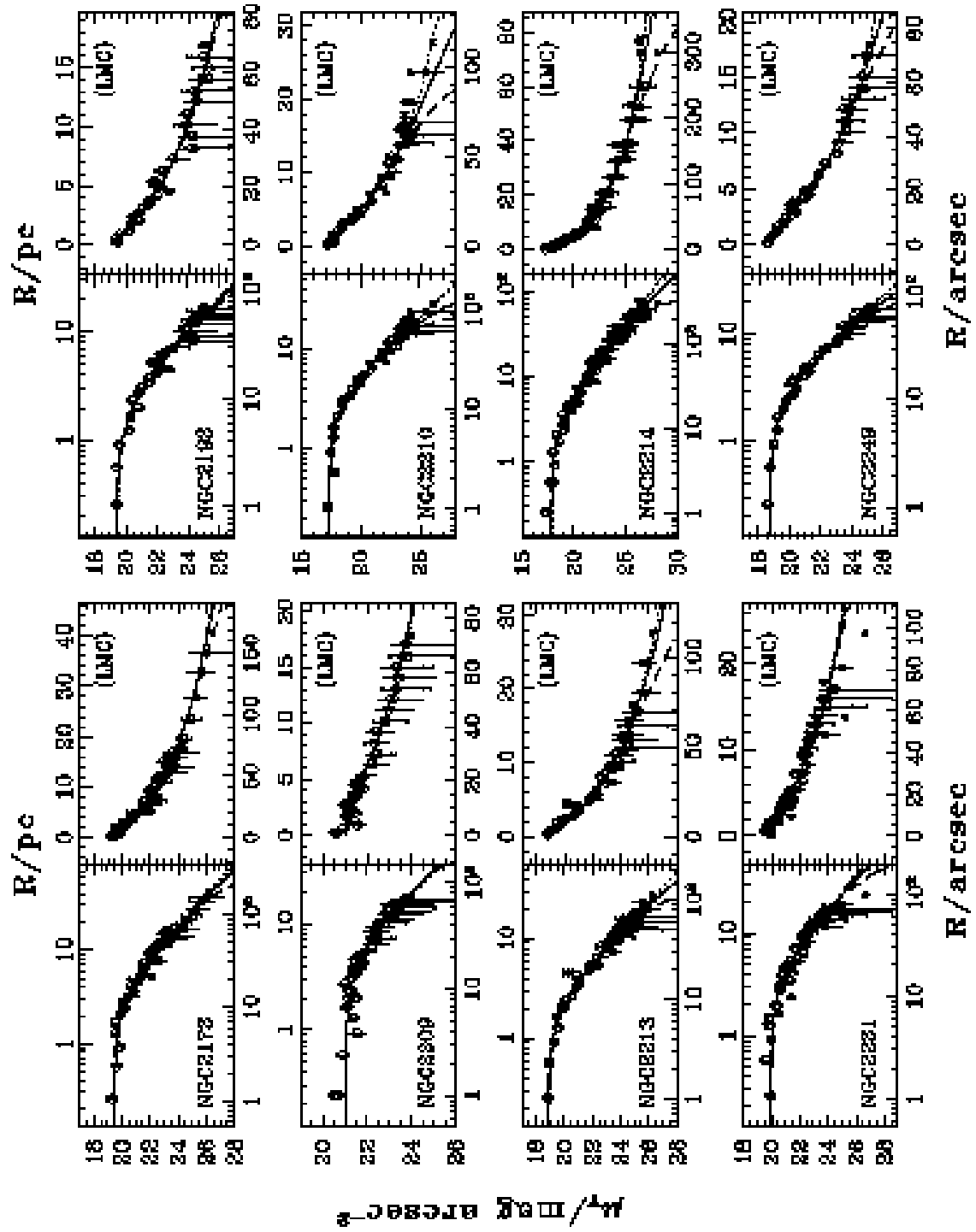


FIG. 12 [CONTINUED].—

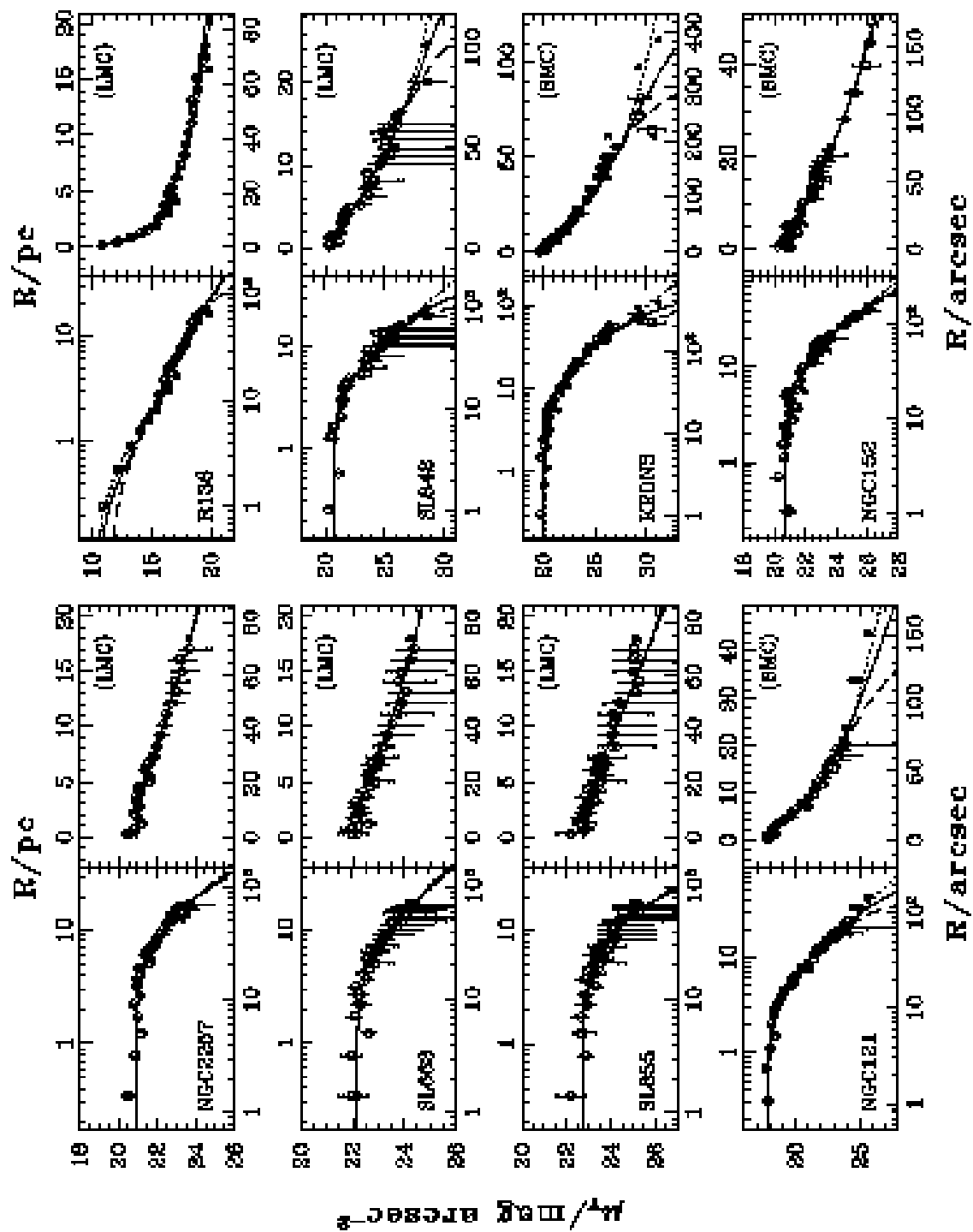


FIG. 12 [CONTINUED].—



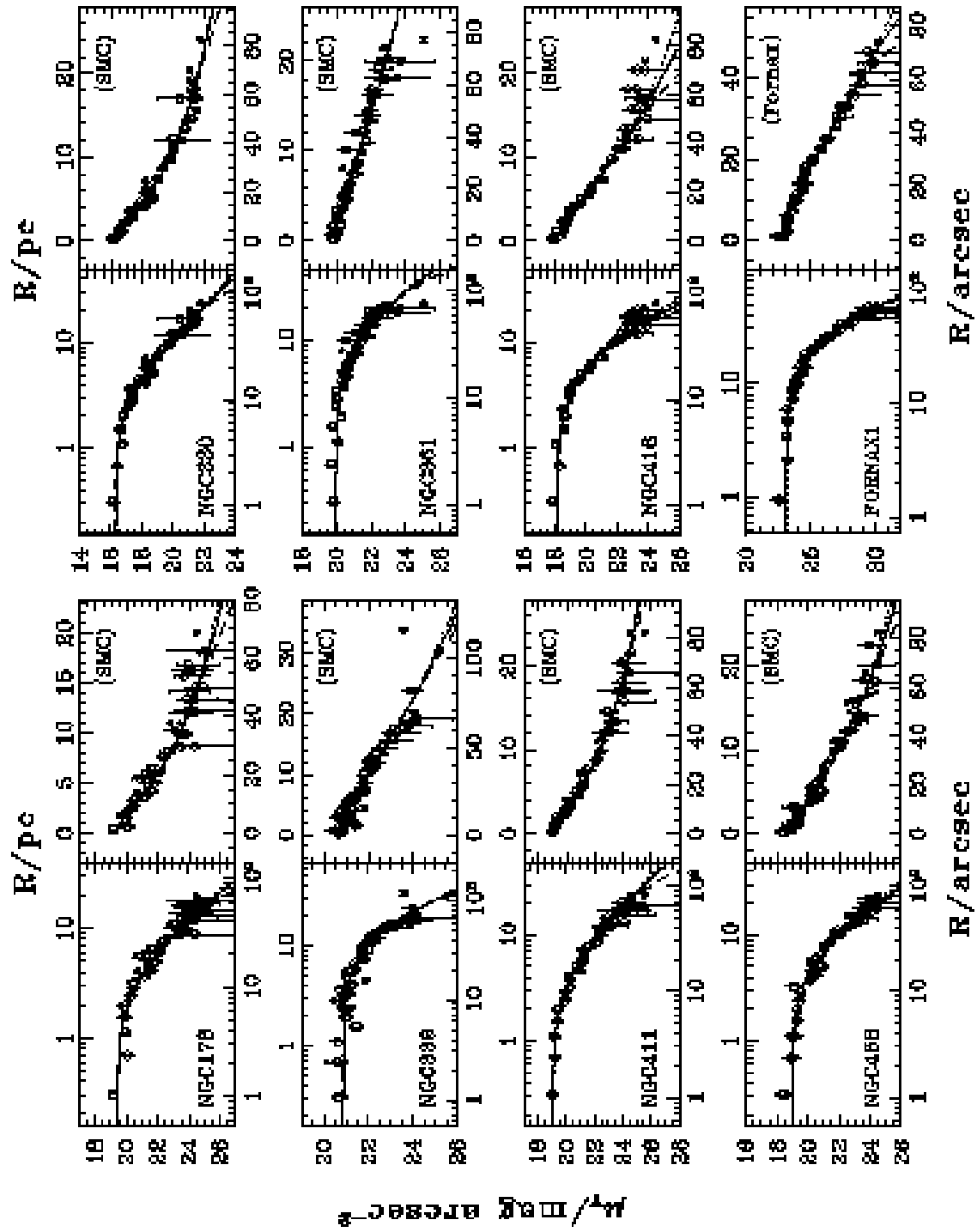


FIG. 12 [CONTINUED].—

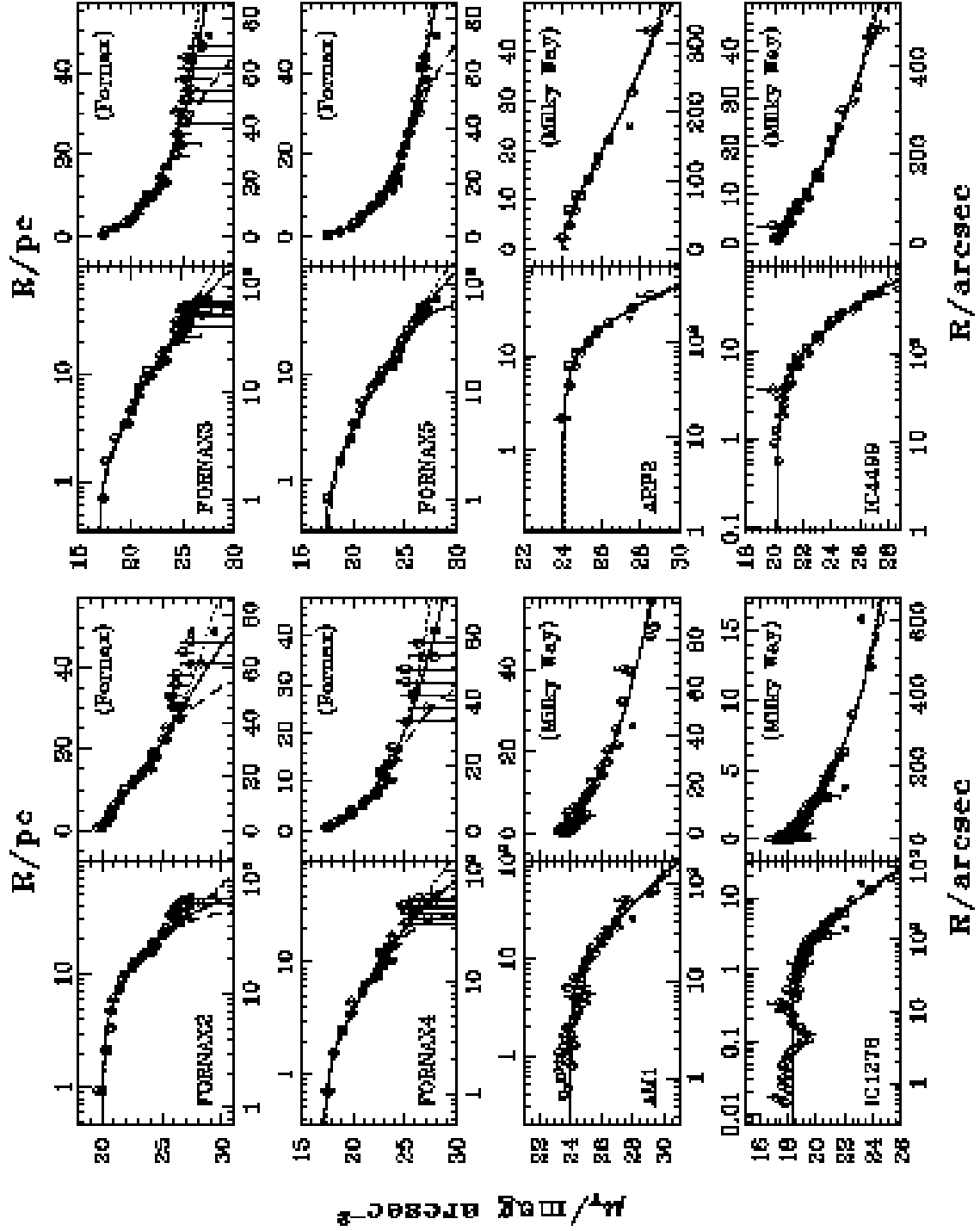


FIG. 12 [CONTINUED].—

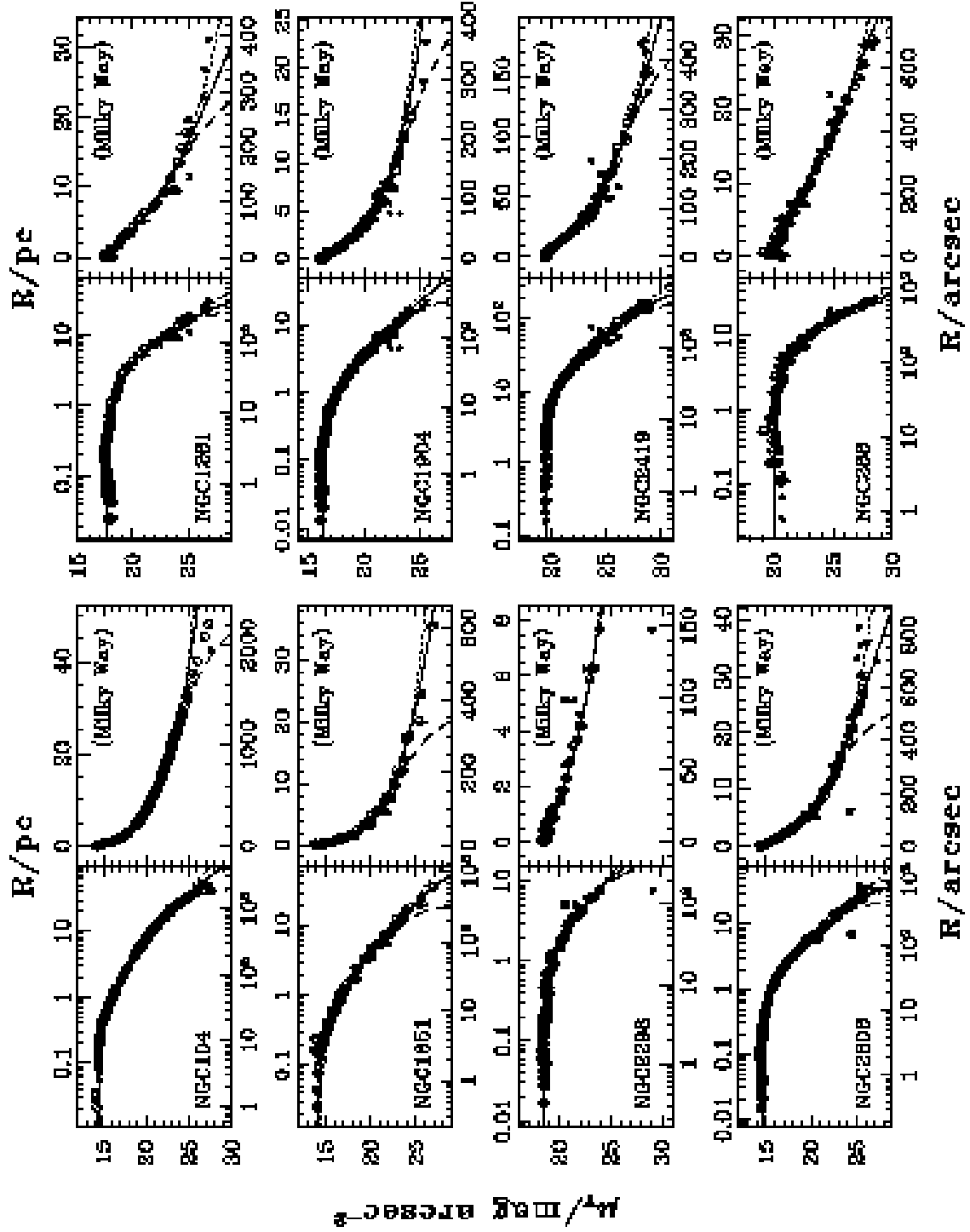


FIG. 12 [CONTINUED].—

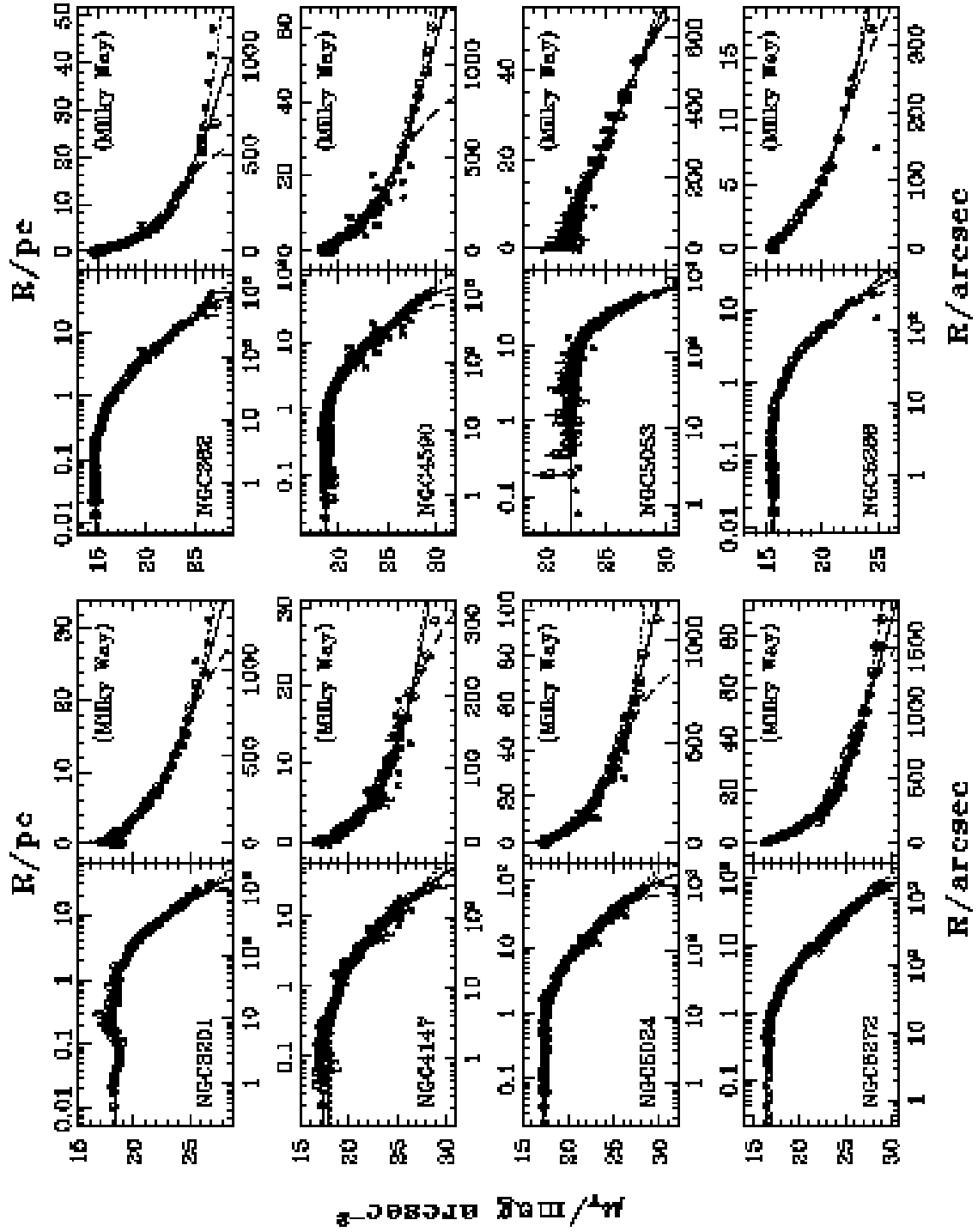


FIG. 12 [CONTINUED].—

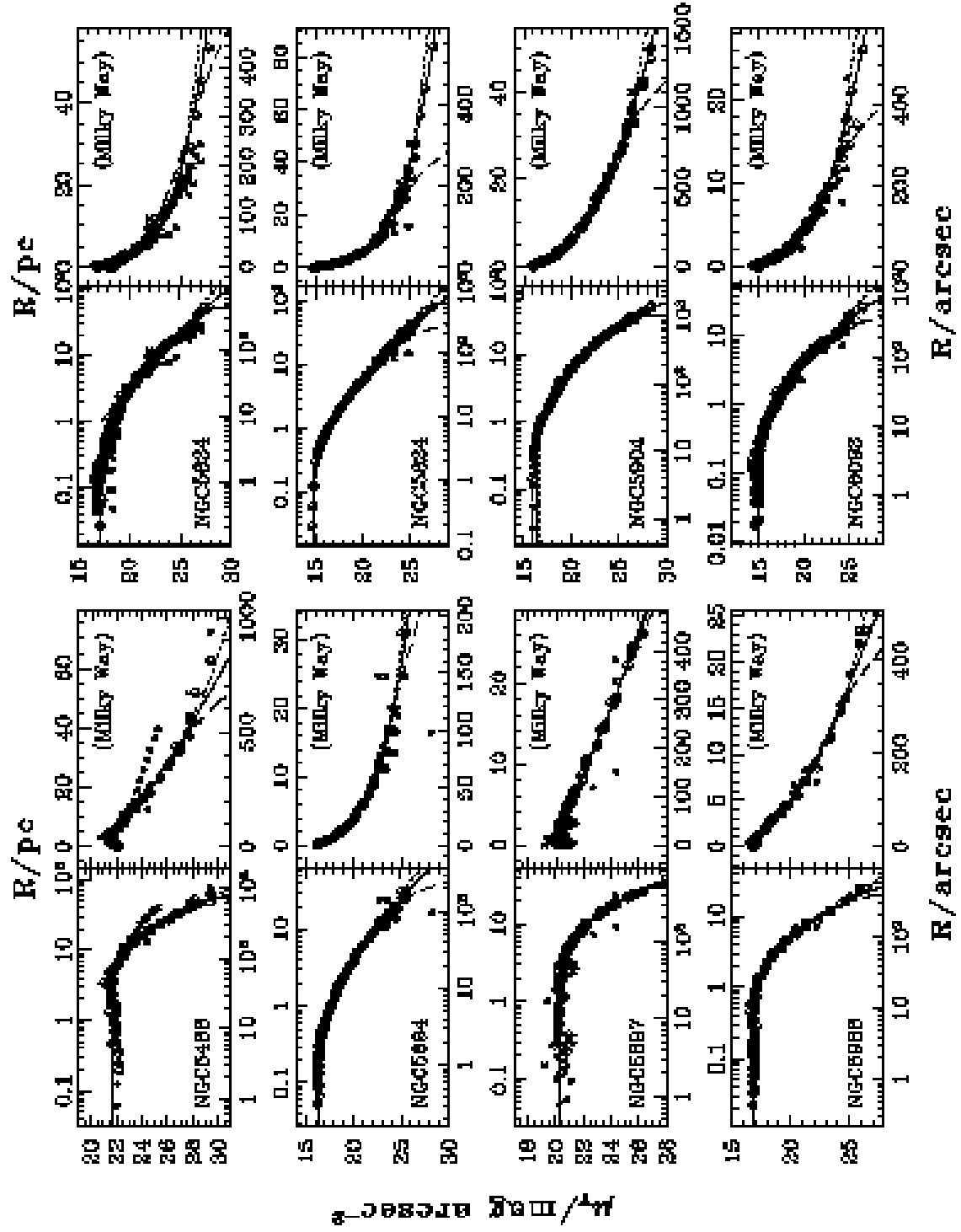


FIG. 12 [CONTINUED].—

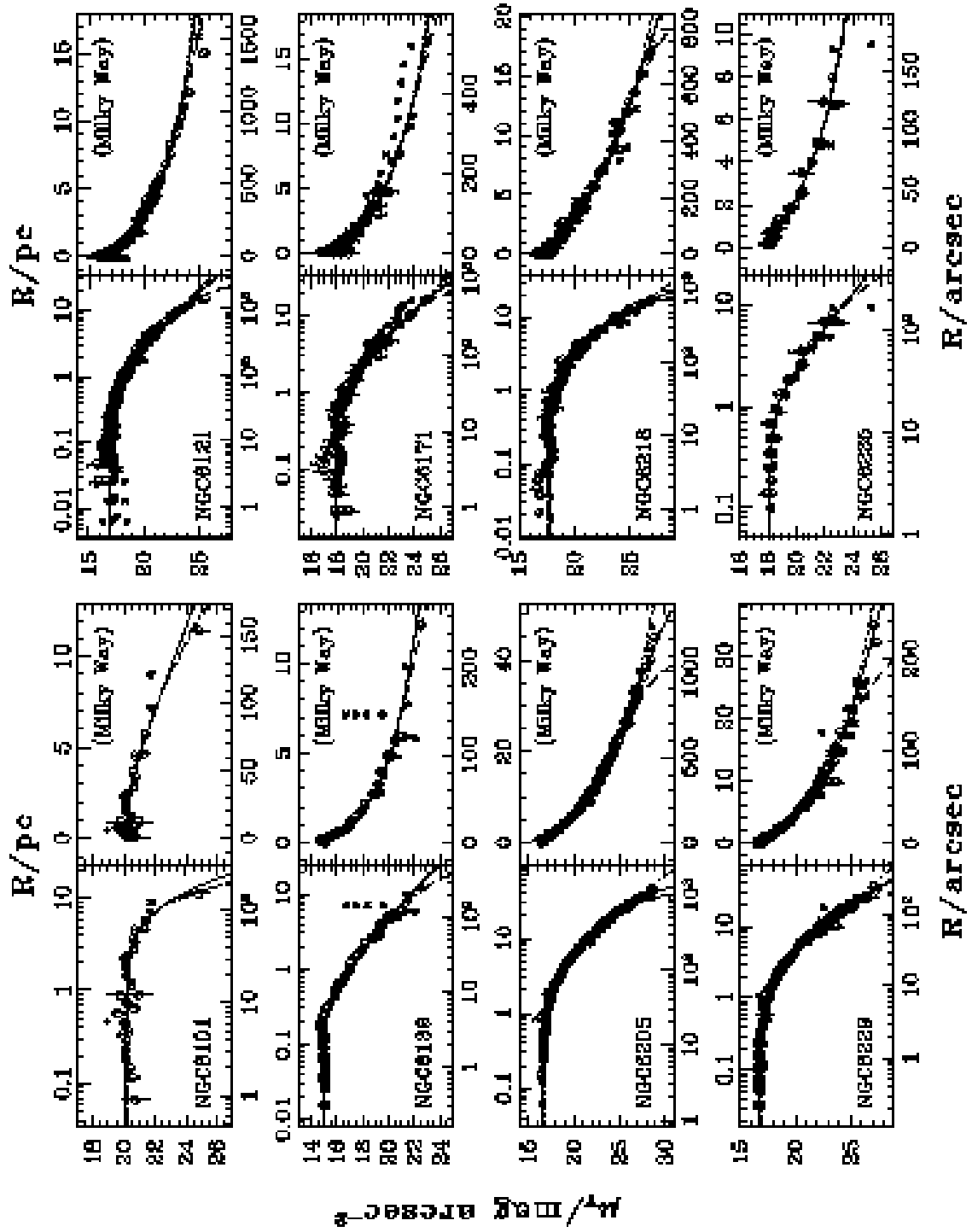


FIG. 12 [CONTINUED].—

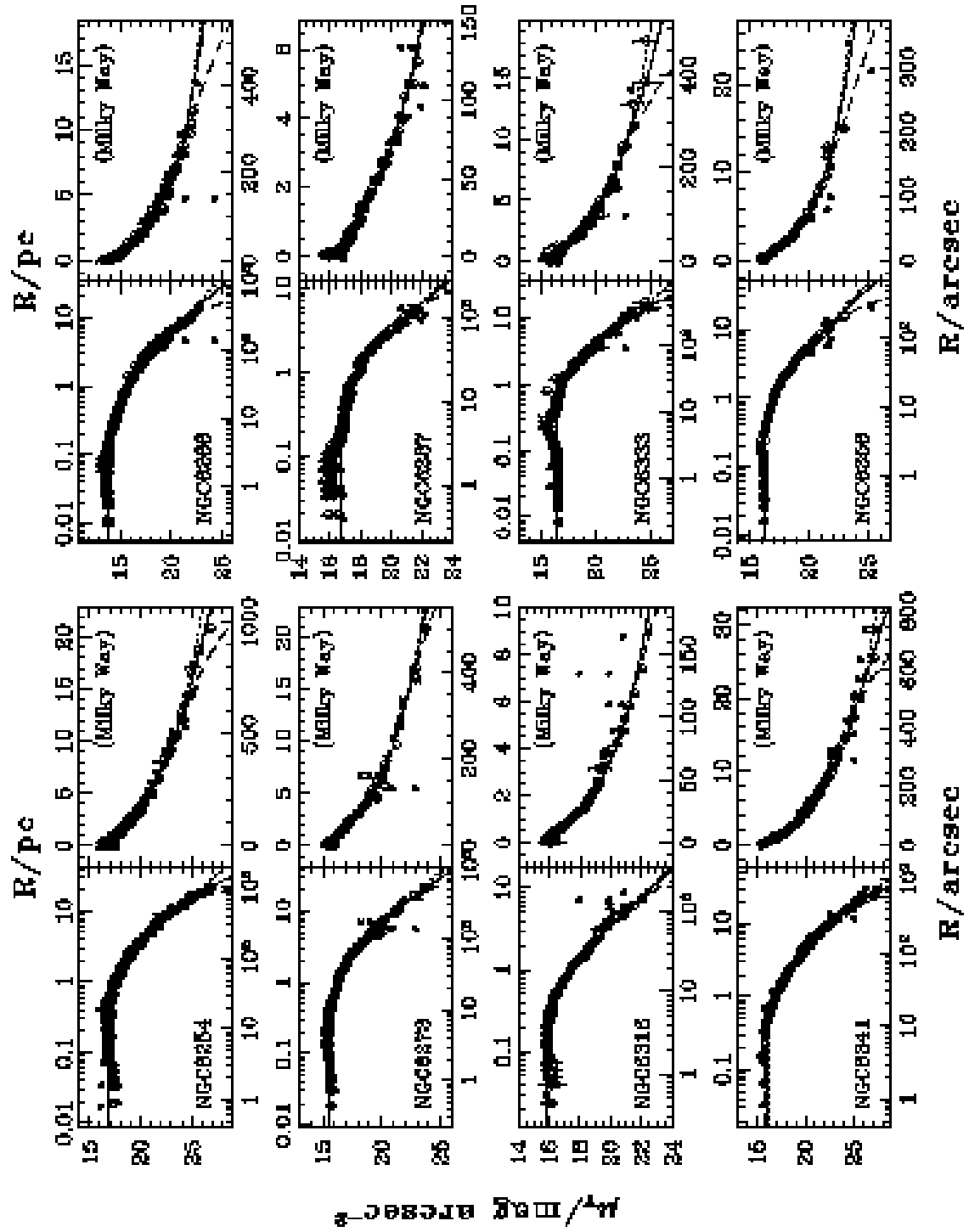


FIG. 12 [CONTINUED].—

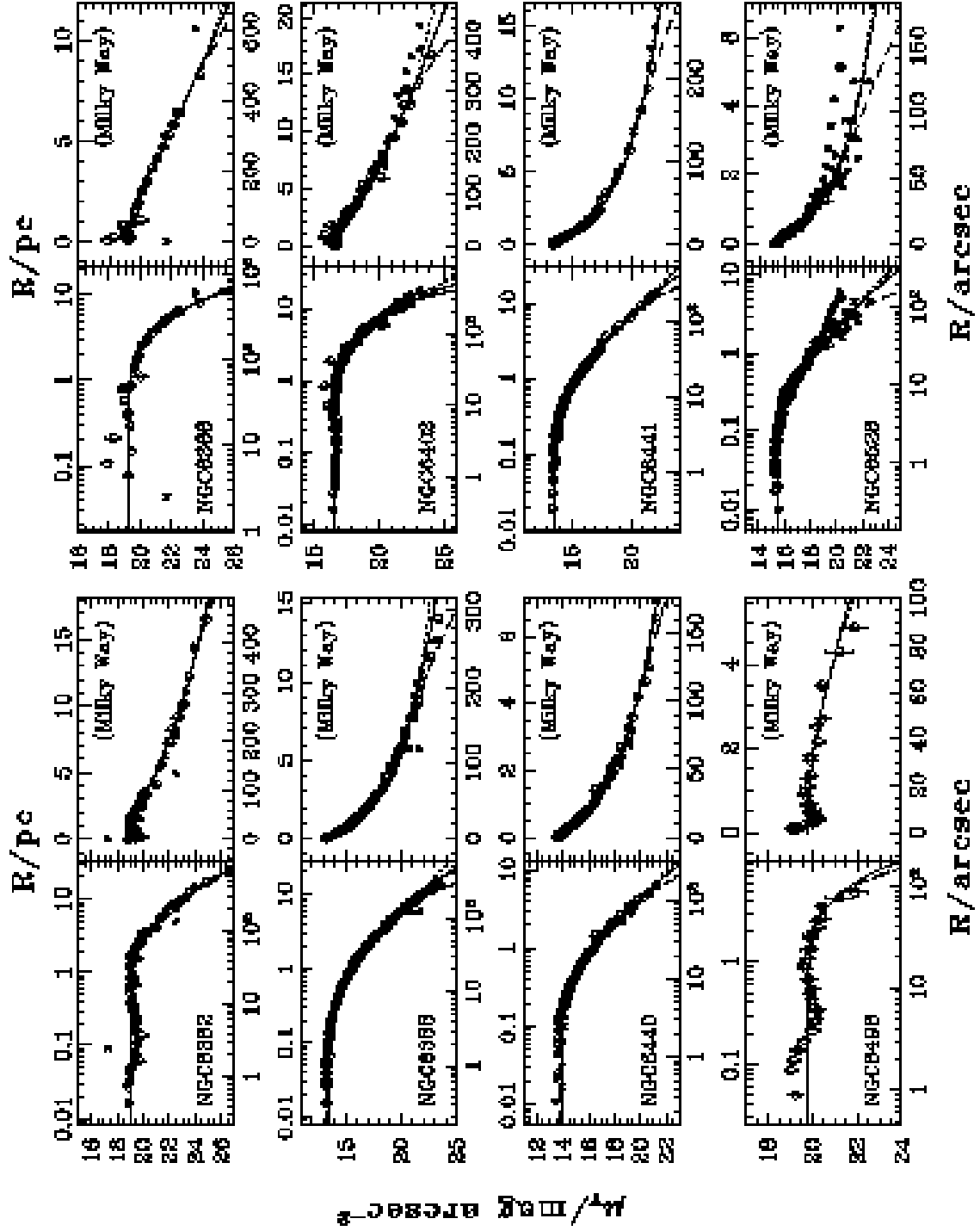


FIG. 12 [CONTINUED].—



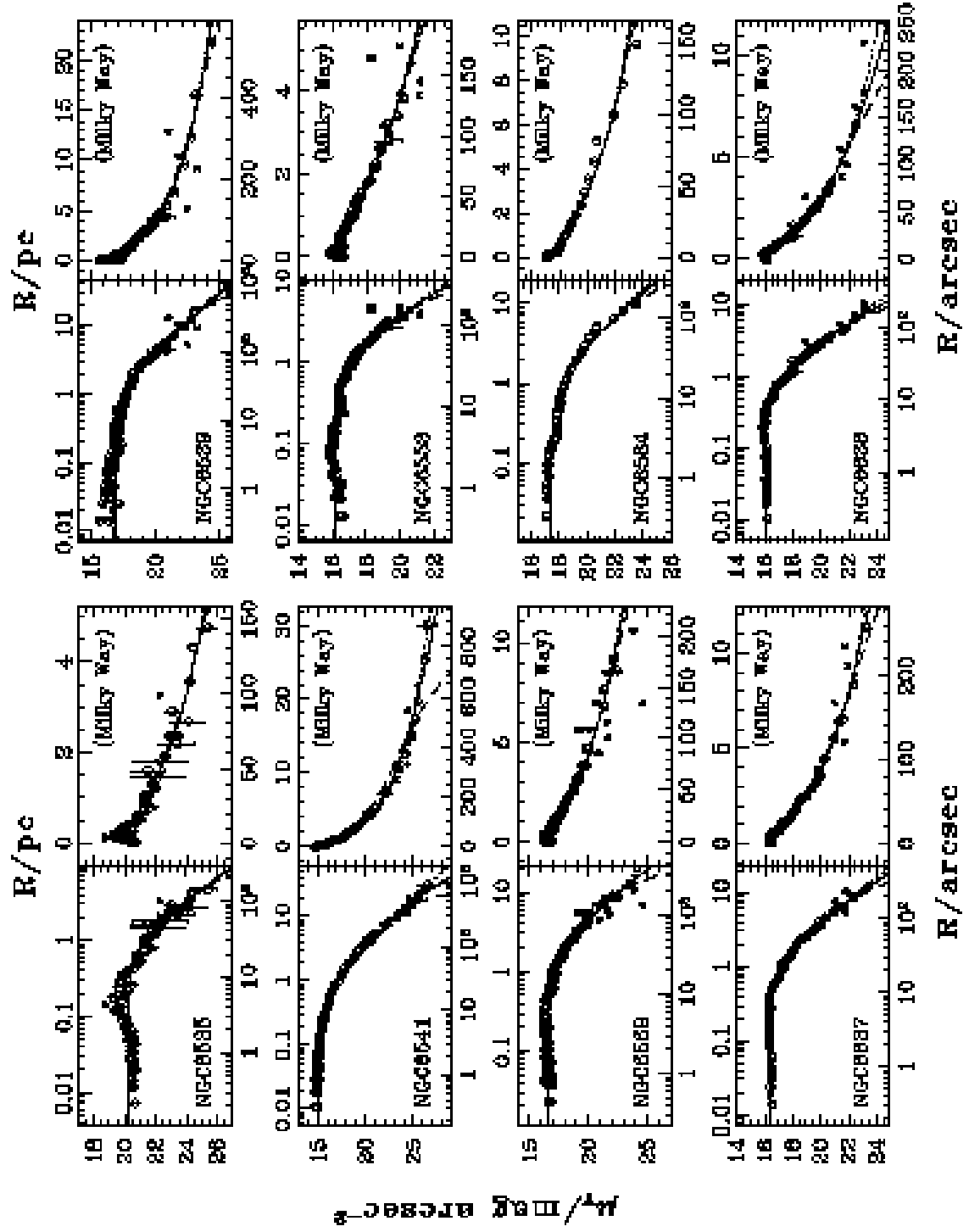


FIG. 12 [CONTINUED].—

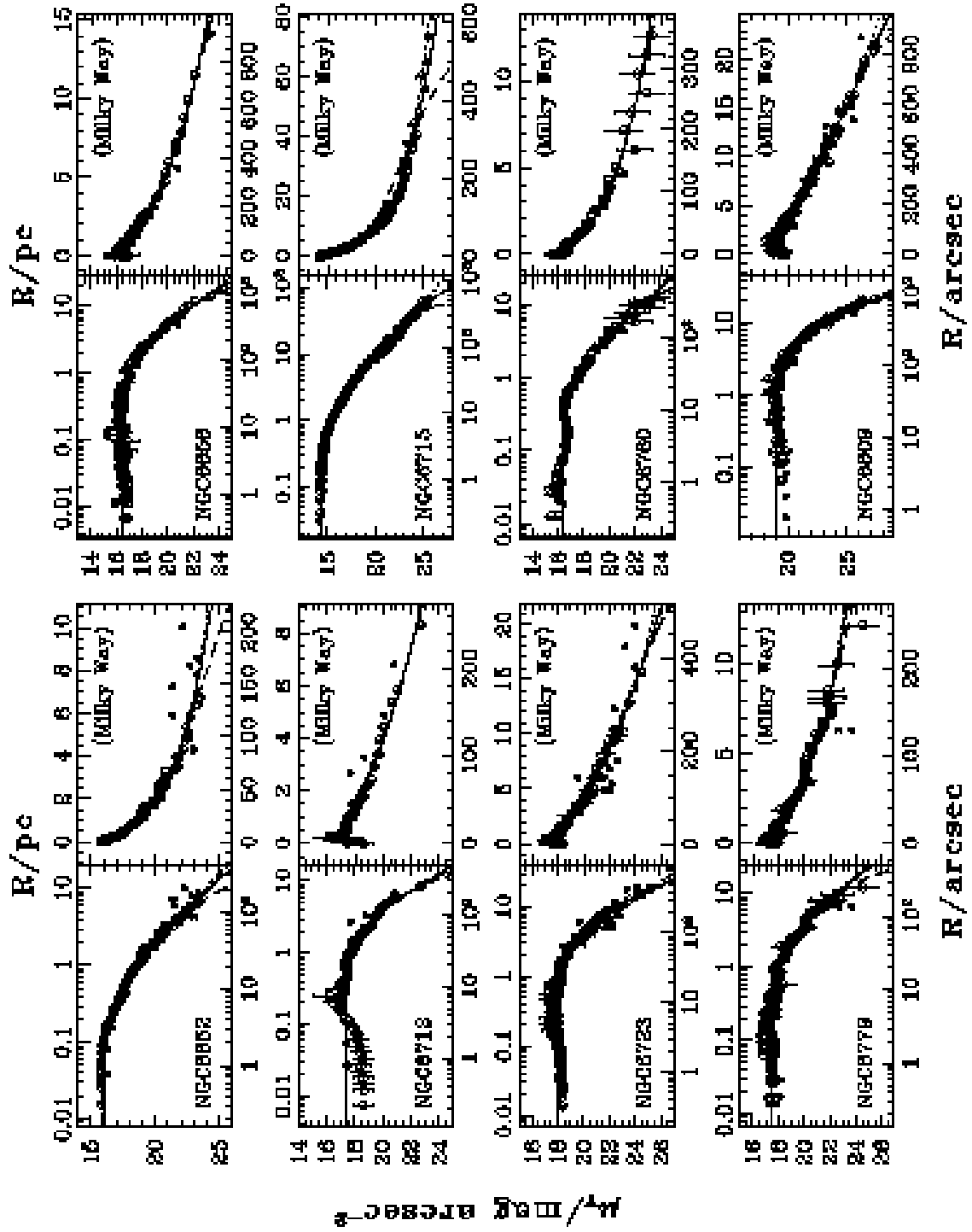


FIG. 12 [CONTINUED].—

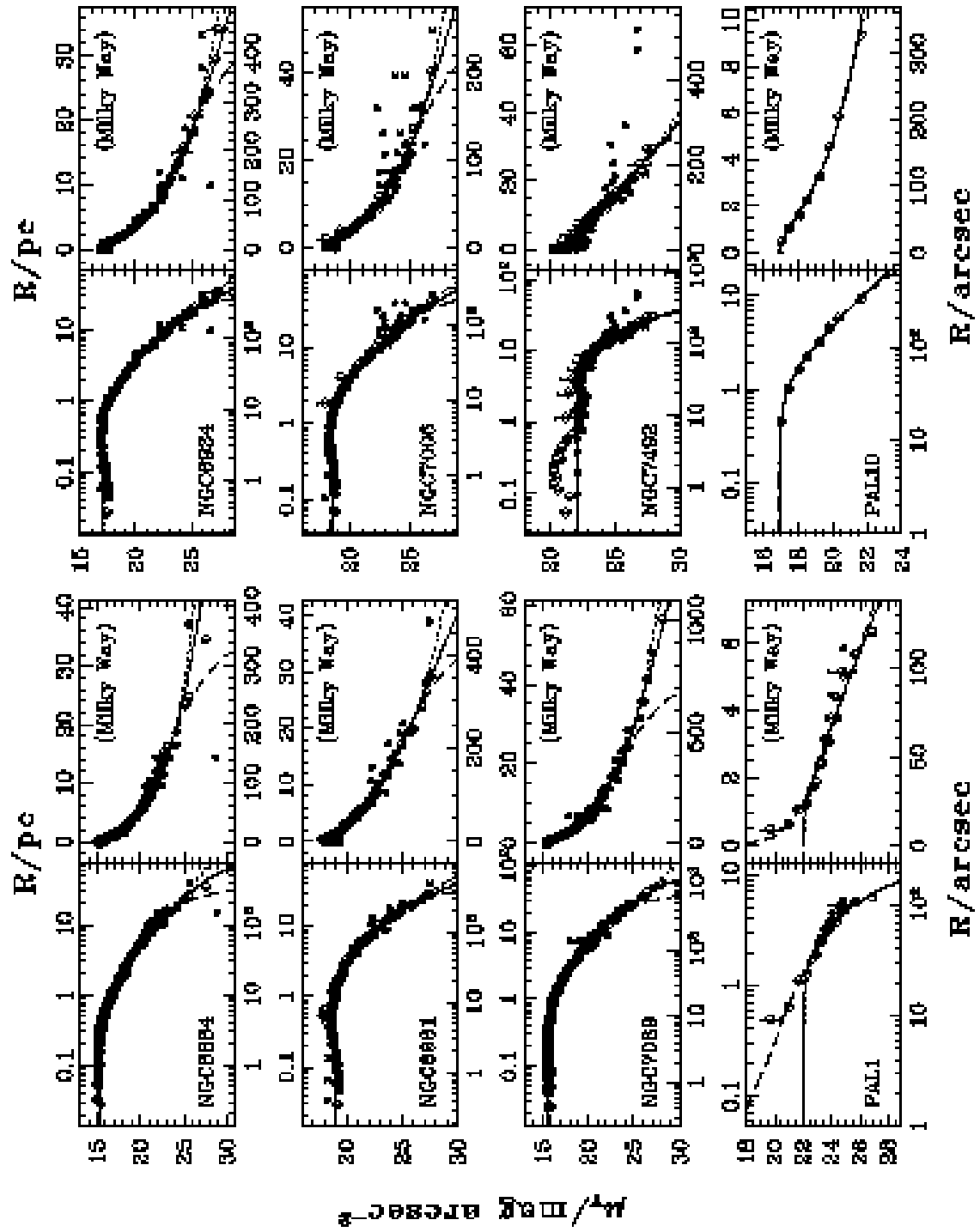


FIG. 12 [CONTINUED].—

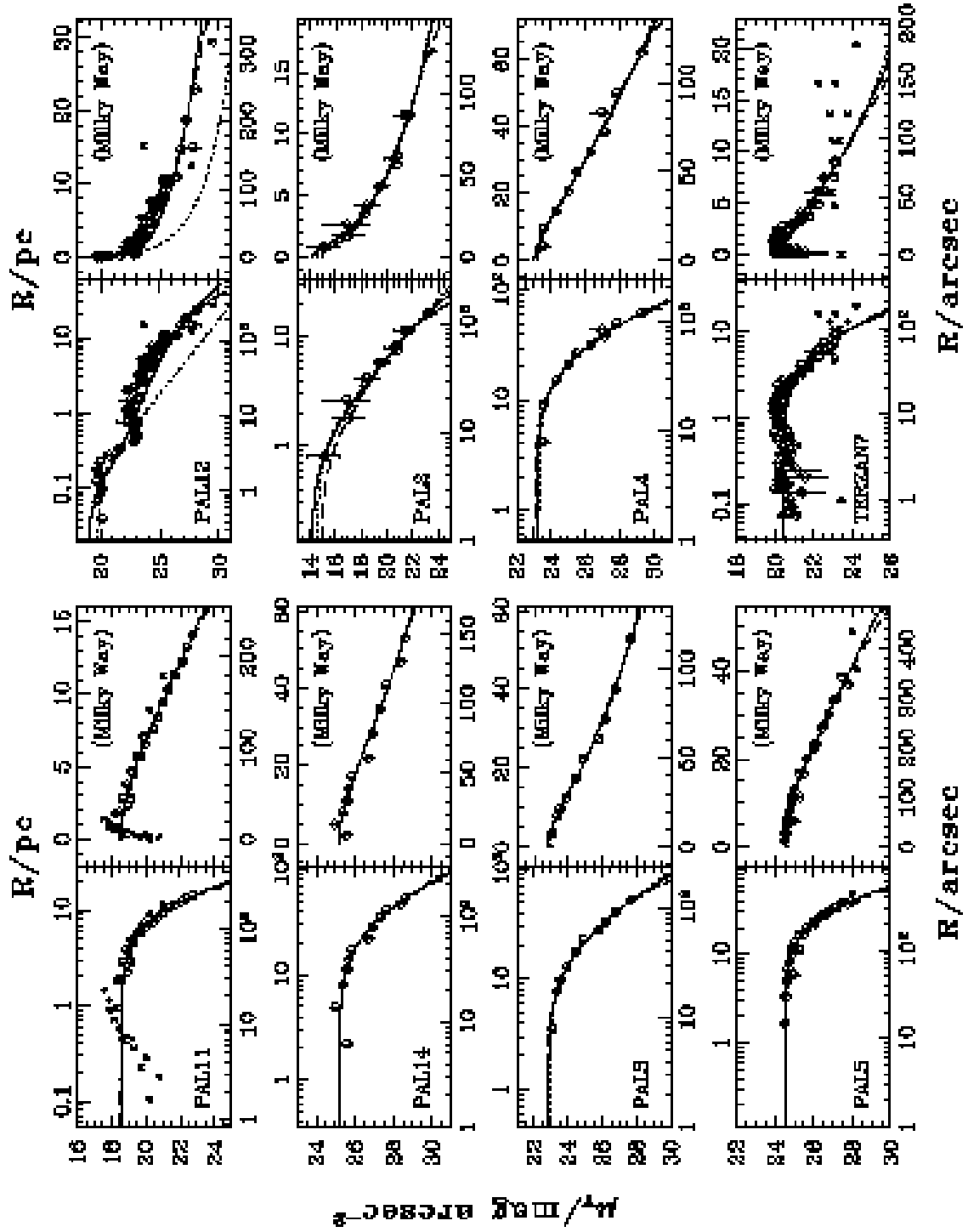


FIG. 12 [CONTINUED].—